Eur. Phys. J. A **10**, 447–486 (2001)

THE EUROPEAN PHYSICAL JOURNAL A

The light-baryon spectrum in a relativistic quark model with instanton-induced quark forces

The strange-baryon spectrum

U. Löring[a], B.Ch. Metsch and H.R. Petry

Institut für Theoretische Kernphysik, Universität Bonn, Nußallee 14-16, D-53115 Bonn, Germany

Received: 27 March 2001
Communicated by V.V. Anisovich

Abstract. This is the third of a series of papers treating light-baryon resonances up to 3 GeV within a relativistically covariant quark model based on the Bethe-Salpeter equation with instantaneous two- and three-body forces. In this last paper we extend our previous work (U. Löring, B.Ch. Metsch, H.R. Petry, this issue, p. 395) on non-strange baryons to a prediction of the complete strange-baryon spectrum and a detailed comparison with experiment. We apply the covariant Salpeter framework, which we developed in the first paper (U. Löring, K. Kretzschmar, B.Ch. Metsch, H.R. Petry, Eur. Phys. J. A **10**, 309 (2001)), to the specific quark models introduced in our work published in this issue. Quark confinement is realized by linearly rising three-body string potentials with appropriate Dirac structures; to describe the hyperfine structure of the baryon spectrum we adopt 't Hooft's two-quark residual interaction based on QCD instanton effects. The investigation of instanton-induced effects in the baryon mass spectrum plays a central role in this work. We demonstrate that several prominent features of the excited strange mass spectrum, *e.g.* the low positions of the strange partners of the Roper resonance or the appearance of approximate "parity doublets" in the Λ spectrum, find a natural, uniform explanation in our relativistic quark model with instanton-induced forces.

PACS. 11.10.St Bound and unstable states; Bethe-Salpeter equations – 12.39.Ki Relativistic quark model – 12.40.Yx Hadron mass models and calculations – 14.20.-c Baryons (including antiparticles)

1 Introduction

In this paper we want to present a description of strange baryons in a relativistic quark model based on the three-particle Bethe-Salpeter equation [1,2] with instantaneous forces (Salpeter equation [3]). The model is characterized by three- and two-particle potentials which we have already fixed in two preceding papers [4,5]; the three-particle potentials simulate (linear) confinement [6–8] and the two-particle potentials are of the form of 't Hooft's instanton-induced quark interaction [9,10]. In ref. [5] we were able to demonstrate that non-strange baryons can be accounted for very well (model $\mathcal{A}$); in particular, the known Regge trajectories are correctly reproduced by the confinement force and the hyperfine structure of the spectrum appears with its characteristic details up to high energies as a consequence of 't Hooft's interaction.

The additional model parameters for models with strangeness are the strange constituent quark mass and the coupling of strange to non-strange quarks in 't Hooft's interaction. We have fixed these parameters already in ref. [5] in order to reproduce the lowest baryon octet alone. This paper contains the complete excited Λ, Σ, Ξ and Ω spectrum (as far as it is experimentally known) which thus is a genuine prediction. We find excellent agreement with experiment, despite the fact that our treatment of baryons is still incomplete in the sense that we do not compute the strong decays of baryon resonances. We are aware that such a calculation [11–16] would influence also the resonance positions computed in our model. Indirectly, the calculations of this paper, which are purely predictive and agree so well with experiment, seem to indicate that such changes can probably be parameterized within our phenomenological quark potentials and constituent quark masses.

The most significant result of this paper is the demonstration of the role of 't Hooft's interaction in the hyperfine structure of the mass spectrum. The details, which we shall present below, seem to establish its superior relevance for light-quark flavors; at least the characteristic operator structure of this interaction seems to be indispensable for a satisfactory calculation. (One-gluon exchange potentials can be ruled out; see ref. [5].) Since we fixed the potentials strength of this interaction by a fit to

[a] e-mail: loering@itkp.uni-bonn.de

experiment, we can, however, not be completely sure that this force is derived from QCD in a strict and unambiguous way. We include a small theoretical consistency check in appendix A, but believe that more work has to be done, probably extending the efforts in refs. [17–23]. The main emphasize of this and the two preceding papers [4,5] is, however, put on the development of a relativistic quark model and the detailed comparison with experimental data.

The paper is organized as follows. Section 2 is concerned with an extensive discussion of our predictions for the excited Λ spectrum in comparison to the hitherto experimentally established Λ-resonances. A principal objective of our investigations is to demonstrate the role of the instanton-induced 't Hooft interaction in generating several prominent structures seen in the experimental Λ spectrum. These are for instance the low position of the Roper analogue or the occurrence of approximate parity doublets. This discussion of instanton effects is extended to the predictions in the other strange sectors, *i.e.* for the Σ- and Ξ-resonances in sects. 3 and 4, respectively. In sect. 5 we briefly present our predictions for the Ω-baryons, where 't Hooft's force does not contribute. In appendix A we check in how far the model parameters, which are fixed from the experimental baryon spectrum, are in fact consistent with QCD relations from the theory of instantons. Finally, we give a summary and conclusion in sect. 6.

2 The Λ-resonance spectrum

In this section we analyze the predictions of model $\mathcal{A}$ and $\mathcal{B}$ of ref. [5] for the excited strange Λ-baryons with strangeness $S^* = -1$ and isospin $T = 0$, and compare our results with the currently available experimental data. For the following discussion it is convenient to begin with some general remarks concerning the action of 't Hooft's force and the experimental status of this flavor sector.

2.1 Remarks — Implications of 't Hooft's force and the experimental situation

Similar to the nucleon spectrum discussed in ref. [5] we expect the instanton-induced interaction to play an essential role also for the description of the excited Λ spectrum. Let us briefly comment on the influence of 't Hooft's force on the different states in this flavor sector. As in the case of the excited nucleon states, the effect of 't Hooft's force in the different Λ states depends on the content of quark pairs with trivial spin being antisymmetric in flavor. But in contrast to the nucleon states these quark pairs can here be non-strange (nn) or non-strange–strange (ns), and 't Hooft's force distinguishes between these types due to the different couplings g_{nn} and g_{ns}. Moreover, the constituent quark model predicts in comparison to the nucleon sector additional degrees of freedom for the Λ sector. This results from inclusion of the strange quark, which leads to a totally antisymmetric flavor singlet state $\Lambda_{\mathbf{1}}$ in addition to the mixed symmetric octet representations $\Lambda_{\mathbf{8}}$. Hence, in addition to the octet states (that possess corresponding counterparts in the nucleon spectrum) also singlet states appear in the Λ spectrum. The positive and negative energy components of the Salpeter amplitude $\Phi^{\Lambda}_{J^\pi}$ describing an excited Λ state with spin and parity J^π are obtained by the embedding map (see ref. [4])

$$\Phi^{\Lambda}_{J^\pi} \;=\; T^{+++}\varphi^{\Lambda}_{J^\pi} \;+\; T^{---}\varphi^{\Lambda}_{J^{-\pi}} \tag{1}$$

of totally S_3-symmetric Pauli spinors $\varphi^{\Lambda}_{J^\pi}$ and $\varphi^{\Lambda}_{J^{-\pi}}$ which then decompose into the following six different spin-flavor $SU(6)$-configurations:

$$\begin{aligned}|\varphi^{\Lambda}_{J^\pm}\rangle = \;& |\Lambda\, J^\pm,\, {}^2\!8[56]\rangle \;+\; |\Lambda\, J^\pm,\, {}^2\!8[70]\rangle \\ &+|\Lambda\, J^\pm,\, {}^4\!8[70]\rangle \;+\; |\Lambda\, J^\pm,\, {}^2\!8[20]\rangle \\ &+\,|\Lambda\, J^\pm,\, {}^2\!1[70]\rangle \;+\; |\Lambda\, J^\pm,\, {}^4\!1[20]\rangle,\end{aligned} \tag{2}$$

with the four flavor octet states (as for the nucleon configurations)

$$|\Lambda\, J^\pm,\, {}^2\!8[56]\rangle :=$$
$$\sum_L \left[|\psi^{L\pm}_{\mathcal{S}}\rangle \otimes \frac{1}{\sqrt{2}}\Big(|\chi^{\frac12}_{\mathcal{M}_\mathcal{A}}\rangle\otimes|\phi^{\Lambda}_{\mathcal{M}_\mathcal{A}}\rangle + |\chi^{\frac12}_{\mathcal{M}_\mathcal{S}}\rangle\otimes|\phi^{\Lambda}_{\mathcal{M}_\mathcal{S}}\rangle\Big)\right]^J,$$

$$|\Lambda\, J^\pm,{}^2\,8[70]\rangle :=$$
$$\sum_L \left[\frac{1}{2}\,|\psi^{L\,\pm}_{\mathcal{M}_\mathcal{A}}\rangle\otimes\Big(|\chi^{\frac12}_{\mathcal{M}_\mathcal{A}}\rangle\otimes|\phi^{\Lambda}_{\mathcal{M}_\mathcal{S}}\rangle + |\chi^{\frac12}_{\mathcal{M}_\mathcal{S}}\rangle\otimes|\phi^{\Lambda}_{\mathcal{M}_\mathcal{A}}\rangle\Big)\right.$$
$$\left. +\frac{1}{2}\,|\psi^{L\,\pm}_{\mathcal{M}_\mathcal{S}}\rangle\otimes\Big(|\chi^{\frac12}_{\mathcal{M}_\mathcal{A}}\rangle\otimes|\phi^{\Lambda}_{\mathcal{M}_\mathcal{A}}\rangle - |\chi^{\frac12}_{\mathcal{M}_\mathcal{S}}\rangle\otimes|\phi^{\Lambda}_{\mathcal{M}_\mathcal{S}}\rangle\Big)\right]^J,$$

$$|\Lambda\, J^\pm,\, {}^4\!8[70]\rangle := \sum_L \left[\frac{1}{\sqrt{2}}\Big(|\psi^{L\,\pm}_{\mathcal{M}_\mathcal{A}}\rangle\otimes|\chi^{\frac32}_{\mathcal{S}}\rangle\otimes|\phi^{\Lambda}_{\mathcal{M}_\mathcal{A}}\rangle - |\psi^{L\,\pm}_{\mathcal{M}_\mathcal{S}}\rangle\otimes|\chi^{\frac32}_{\mathcal{S}}\rangle\otimes|\phi^{\Lambda}_{\mathcal{M}_\mathcal{S}}\rangle\Big)\right]^J,$$

$$|\Lambda\, J^\pm,\, {}^2\!8[20]\rangle :=$$
$$\sum_L \left[|\psi^{L\,\pm}_{\mathcal{A}}\rangle\otimes\frac{1}{\sqrt{2}}\Big(|\chi^{\frac12}_{\mathcal{M}_\mathcal{A}}\rangle\otimes|\phi^{\Lambda}_{\mathcal{M}_\mathcal{S}}\rangle - |\chi^{\frac12}_{\mathcal{M}_\mathcal{S}}\rangle\otimes|\phi^{\Lambda}_{\mathcal{M}_\mathcal{A}}\rangle\Big)\right]^J, \tag{3}$$

and the two flavor singlet states

$$|\Lambda\, J^\pm,\, {}^2\!1[70]\rangle :=$$
$$\sum_L \left[\frac{1}{\sqrt{2}}\Big(|\psi^{L\,\pm}_{\mathcal{M}_\mathcal{S}}\rangle\otimes|\chi^{\frac12}_{\mathcal{M}_\mathcal{A}}\rangle - |\psi^{L\,\pm}_{\mathcal{M}_\mathcal{A}}\rangle\otimes|\chi^{\frac12}_{\mathcal{M}_\mathcal{S}}\rangle\Big)\right]^J\otimes|\phi^{\Lambda}_{\mathcal{A}}\rangle,$$

$$|\Lambda\, J^\pm,\, {}^4\!1[20]\rangle := \sum_L \left[|\psi^{L\,\pm}_{\mathcal{A}}\rangle\otimes|\chi^{\frac32}_{\mathcal{S}}\rangle\right]^J\otimes|\phi^{\Lambda}_{\mathcal{A}}\rangle. \tag{4}$$

Here $\psi^{L\,\pm}_{R_L}$, $\chi^{S}_{R_S}$ and $\phi^{N}_{R_F}$ are the spatial, spin and flavor wave functions with definite S_3-symmetries $R_L, R_S, R_F \in$

$\{\mathcal{S}, \mathcal{M}_\mathcal{S}, \mathcal{M}_\mathcal{A}, \mathcal{A}\}$. The sum runs over the possible orbital angular momenta L that can be coupled with the internal spin S to the total spin J as denoted by the brackets $[\ldots]^J$. To explore the implications of the strong selection rules of 't Hooft's force for the different Λ states, let us discuss qualitatively what one naively expects in a simplified picture (disregarding the negative energy component and the relativistic effects from the embedding map of the Salpeter amplitudes (non-relativistic limit)). Recalling the selection rules of 't Hooft's force for the flavor octet states from our earlier discussion of the nucleon sector (see ref. [5]), we expect the dominantly ^{4}8[70] and ^{2}8[20] states to be hardly influenced, whereas dominantly ^{2}8[56] and ^{2}8[70] states should be shifted downward. Moreover, 't Hooft's force generally mixes the configurations ^{2}8[56] and ^{2}8[70]. Concerning the additional flavor singlet states we expect dominantly ^{4}1[20] states to remain essentially unaffected due to the internal totally symmetric spin function $\chi_\mathcal{S}^{3/2}$ in the ^{4}1[20] configurations. But similar to dominantly ^{2}8[56] and ^{2}8[70] states we likewise expect a lowering of dominantly ^{2}1[70] states. Finally, we should mention here that the difference $g_{nn} - g_{ns} > 0$ between the 't Hooft couplings as required by the Σ-Λ ground-state splitting (see ref. [5]) implies further flavor $SU(3)$ symmetry breaking effects in addition to those arising already from the difference $m_s - m_n > 0$ between the non-strange and strange quark masses. This leads to a further mixing of the flavor singlet configuration ^{2}1[70] with the flavor octet configurations ^{2}8[70] and ^{2}8[56], which depends on the difference $g_{nn} - g_{ns}$ of the two couplings and vanishes in the case $g_{ns} = g_{nn}$.

Once again we should be aware of the simplicity of these naive non-relativistic considerations: In the same manner as observed for the excited nucleon states [5], the relativistic effects in our fully relativistic framework, especially the interplay of 't Hooft's force with relativistic effects from confinement, should also here be crucial for the influence of 't Hooft's residual force on the excited Λ states. In the course of the following discussion we therefore will again analyze how instanton-induced effects in our fully relativistic approach do really shape the hyperfine structures in the excited Λ spectrum. From the discussion of the nucleon spectrum we expect again substantial differences between the results of the confinement models $\mathcal{A}$ and $\mathcal{B}$.

Before quoting our predictions, let us first discuss heuristically what we do expect from our earlier investigations of the nucleon sector (see ref. [5]) in view of the rather similar structures that can be found in the experimental Λ and nucleon spectra. In this respect, it is instructive to consider the flavor $SU(3)$ symmetric limit, *i.e.* $m_s = m_n$ and $g_{ns} = g_{nn}$. In this limit the flavor octet and flavor singlet states completely decouple due to the explicit flavor-independence of the confinement kernel and due to the flavor $SU(3)$ invariance of the embedding map, the kinetic energy operator and 't Hooft's force in this case. Consequently, the flavor octet states of the Λ spectrum and the nucleon spectrum have exactly the same masses and configuration mixings. The singlet states just additionally appear with the ^{2}1[70] states lowered with respect to the ^{4}1[20] states. Of course, in the realistic case (with $m_s > m_n$ and $g_{ns} < g_{nn}$) this degeneracy is lifted and singlet and octet states mix. Nonetheless, we expect the dominantly flavor octet states of the Λ spectrum forming hyperfine structures that have their direct counterparts in the excited-nucleon spectrum. This, in fact, one really observes in the experimental Λ-resonance spectrum. Figure 1 shows a direct comparison of the present experimental situation for the nucleon- and Λ-resonances for each sector with spin and parity J^π. The nucleon states are displayed on the left-hand side in each column and the Λ states on the right-hand side. To correct approximately for the flavor $SU(3)$ breaking effects in the Λ states, the mass scales for N- and Λ-resonances are mutually shifted by 177 MeV, such that the ground states appear at the same level. The figure nicely demonstrates that the positive- and negative-parity Λ spectra indeed exhibit several structures showing similar hyperfine splittings as in the nucleon spectrum. The corresponding states thus presumably are the flavor octet counterparts of the nucleon spectrum. According to fig. 1, let us briefly summarize the most striking features of the experimentally observed Λ spectrum that have (and have not) counterparts in the experimental nucleon spectrum:

- The pattern of four low-lying Λ-resonances in the positive-parity $2\hbar\omega$ band indeed shows a very striking similarity to the structure of the four low-lying states in $2\hbar\omega$ shell of the nucleon spectrum: The lowest-lying resonance $\Lambda\frac{1}{2}^+(1600, ***)$, which is the first isoscalar/scalar excitation of the Λ ground state, may be viewed as the strange counterpart of the Roper resonance $N\frac{1}{2}^+(1440, ****)$. The remaining three well-established resonances $\Lambda\frac{1}{2}^+(1810, ***)$, $\Lambda\frac{3}{2}^+(1890, ****)$, and $\Lambda\frac{5}{2}^+(1820, ****)$ are approximately degenerate at around 1850 MeV quite similar to the three nucleon resonances $N\frac{1}{2}^+(1710, ***)$, $N\frac{3}{2}^+(1720, ****)$, and $N\frac{5}{2}^+(1680, ****)$ which are nearly degenerate at around 1700 MeV in the nucleon $2\hbar\omega$ band. Here the $\Lambda\frac{3}{2}^+(1890, ****)$ and the $\Lambda\frac{5}{2}^+(1820, ****)$ are presumably the octet partners of the $N\frac{3}{2}^+(1720, ****)$ and the $N\frac{5}{2}^+(1680, ****)$, respectively. The correspondence of $\Lambda\frac{1}{2}^+(1810, ***)$ with $N\frac{1}{2}^+(1710, ***)$, however, seems to be less clear.
- In the upper part of the negative-parity $1\hbar\omega$ band between 1600 and 1900 MeV, the four well-established three- and four-star Λ-resonances stated by the Particle Data Group exhibit hyperfine splittings which are similar to those of the five resonances observed in the $1\hbar\omega$ shell of the nucleon spectrum: The two lower-lying resonances $\Lambda\frac{1}{2}^-(1670, ****)$ and $\Lambda\frac{3}{2}^-(1690, ****)$, which form a nearly degenerate doublet at around 1680 MeV, may be interpreted as the octet partners of the two approximately degenerate (dominantly ^{2}8[70]) states $N\frac{1}{2}^-(1535, ****)$ and

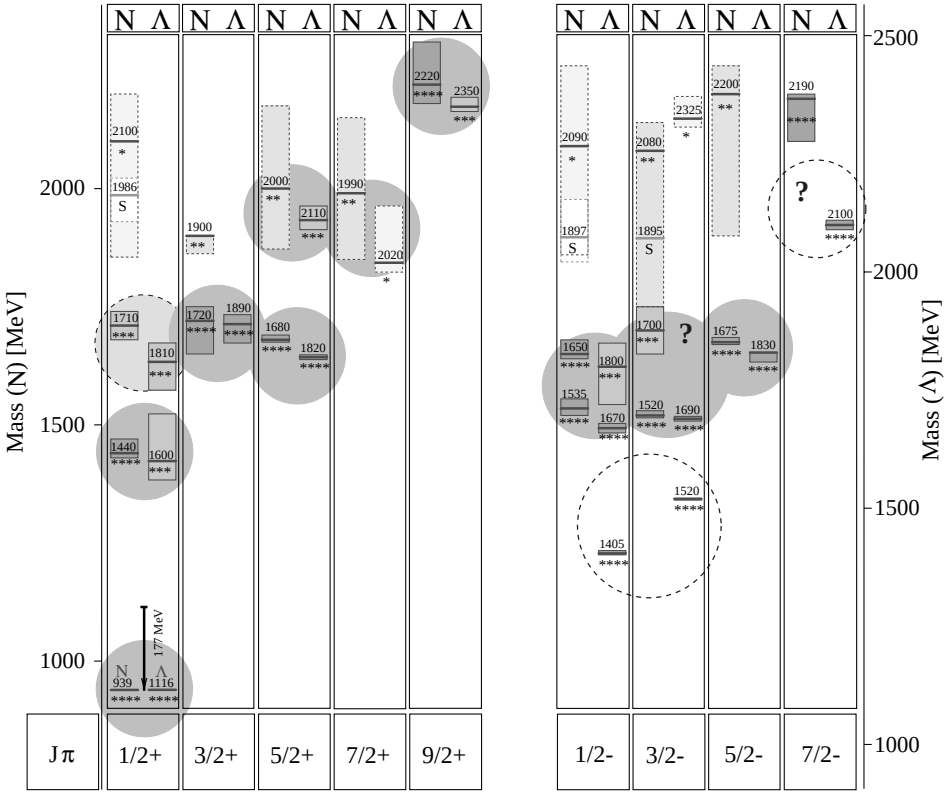

Fig. 1. Comparison of the present experimental situation for nucleon- and Λ-resonances. The resonances are classified due to their total spin and parity J^π. On the left in each column, the nucleon resonances are shown. For comparison, the Λ-resonances are shown on the right-hand side in each column. Note, that the mass scale for the Λ states is shifted downwards with respect to the mass scale of nucleon states by 177 MeV, so that the ground states appear on the same level. In fact, there are a lot of Λ states (expected to be dominantly flavor octet), that have their direct counterparts in the nucleon spectrum. See, the text for further explanations.

$N\frac{3}{2}^-(1520,***)$ in the lower part of the nucleon $1\hbar\omega$ shell. The two higher-lying resonances $\Lambda\frac{1}{2}^-(1800,***)$ and $\Lambda\frac{5}{2}^-(1830,****)$ positioned approximately degenerate at roughly 1800 MeV should then be the octet counterparts to the $J^\pi = \frac{1}{2}^-$ and $J^\pi = \frac{5}{2}^-$ nucleon states of the triplet formed by the nearly degenerate (dominantly ^{4}8[70]) resonances $N\frac{1}{2}^-(1650,****)$, $N\frac{3}{2}^-(1700,***)$, and $N\frac{5}{2}^-(1675,****)$ in the upper part of the nucleon $1\hbar\omega$ shell. The octet partner of $N\frac{3}{2}^-(1700,***)$, however, which likewise should appear at roughly 1800–1900 MeV in the $\Lambda\frac{3}{2}^-$ sector, has not been observed so far.

The two lowest-lying Λ-resonances in the $1\hbar\omega$ band, *i.e.* the two four-star states $\Lambda\frac{1}{2}^-(1405,****)$ and $\Lambda\frac{3}{2}^-(1520,****)$, have no counterparts in the nucleon spectrum. Consequently, they are expected to be dominantly flavor singlet states. Apart from the significantly lower position with respect to the octet states, a very striking feature of these two resonances is the very low position of the $\Lambda\frac{1}{2}^-(1405,****)$ relative to the $\Lambda\frac{3}{2}^-(1520,****)$. The $\Lambda\frac{1}{2}^-(1405,****)$ lies even below the lowest nucleon excitations and is the lowest negative-parity excitation in the light-baryon spectrum measured at all. The failure of several constituent quark models in reproducing the low position of this well-established four-star state is a long-standing problem and there is still controversy about the real physical nature of this state, see, for instance, [25].

– Similar to the nucleon spectrum, one observes overlapping parts of alternating even- and odd-parity bands which likewise lead to the appearance of approximate "parity doublets" in the experimental Λ spectrum. The best established parity doublet structure is formed by the two lowest four-star excitations in the sectors with total spin $J = \frac{5}{2}$:

$$\Lambda\tfrac{5}{2}^+(1820,****) \quad - \quad \Lambda\tfrac{5}{2}^-(1830,****).$$

This doublet is due to the overlap of the negative-parity $1\hbar\omega$ and the positive-parity $2\hbar\omega$ shell. A further parity doublet in the same energy range between 1800 and 1850 MeV is found in the sectors with total spin $J = \frac{1}{2}$ with the two three-star states

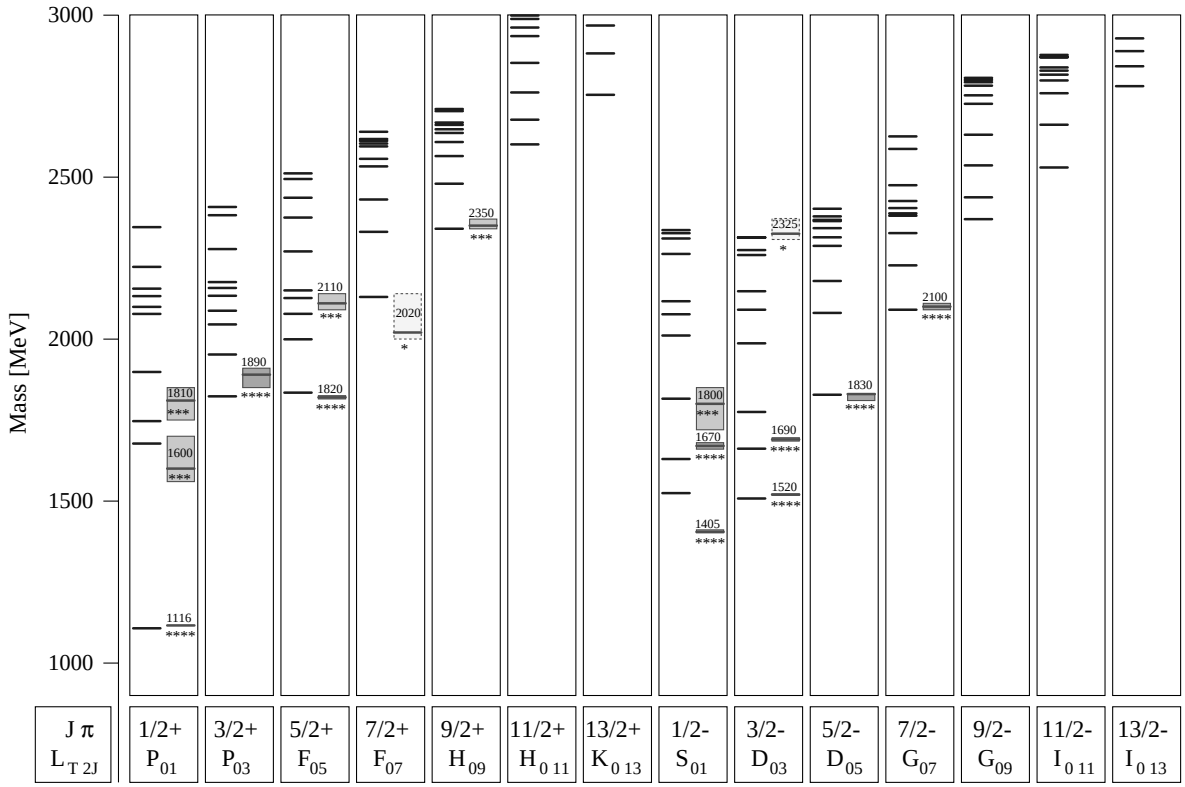

Fig. 2. The calculated positive- and negative-parity *Λ-resonance spectrum* with isospin $T = 0$ and strangeness $S^* = -1$ in *model* $\mathcal{A}$ (left part of each column) in comparison to the experimental spectrum taken from Particle Data Group [24] (right part of each column). The resonances are classified by the total spin J and parity π. The experimental resonance position is indicated by a bar, the corresponding uncertainty by the shaded box, which is darker for better-established resonances; the status of each resonance is additionally indicated by stars.

$$\Lambda\tfrac{1}{2}^+(1810,***) \quad - \quad \Lambda\tfrac{1}{2}^-(1800,***).$$

In the higher mass region of the Λ spectrum such a parity doublet pattern is indicated by the lowest resonances observed in the $\Lambda\frac{7}{2}^{\pm}$ sectors[1]:

$$\Lambda\tfrac{7}{2}^+(2020,*) \quad - \quad \Lambda\tfrac{7}{2}^-(2100,****).$$

Since all corresponding structures of the excited-nucleon spectrum could be nicely reproduced by means of 't Hooft's residual interaction, our approach (model $\mathcal{A}$) looks very promising to work as well for the counterparts in the Λ spectrum. So let us see now how far the predictions of both models can really account for these observed structures using the parameter sets of ref. [5] as they were fixed on the phenomenology of the Δ and the ground-state spectrum alone. In this respect, we should stress once more that also in the Λ sector all calculated positions of excited states are *real parameter-free predictions*. As already in the nucleon spectrum, *no* structure in the Λ spectrum has been explicitly adjusted.

[1] It is worth noting in this respect the striking difference to the present experimental situation in the nucleon spectrum (see fig. 1) and to refer back to our predictions for the lowest excitations in the corresponding $N\frac{7}{2}^{\pm}$ sectors (see ref. [5]): In contrast to our model calculation the currently available experimental data do not exhibit a clear parity doublet structure of the lowest excitations in $N\frac{7}{2}^{\pm}$ due to the rather high position of the $N\frac{7}{2}^-(2190,****)$ with respect to the $N\frac{7}{2}^+(1990,**)$. In view of the otherwise striking similarities between the experimental nucleon and Λ spectra the comparatively low position of $\Lambda\frac{7}{2}^-(2100,****)$ might be a further strong *experimental* indication for a $N\frac{7}{2}^-$ resonance even below the $N\frac{7}{2}^-(2190,****)$.

2.2 Discussion of the complete Λ spectrum

Our predictions for the Λ spectrum in both model variants $\mathcal{A}$ and $\mathcal{B}$ are depicted in figs. 2 and 3, respectively. The resonances in each column are classified by their total spin J and parity π. For both parities the predictions are shown up to $J = \frac{13}{2}$. For each sector $[\Lambda\, J^\pi]$ at most ten radially excited states are displayed on the left-hand side of the column. In comparison, the currently experimentally known Λ-resonances [24] are shown on the right-hand side in each column. The corresponding uncertainties in the measured resonance positions are indicated by the shaded

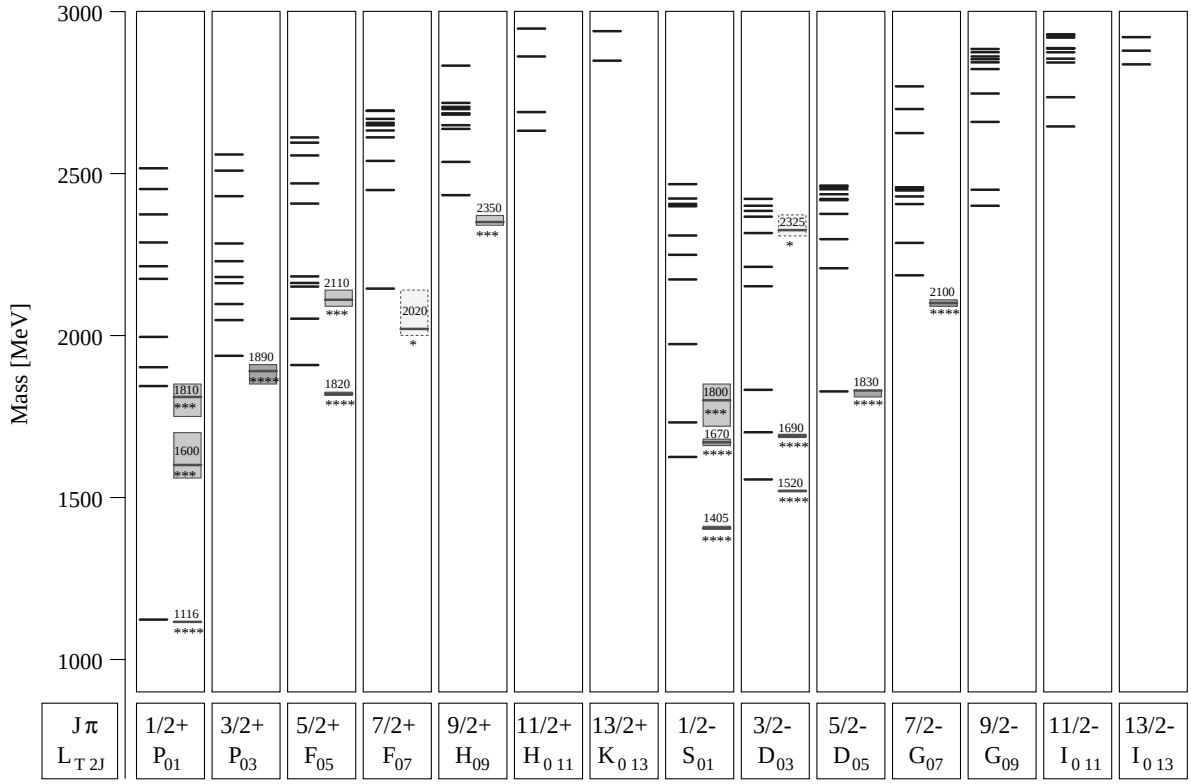

Fig. 3. The calculated positive- and negative-parity *Λ-resonance spectrum* with isospin $T = 0$ and strangeness $S^* = -1$ in *model* $\mathcal{B}$ (left part of each column) in comparison to the experimental spectrum taken from Particle Data Group [24] (right part of each column). The resonances are classified by the total spin J and parity π. See also caption to fig. 2.

areas. The status of each resonance is denoted by the corresponding number of stars following the notation of the Particle Data Group [24] and moreover, by the shading of the error box which is darker for better established resonances. The following discussion is organized according to a separate investigation of each shell. The predicted masses for the states of each shell in comparison with corresponding resonance positions measured experimentally are explicitly given in tables 1, 3, 5 and 6, respectively.

2.2.1 A first glimpse of the resulting spectra — comparing model $\mathcal{A}$ and model $\mathcal{B}$

Comparing globally the predictions of model $\mathcal{A}$ and model $\mathcal{B}$ in figs. 2 and 3, respectively, we again observe that model $\mathcal{A}$ leads to consistently better agreement with experiment than model $\mathcal{B}$: As in the non-strange nucleon sector, model $\mathcal{A}$ can excellently explain the positions of several well-established four- and three-star resonances of the complete Λ spectrum presently known (most of them belonging to the $1\hbar\omega$ and $2\hbar\omega$ shell): Since this is in fact a *parameter-free prediction*, the excellent quantitative agreement is very remarkable and strongly supports the credibility and predictive power of our model $\mathcal{A}$.

The only feature which model $\mathcal{A}$ unfortunately cannot account for is the puzzling low position of $\Lambda\frac{1}{2}^-(1405, ****)$. Hence, the notorious difficulty of *all* previous constituent quark models in explaining the position of $\Lambda\frac{1}{2}^-(1405, ****)$ remains unsolved also in our fully relativistic approach which uses instanton-induced, flavor-dependent forces. In view of the otherwise excellent results, this shortcoming strongly indicates that something in the present dynamics is missing which must be very specific to that single state. We will come back to this question during the following more detailed discussion.

As one would already anticipate from our discussion of the nucleon spectrum [5], the most distinct deviations between model $\mathcal{A}$ and $\mathcal{B}$ again show up in the sectors with total spin $J = \frac{1}{2}$. In particular, model $\mathcal{B}$ once again strongly fails in describing the striking low position of the first scalar/isoscalar excitation in the $\frac{1}{2}^+$ sector, which in this flavor sector is the counterpart $\Lambda\frac{1}{2}^+(1600, ***)$ of the Roper resonance. Furthermore, several positions of higher mass states (in the $2\hbar\omega$ shell and beyond) are generally predicted too high in model $\mathcal{B}$. This result once more confirms that model $\mathcal{A}$ is more realistic and thus the favored model for describing light baryons. For this reason, the following detailed comparison of our predictions with experiment will henceforth mainly focus to the results of the more successful model $\mathcal{A}$. Now let us discuss and investigate in detail the hyperfine structures in each shell. We start with the predictions in the positive-parity $2\hbar\omega$ shell.

Table 1. Calculated positions of all Λ states assigned to the positive-parity $2\hbar\omega$ shell in comparison to the corresponding experimental mass values taken from [24]. PW denotes the partial wave and the rating is given according to the PDG classification [24]. Here and throughout this work we use the notation $[B\ J^\pi]_n(M)$ for the predicted model states in model $\mathcal{A}$ and $\mathcal{B}$, respectively, where B denotes the baryon (*i.e.* the flavor), J^π are spin and parity, and M is the predicted mass given in MeV. $n = 1, 2, 3, \ldots$ is the principal quantum number counting the states in each sector J^π beginning with the lowest state.

Experimental state [24]	PW	J^π	Rating	Mass range [MeV] [24]	Model state in model $\mathcal{A}$	Model state in model $\mathcal{B}$
$\Lambda(1600)$	P_{01}	$\frac{1}{2}^+$	***	1560–1700	$[\Lambda\frac{1}{2}^+]_2(1677)$	$[\Lambda\frac{1}{2}^+]_2(1844)$
$\Lambda(1810)$	P_{01}	$\frac{1}{2}^+$	***	1750–1850	$[\Lambda\frac{1}{2}^+]_3(1747)$	$[\Lambda\frac{1}{2}^+]_3(1902)$
					$[\Lambda\frac{1}{2}^+]_4(1898)$	$[\Lambda\frac{1}{2}^+]_4(1996)$
					$[\Lambda\frac{1}{2}^+]_5(2077)$	$[\Lambda\frac{1}{2}^+]_5(2175)$
					$[\Lambda\frac{1}{2}^+]_6(2099)$	$[\Lambda\frac{1}{2}^+]_6(2214)$
					$[\Lambda\frac{1}{2}^+]_7(2132)$	$[\Lambda\frac{1}{2}^+]_7(2287)$
$\Lambda(1890)$	P_{03}	$\frac{3}{2}^+$	****	1850–1910	$[\Lambda\frac{3}{2}^+]_1(1823)$	$[\Lambda\frac{3}{2}^+]_1(1937)$
					$[\Lambda\frac{3}{2}^+]_2(1952)$	$[\Lambda\frac{3}{2}^+]_2(2047)$
					$[\Lambda\frac{3}{2}^+]_3(2045)$	$[\Lambda\frac{3}{2}^+]_3(2097)$
					$[\Lambda\frac{3}{2}^+]_4(2087)$	$[\Lambda\frac{3}{2}^+]_4(2161)$
					$[\Lambda\frac{3}{2}^+]_5(2133)$	$[\Lambda\frac{3}{2}^+]_5(2180)$
					$[\Lambda\frac{3}{2}^+]_6(2157)$	$[\Lambda\frac{3}{2}^+]_6(2229)$
					$[\Lambda\frac{3}{2}^+]_7(2167)$	$[\Lambda\frac{3}{2}^+]_7(2285)$
$\Lambda(1820)$	F_{05}	$\frac{5}{2}^+$	****	1815–1825	$[\Lambda\frac{5}{2}^+]_1(1834)$	$[\Lambda\frac{5}{2}^+]_1(1909)$
					$[\Lambda\frac{5}{2}^+]_2(1999)$	$[\Lambda\frac{5}{2}^+]_2(2052)$
					$[\Lambda\frac{5}{2}^+]_3(2078)$	$[\Lambda\frac{5}{2}^+]_3(2151)$
$\Lambda(2110)$	F_{05}	$\frac{5}{2}^+$	***	2090–2140	$[\Lambda\frac{5}{2}^+]_4(2127)$	$[\Lambda\frac{5}{2}^+]_4(2162)$
					$[\Lambda\frac{5}{2}^+]_5(2150)$	$[\Lambda\frac{5}{2}^+]_5(2182)$
$\Lambda(2020)$	F_{07}	$\frac{7}{2}^+$	*	2000–2140	$[\Lambda\frac{7}{2}^+]_1(2130)$	$[\Lambda\frac{7}{2}^+]_1(2145)$

2.2.2 States of the positive-parity $2\hbar\omega$ band

The $2\hbar\omega$ band includes states with spin $J^\pi = \frac{1}{2}^+$, $\frac{3}{2}^+$, $\frac{5}{2}^+$, and $\frac{7}{2}^+$. The positions predicted for these states (in both models) are summarized in table 1 together with the assignment to the observed states according to a comparison of the predicted and measured masses. The number of predicted $2\hbar\omega$ states is even larger than in the nucleon spectrum owing to the additional flavor singlet states. On the other hand, there are considerably fewer states observed experimentally, especially in the upper part of this band (beyond 2 GeV), where so far only two resonances have been seen in the $\Lambda\frac{5}{2}^+$ and $\Lambda\frac{7}{2}^+$ sectors. Hence a quite large number of Λ-resonances in this mass region is expected to be "missing", *i.e.* hitherto these states have not been seen in multichannel phase-shift analysis of $\bar{K}N$ scattering data. In this respect, the study of strong two-body decay amplitudes of baryons within our covariant Bethe-Salpeter framework would be very favorable again. This should offer the possibility to explain that model states, assigned to observed resonances (according to their position), strongly couple to the $\bar{K}N$ channel, whereas the others do not (or only weakly couple to $\bar{K}N$) and thus escape from observation [26]. Since these investigations are still in progress, here the assignment of model states to experimental states has again to be made on the basis of the masses alone. To distinguish between dominantly flavor octet and flavor singlet states, we additionally tabulated for each state of model $\mathcal{A}$ the corresponding spin-flavor $SU(6)$ contributions in table 2. This piece of information is useful for identifying those structures that have their direct counterparts in the nucleon spectrum.

Figure 2 shows that the agreement between the predictions of model $\mathcal{A}$ and the few presently known resonances of the $2\hbar\omega$ shell is of similar good quality as that of the corresponding nucleon states. Due to 't Hooft's force, we again observe in the sectors $J^\pi = \frac{1}{2}^+$, $\frac{3}{2}^+$ and $\frac{5}{2}^+$ a selective lowering of particular states with respect to the majority of states grouped between 2000 and 2200 MeV, which essentially remain unaffected by 't Hooft's interaction. The centroid of the bulk of unaffected states fairly agrees with the positions of the $\Lambda\frac{5}{2}^+(2110, ***)$ and the $\Lambda\frac{7}{2}^+(2020, *)$ observed so far in the upper energy range. With the couplings g_{nn} and g_{ns} fixed from the ground-state hyperfine pattern, four of the separated states are lowered even deeply enough to fit rather well into the conspicuous low-lying pattern formed by the four experimentally observed resonances $\Lambda\frac{1}{2}^+(1600, ***)$, $\Lambda\frac{1}{2}^+(1810, ***)$, $\Lambda\frac{3}{2}^+(1890, ****)$, and $\Lambda\frac{5}{2}^+(1820, ****)$. Their structure is very similar to that found in the nucleon spectrum (see fig. 1). Figure 4 demonstrates how in model $\mathcal{A}$ the instanton-induced 't Hooft interaction shapes this

Table 2. Configuration mixing of positive-parity Λ states in model $\mathcal{A}$ assigned to the $2\hbar\omega$ band. For each contribution to the Salpeter amplitude the corresponding Salpeter norm is given in %. In each row the upper line shows the positive- and the lower line the negative-energy contributions. Dominant contributions are bold printed and underlined.

J^π	Model state in model $\mathcal{A}$	pos. neg.	^{2}8[56] ^{2}8[56]	^{2}8[70] ^{2}8[70]	^{4}8[70] ^{4}8[70]	^{2}8[20] ^{2}8[20]	^{2}1[70] ^{2}1[70]	^{4}1[20] ^{4}1[20]
$\frac{1}{2}^+$	$[\Lambda\frac{1}{2}^+]_1(1108)$	98.6	**94.3**	3.9	0.0	0.0	0.3	0.0
	Λ ground state	1.4	0.4	0.6	0.3	0.0	0.0	0.0
$\frac{1}{2}^+$	$[\Lambda\frac{1}{2}^+]_2(1677)$	98.6	**88.4**	6.2	0.1	0.2	3.7	0.1
		1.4	0.3	0.6	0.4	0.0	0.1	0.0
	$[\Lambda\frac{1}{2}^+]_3(1747)$	98.9	5.1	2.1	0.0	0.1	**90.6**	0.9
		1.1	0.0	0.0	0.0	0.0	1.0	0.1
	$[\Lambda\frac{1}{2}^+]_4(1898)$	99.1	9.1	**84.2**	1.0	0.8	3.8	0.2
		0.9	0.2	0.3	0.3	0.1	0.1	0.0
	$[\Lambda\frac{1}{2}^+]_5(2077)$	99.0	0.5	1.2	**85.8**	11.2	0.1	0.3
		1.0	0.0	0.1	0.8	0.0	0.0	0.0
	$[\Lambda\frac{1}{2}^+]_6(2099)$	98.9	1.1	0.6	1.5	11.7	0.9	**83.0**
		1.1	0.0	0.1	0.1	0.0	0.8	0.1
	$[\Lambda\frac{1}{2}^+]_7(2132)$	98.9	2.2	1.6	11.2	**69.8**	0.6	13.5
		1.1	0.0	0.3	0.4	0.2	0.1	0.0
$\frac{3}{2}^+$	$[\Lambda\frac{3}{2}^+]_1(1823)$	98.5	**60.0**	28.2	0.3	0.1	9.9	0.1
		1.5	0.4	0.3	0.6	0.0	0.2	0.0
	$[\Lambda\frac{3}{2}^+]_2(1952)$	98.4	3.8	7.6	0.8	0.1	**84.0**	2.2
		1.6	0.0	0.0	0.1	0.0	1.4	0.1
	$[\Lambda\frac{3}{2}^+]_3(2045)$	99.2	0.5	0.2	**96.9**	1.1	0.3	0.2
		0.8	0.1	0.2	0.5	0.0	0.0	0.0
	$[\Lambda\frac{3}{2}^+]_4(2087)$	99.0	1.3	1.6	**84.0**	11.2	0.6	0.3
		1.0	0.0	0.4	0.6	0.0	0.0	0.0
	$[\Lambda\frac{3}{2}^+]_5(2133)$	99.1	25.2	**56.2**	7.2	9.1	1.2	0.2
		0.9	0.1	0.4	0.4	0.0	0.0	0.0
	$[\Lambda\frac{3}{2}^+]_6(2157)$	99.0	5.1	8.0	8.5	**70.8**	1.1	5.5
		1.0	0.0	0.3	0.4	0.1	0.0	0.1
	$[\Lambda\frac{3}{2}^+]_7(2176)$	99.0	0.3	0.4	0.7	5.8	4.2	**87.5**
		1.0	0.0	0.0	0.0	0.0	0.1	0.8
$\frac{5}{2}^+$	$[\Lambda\frac{5}{2}^+]_1(1834)$	98.5	**57.8**	28.3	0.2	0.1	12.1	0.0
		1.5	0.4	0.4	0.4	0.1	0.1	0.1
	$[\Lambda\frac{5}{2}^+]_2(1999)$	98.7	4.5	8.9	1.0	0.1	**84.1**	0.2
		1.3	0.1	0.1	0.1	0.0	0.6	0.5
	$[\Lambda\frac{5}{2}^+]_3(2078)$	99.0	9.0	9.9	**77.1**	0.0	2.0	0.9
		1.0	0.4	0.3	0.3	0.0	0.0	0.0
	$[\Lambda\frac{5}{2}^+]_4(2127)$	99.0	20.9	**45.9**	12.9	0.0	0.6	18.7
		1.0	0.1	0.2	0.1	0.3	0.1	0.1
	$[\Lambda\frac{5}{2}^+]_5(2150)$	99.0	4.6	7.6	7.8	0.0	0.7	**78.3**
		1.0	0.0	0.1	0.0	0.1	0.5	0.4
$\frac{7}{2}^+$	$[\Lambda\frac{7}{2}^+]_1(2130)$	99.2	0.0	0.0	**99.1**	0.0	0.0	0.1
		0.8	0.1	0.1	0.6	0.1	0.0	0.0

pattern along with the right position of the ground-state $\Lambda\frac{1}{2}^+(1116, ****)$.

The figure illustrates the influence of 't Hooft's force on the energy levels of all positive-parity Λ states, where the effects of non-strange (nn) and non-strange–strange (ns) diquark correlations are shown separately[2]. Starting from the case with confinement only ($g_{nn} = g_{ns} = 0$) which is shown in the leftmost spectrum of each column, first the non-strange coupling g_{nn} is gradually increased up to its value $g_{nn} = 136$ MeV fm^3 fixed from the $\Delta - N$-splitting while the non-strange–strange coupling still is kept at $g_{ns} = 0$ MeV fm^3. Then, the non-strange–strange

[2] The different behavior of the states under the influence of the two distinct (nn) and (ns) parts of 't Hooft's force then reflects the (scalar) diquark content of both flavor types within the states.

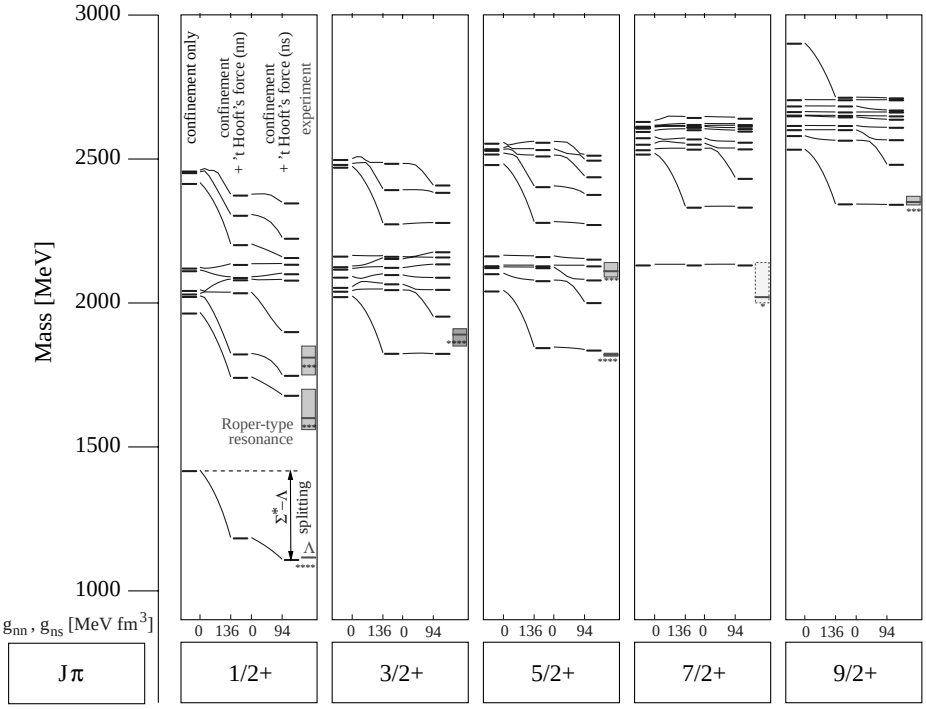

Fig. 4. Influence of the instanton-induced interaction on the energy levels of the positive-parity Λ states in model $\mathcal{A}$. The effects of non-strange (nn) and non-strange–strange (ns) diquark correlations are shown separately: In each column the leftmost spectrum shows the result with confinement only. The curves illustrate the variation of the spectrum with increasing 't Hooft couplings g_{nn} and g_{ns}, respectively. The middle spectrum shows first the result with 't Hooft's force acting only for non-strange quark pairs ($g_{nn} = 136$ MeV fm^3, $g_{ns} = 0$ MeV fm^3). Finally, the right spectrum shows the prediction with 't Hooft's force acting for both, non-strange and non-strange–strange quark pairs ($g_{nn} = 136$ MeV fm^3, $g_{ns} = 94$ MeV fm^3). For comparison the rightmost spectrum shows the experimental data with the corresponding uncertainties.

coupling g_{ns} is increased until the Λ ground state together with the other octet hyperons Σ and Ξ (here compare to ref. [5]) is correctly reproduced ($g_{nn} = 136$ MeV fm^3, $g_{ns} = 94$ MeV fm^3). The spectrum predicted finally in model $\mathcal{A}$ is shown on the right-hand side of each column in comparison to the experimental resonance positions. Indeed, it turns out that, once the couplings are fixed to reproduce the hyperfine pattern of ground states, the positions of the four comparatively low-lying states $\Lambda\frac{1}{2}^+(1600,***)$, $\Lambda\frac{1}{2}^+(1810,***)$, $\Lambda\frac{3}{2}^+(1890,****)$, and $\Lambda\frac{5}{2}^+(1820,****)$ are *simultaneously* well described. Apart from the distinct action of 't Hooft's force in the non-strange and non-strange–strange diquark channels, the systematics observed here is quite similar to that found for the corresponding $2\hbar\omega$ nucleon states. For a more detailed discussion let us investigate the situation for each spin sector from $\frac{1}{2}^+$ to $\frac{7}{2}^+$ in turn:

In the $\Lambda\frac{7}{2}^+$ sector with maximal possible spin $J_{\max}(N) = N + \frac{3}{2}$ in the $N = 2$ oscillator shell, our model predicts a single well-isolated state in the upper part of the shell, which coincides with the only resonance $\Lambda\frac{7}{2}^+(2020,*)$ "seen" in this mass range of the F_{07} partial wave. The mass predicted at 2130 MeV lies within the quite large range of possible values of this poorly determined one-star resonance. To achieve this maximal total spin, this state contains a symmetric spin-quartet wave function. Consequently, this state, *i.e.* its mass as well as its Salpeter amplitude remains totally unaffected by 't Hooft's force as confirmed in fig. 4. In fact, this state shows an almost pure ^{4}8[70] configuration ($> 97\%$, see table 2) and thus is the octet partner of the resonance $N\frac{7}{2}^+(1990,**)$ in the corresponding $N\frac{7}{2}^+$ sector of the nucleon spectrum.

In the $\Lambda\frac{5}{2}^+$ sector model $\mathcal{A}$ predicts altogether five states. As in the corresponding nucleon sector, the dominantly ^{2}8[56] state shows the largest downward mass shift of roughly 200 MeV relative to its position in the pure confinement spectrum. Note that this lowering originates mainly from an attractive correlation in the scalar *non-strange* (nn) diquark channel, whereas the contribution from the non-strange–strange (ns) diquark correlation is almost negligible. With the couplings g_{nn} and g_{ns} fixed from the ground-state hyperfine pattern the predicted mass of this lowest $\Lambda\frac{5}{2}^+$ excitation at 1834 MeV is in nice agreement with the lowest observed four-star resonance $\Lambda\frac{5}{2}^+(1820,****)$. The admixture of flavor singlet contributions amounts to only $\sim 12\%$. Hence, this low-lying, dominantly ^{2}8[56] state may be considered as the octet

counterpart of the $N\frac{5}{2}^+(1680,****)$. The second excited state is predicted at 1999 MeV. It exhibits a dominant ^{2}1[70] configuration ($\sim 85\%$) and 't Hooft's force induces a moderate downward mass shift of roughly 120 MeV, where now this lowering originates mainly due to an attractive non-strange–strange (ns) scalar diquark correlation. This dominantly flavor singlet state has no counterpart in the N^* spectrum and a corresponding resonance observed experimentally in this region is still "missing" although its position lies rather isolated between the $\Lambda\frac{5}{2}^+(1820,****)$ and the three remaining states predicted in this sector. The other three states are hardly influenced by 't Hooft's force and are all predicted to lie in the narrow range between $\sim$ 2080 and $\sim$ 2150 MeV around the three-star resonance $\Lambda\frac{5}{2}^+(2110,***)$.

In the $\Lambda\frac{3}{2}^+$ sector our model predicts seven $2\hbar\omega$ states. Here the situation is quite similar to the $\Lambda\frac{5}{2}^+$ sector. Again, the dominantly ^{2}8[56] state is lowered by an equally big downward shift of roughly 200 MeV. As in the $\Lambda\frac{5}{2}^+$ sector, this state apparently has no scalar non-strange–strange (ns) diquark contributions and the whole mass shift turns out to be due to an attractive non-strange (nn) diquark correlation alone. With the 't Hooft couplings fixed on the ground-state spectrum, the lowest-excited state is then predicted at 1823 MeV and thus can be uniquely identified with the well-established low-lying resonance $\Lambda\frac{3}{2}^+(1890,****)$ observed experimentally in the P_{03} partial wave. Once again, the flavor singlet admixtures of roughly 10% are moderate, and thus the $\Lambda\frac{3}{2}^+(1890,****)$ is the octet partner of the $N\frac{3}{2}^+(1720,****)$. Unfortunately, apart from the low-lying $\Lambda\frac{3}{2}^+(1890,****)$, no further resonance has been seen in the P_{03} partial wave so far. Similar to the $\Lambda\frac{5}{2}^+$ sector, the second state predicted at 1952 MeV again reveals a dominantly flavor singlet ^{2}1[70] configuration ($\sim 85\%$). Compared to the dominantly ^{2}8[56] state, it exhibits again a rather moderate downward mass shift of roughly 130 MeV due to a dominantly non-strange–strange (ns) scalar diquark correlation. Hence this state, which has no counterpart in the nucleon spectrum, comes to lie fairly in between the lowest excitation and the five remaining states in this sector, whose positions are virtually not affected by 't Hooft's force and are predicted to lie in the range between $\sim$ 2045 and $\sim$ 2180 MeV.

Finally, let us focus on the $\Lambda\frac{1}{2}^+$ sector with the scalar/isoscalar excitations of the Λ ground state. Here we expect six excited $2\hbar\omega$ states. Again, the lowest state predicted at 1677 MeV turns out to be dominantly ^{2}8[56] ($\sim$ 89%). Due to 't Hooft's force this state is strongly lowered by almost the same amount (roughly 300 MeV) as the ground state. In fact, this downward mass shift is even large enough to account for the striking low position of $\Lambda\frac{1}{2}^+(1600,***)$. This state behaves quite similar to the corresponding lowest state in the nucleon sector which is assigned to the Roper resonance $N\frac{1}{2}^+(1440,****)$ and hence it may readily be associated with the octet partner of the Roper resonance. In the nucleon sector we found [5] the Roper state in model $\mathcal{A}$ showing a very similar behavior under the influence of 't Hooft's instanton-induced interaction like the ground state. Here we make a similar observation: Both, the Λ ground state and the Roper-type state, show almost the same contributions of non-strange and non-strange–strange scalar diquarks. Consequently, in both cases, the equally large energy shift originates mainly from the non-strange and partly from the non-strange–strange diquark correlations (here compare to the discussion of the ground-state spectrum in ref. [5]). It is interesting to note that exactly the same behavior is also observed for the second radially excited state predicted at 1747 MeV, which lies at the lower end of the uncertainty range quoted for the resonance $\Lambda\frac{1}{2}^+(1810,***)$. As the Roper-type state, this resonance likewise reveals almost the same strong downward mass shift of about 300 MeV. Hence, the calculated mass splitting of about 70 MeV between the first two radial excitations in $\Lambda\frac{1}{2}^+$ is primarily a relativistic spin-orbit effect of the confinement force. Unlike the nucleon $N\frac{1}{2}^+$ sector, this second excitation predicted is *not* the dominantly flavor octet ^{2}8[70] state, but a dominantly flavor singlet ^{2}1[70] state ($\sim 92\%$). The dominantly flavor octet ^{2}8[70] state, however, appears here as the third radial excitation predicted at 1898 MeV. Consequently, we would identify the $\Lambda\frac{1}{2}^+(1810,***)$ as being a dominantly flavor singlet state, hence *not* being the octet counterpart of the $N\frac{1}{2}^+(1710,***)$ in the corresponding $N\frac{1}{2}^+$ sector. However, our assignment is less clear, since the reported central value of 1810 MeV of the second observed excitation lies fairly in between our two model predictions at 1747 and 1898 MeV. Perhaps the $\Lambda\frac{1}{2}^+(1810,***)$ might be resolved into two separate states by future experiments.

2.2.3 States of the negative-parity $1\hbar\omega$ band

We now turn to the discussion of negative-parity Λ states in the $1\hbar\omega$ shell. As usual in constituent quark models for baryons, our models predict altogether seven states with spins $J^\pi = \frac{1}{2}^-$, $\frac{3}{2}^-$ and $\frac{5}{2}^-$ in this shell. In the baryon summary table of the Particle Data Group [24] six well-established four- and three-star resonances with these spins below 2 GeV are listed. In model $\mathcal{A}$ the assignment to these observed resonances due to a comparison of predicted and measured masses is unambiguous and a clear identification of the states is thus readily possible. Only one resonance of the $1\hbar\omega$ shell has not been observed hitherto: the third radial excitation in the $\Lambda\frac{3}{2}^-$ is still missing.

Table 3 gives the predicted masses of both models in comparison to the six corresponding experimental resonance positions. In addition, table 4 shows the contributions of the different spin-flavor $SU(6)$ configurations to each state of model $\mathcal{A}$. Again let us focus in this discussion on the (better) results of model $\mathcal{A}$. As shown in fig. 2 the masses predicted in model $\mathcal{A}$ can considerably well account for all resonance positions quoted by the Particle Data Group, however, as already mentioned, with

Table 3. Calculated positions of all Λ states assigned to the negative-parity $1\hbar\omega$ shell in comparison to the corresponding experimental mass values taken from [24]. Notation as in table 1.

Experimental state [24]	PW	J^π	Rating	Mass range [MeV] [24]	Model state in model $\mathcal{A}$	Model state in model $\mathcal{B}$
$\Lambda(1405)$	S_{01}	$\frac{1}{2}^-$	****	1402–1411	$[\Lambda\frac{1}{2}^-]_1(1524)$	
$\Lambda(1670)$	S_{01}	$\frac{1}{2}^-$	****	1660–1680	$[\Lambda\frac{1}{2}^-]_2(1630)$	$[\Lambda\frac{1}{2}^-]_1(1625)$
$\Lambda(1800)$	S_{01}	$\frac{1}{2}^-$	***	1720–1850	$[\Lambda\frac{1}{2}^-]_3(1816)$	$[\Lambda\frac{1}{2}^-]_2(1732)$
						$[\Lambda\frac{1}{2}^-]_3(1973)$
$\Lambda(1520)$	D_{03}	$\frac{3}{2}^-$	****	1518–1522	$[\Lambda\frac{3}{2}^-]_1(1508)$	$[\Lambda\frac{3}{2}^-]_1(1555)$
$\Lambda(1690)$	D_{03}	$\frac{3}{2}^-$	****	1685–1695	$[\Lambda\frac{3}{2}^-]_2(1662)$	$[\Lambda\frac{3}{2}^-]_2(1701)$
					$[\Lambda\frac{3}{2}^-]_3(1775)$	$[\Lambda\frac{3}{2}^-]_3(1832)$
$\Lambda(1830)$	D_{05}	$\frac{5}{2}^-$	****	1810–1830	$[\Lambda\frac{5}{2}^-]_1(1828)$	$[\Lambda\frac{5}{2}^-]_1(1827)$

Table 4. Configuration mixing of negative-parity Λ states in model $\mathcal{A}$ assigned to the $1\hbar\omega$ band. For each contribution to the Salpeter amplitude the corresponding Salpeter norm is given in %. In each row the upper line shows the positive- and the lower line the negative-energy contributions. Dominant contributions are bold printed and underlined.

J^π	Model state in model $\mathcal{A}$	pos. neg.	^{2}8[56] ^{2}8[56]	^{2}8[70] ^{2}8[70]	^{4}8[70] ^{4}8[70]	^{2}8[20] ^{2}8[20]	^{2}1[70] ^{2}1[70]	^{4}1[20] ^{4}1[20]
$\frac{1}{2}^-$	$[\Lambda\frac{1}{2}^-]_1(1524)$	98.8	2.9	26.0	0.3	0.0	**69.4**	0.2
		1.2	0.3	0.1	0.0	0.1	0.3	0.5
	$[\Lambda\frac{1}{2}^-]_2(1630)$	98.7	5.5	**61.6**	2.1	0.3	29.2	0.1
		1.3	0.6	0.2	0.0	0.2	0.1	0.2
	$[\Lambda\frac{1}{2}^-]_3(1816)$	99.4	0.2	3.1	**94.9**	0.6	0.1	0.6
		0.6	0.0	0.0	0.5	0.1	0.0	0.0
$\frac{3}{2}^-$	$[\Lambda\frac{3}{2}^-]_1(1508)$	98.6	2.0	18.7	0.1	0.0	**77.7**	0.1
		1.4	0.1	0.1	0.1	0.0	0.9	0.3
	$[\Lambda\frac{3}{2}^-]_2(1662)$	98.9	4.4	**72.0**	2.2	0.2	20.1	0.0
		1.1	0.1	0.2	0.3	0.1	0.2	0.0
	$[\Lambda\frac{3}{2}^-]_3(1775)$	99.3	0.8	1.5	**96.1**	0.0	0.4	0.4
		0.7	0.1	0.2	0.3	0.1	0.0	0.0
$\frac{5}{2}^-$	$[\Lambda\frac{5}{2}^-]_1(1828)$	99.4	0.0	0.0	**99.0**	0.0	0.0	0.4
		0.6	0.0	0.1	0.4	0.1	0.0	0.0

one striking exception: The notorious difficulty in explaining the low position of the $\Lambda\frac{1}{2}^-(1405, ****)$ with respect to $\Lambda\frac{3}{2}^-(1520, ****)$ cannot be resolved by using instanton-induced forces also within our fully relativistic framework based on the Salpeter equation. Otherwise, the hyperfine structure of the other $1\hbar\omega$ Λ states can be nicely explained by 't Hooft's residual force. Figure 5 shows how 't Hooft's residual interaction shapes this hyperfine structure of the negative-parity $1\hbar\omega$ shell due to the correlation of non-strange and non-strange–strange diquarks within these states.

Analogous to fig. 4, which shows instanton-induced effects for the positive-parity Λ states, fig. 5 likewise shows the influence of 't Hooft's force on the energy levels of all negative-parity Λ states. As before, we start with the pure confinement spectrum and in succession the couplings g_{nn} and g_{ns} are gradually increased. Once again we observe the remarkable feature of the instanton-induced interaction that, once the 't Hooft couplings are fixed to account for the octet-decuplet ground-state splittings, the excited states, in this case the well-established resonances $\Lambda\frac{1}{2}^-(1800, ***)$, $\Lambda\frac{5}{2}^-(1830, ****)$, $\Lambda\frac{1}{2}^-(1670, ****)$, $\Lambda\frac{3}{2}^-(1690, ****)$, and $\Lambda\frac{3}{2}^-(1520, ****)$ of the $1\hbar\omega$ shell, are *at the same time* excellently described. Again, let us discuss the situation for each spin sector $\frac{1}{2}^-$, $\frac{3}{2}^-$, and $\frac{5}{2}^-$ in turn:

In the $\Lambda\frac{5}{2}^-$ sector our model predicts a single $1\hbar\omega$ state at 1828 MeV. Its mass exactly agrees with the resonance position of the single four-star resonance $\Lambda\frac{5}{2}^-(1830, ****)$ observed in the D_{05} partial wave. Note that $J = \frac{5}{2}$ is the highest possible spin in the $1\hbar\omega$ shell and thus requires an internal spin-quartet function for this state. Table 4 shows the $\Lambda\frac{5}{2}^-$ resonance being a pure flavor octet ^{4}8[70] state, which is by no means influenced by 't Hooft's force as

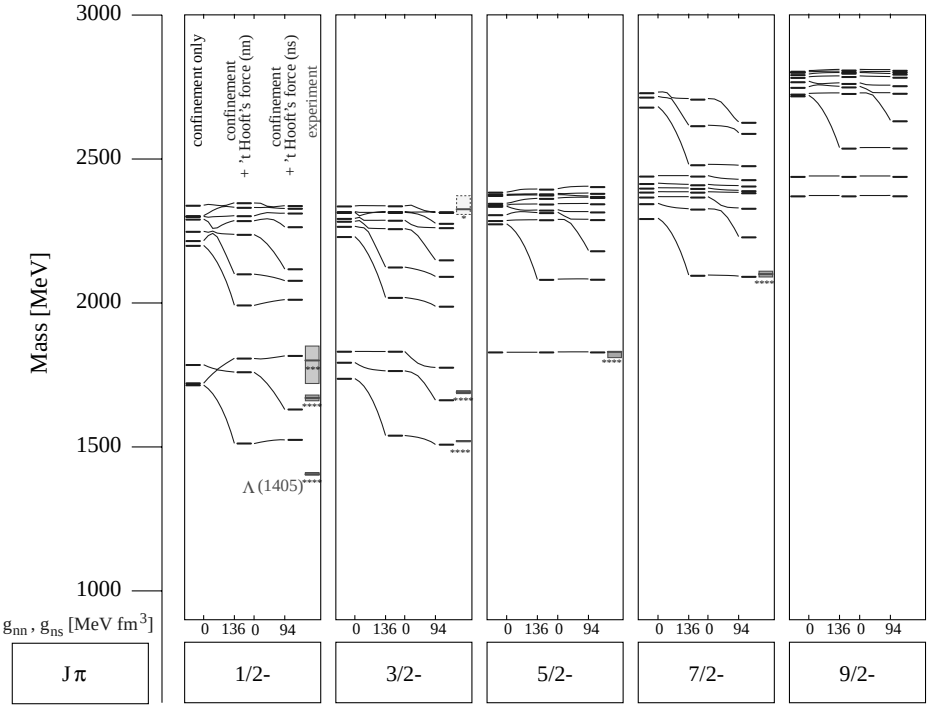

Fig. 5. Influence of the instanton-induced interaction on the energy levels of the negative-parity Λ states in model $\mathcal{A}$. The effects of non-strange (nn) and non-strange–strange (ns) diquark correlations are shown separately. See also caption of fig. 4 and text for further explanations.

illustrated in fig. 5. Similar to its counterpart $N\frac{5}{2}^-(1675,****)$ in the nucleon spectrum, this state is thus determined by the confinement force alone. This selection rule of 't Hooft's force once again nicely conforms with the experimental findings, since already in the pure confinement spectrum the $\Lambda\frac{5}{2}^-(1830,****)$ is well described. The excellent agreement of our prediction with the resonance position of $\Lambda\frac{5}{2}^-(1830,****)$ thus provides good support for the flavor-independent confinement force, whose parameters have been fixed on the phenomenology of the (non-strange) Δ spectrum alone: concerning the positioning of the shells the confinement force works obviously equally well in this strange ($S^*=-1$) sector.

In the $\Lambda\frac{3}{2}^-$ sector the hyperfine splitting between the first resonance $\Lambda\frac{3}{2}^-(1520,****)$ and the second resonance $\Lambda\frac{3}{2}^-(1690,****)$ can be fairly well reproduced by 't Hooft's force: The first excitation is predicted at 1508 MeV and the second one at 1662 MeV, thus both states are predicted close to the resonance positions quoted by the Particle Data Group [24]. Indeed, the first state associated with the $\Lambda\frac{3}{2}^-(1520,****)$ turns out to be dominantly ^{2}1[70] ($\sim 79\%$) with an additional moderate admixture of a flavor octet ^{2}8[70] contribution ($\sim 19\%$). This dominantly flavor singlet state, which has no counterpart in the N^* spectrum, shows the largest downward mass shift of almost the same amount as the Roper-type state and the Λ ground state in the positive-parity sector. The biggest part of this shift originates from the attractive non-strange and only a small fraction comes from the non-strange–strange diquark correlation. The second state predicted reveals a dominant ^{2}8[70] configuration ($\sim 72\%$) with an additional moderate contribution of a flavor singlet ^{2}1[70] configuration ($\sim 20\%$). Hence, the associated resonance $\Lambda\frac{3}{2}^-(1690,****)$ indeed may be viewed as the octet partner of $N\frac{3}{2}^-(1520,****)$. Compared to the lowest state predicted, here the lowering by 't Hooft's force is rather moderate and is primarily due to an attractive non-strange–strange diquark correlation. The third $\Lambda\frac{3}{2}^-$ state, which so far has not been observed experimentally, is predicted at 1816 MeV nearly degenerate to the single state in $\Lambda\frac{5}{2}^-$. This state turns out to be an almost pure ^{4}8[56] state ($\sim 97\%$) and hence is the expected flavor octet partner of the nucleon resonance $N\frac{3}{2}^-(1700,***)$.

Finally, we turn to the $\Lambda\frac{1}{2}^-$ sector, where the situation is quite similar to the $\Lambda\frac{3}{2}^-$ sector. The lowest state predicted at 1524 MeV again turns out to be a dominantly ($\sim 70\%$) flavor singlet ^{2}1[70] state with a rather strong ($\sim 27\%$) contribution of a flavor octet ^{2}8[70] configuration. As in the $\Lambda\frac{3}{2}^-$ sector, this state exhibits the strongest lowering due to 't Hooft's force, but unfortunately *not* deeply enough to account for the puzzling low position of the well-established four-star resonance $\Lambda\frac{1}{2}^-(1405,****)$ below the $\Lambda\frac{3}{2}^-(1520,****)$. Actually, the behavior of this state under the influence of 't Hooft's force is rather

similar to the lowest state in the $\Lambda\frac{3}{2}^-$ sector. Both states show an equally big lowering which primarily originates from a scalar non-strange diquark correlation, thus both becoming degenerate close to the position of the $\Lambda\frac{3}{2}^-(1520,****)$. Nonetheless, there is no doubt to associate the lowest predicted state to the $\Lambda\frac{1}{2}^-(1405,****)$, since 't Hooft's force otherwise provides a quite good explanation of the remaining states in this sector. The second state is predicted at 1630 MeV and may readily be associated with the $\Lambda\frac{1}{2}^-(1670,****)$. This state exhibits a dominantly flavor octet ^{2}8[70] configuration ($\sim$ 62%) with an admixed ^{2}1[70] contribution ($\sim$ 29%) and it is moderately lowered by 't Hooft's interaction mainly due to a scalar non-strange–strange correlation. The third state predicted at 1816 MeV nicely agrees with the $\Lambda\frac{1}{2}^-(1800,***)$ and turns out to be an almost pure flavor octet ^{4}8[70] state. Hence, $\Lambda\frac{1}{2}^-(1670,****)$ and $\Lambda\frac{1}{2}^-(1800,***)$ indeed may be viewed as the octet partners of $N\frac{1}{2}^-(1535,****)$ and $N\frac{1}{2}^-(1650,****)$ in the corresponding $N\frac{1}{2}^-$ sector. Note that similar to the $N\frac{1}{2}^-$ sector the second state reveals an *upwards* mass shift due to the repulsive part in the relativistic version of 't Hooft's force acting in the *pseudo-scalar* diquark sector. This upwards mass shift in fact is necessary here to match the $\Lambda\frac{1}{2}^-(1800,***)$ and finally to correctly reproduce the hyperfine splitting between $\Lambda\frac{1}{2}^-(1670,****)$ and $\Lambda\frac{1}{2}^-(1800,***)$.

Altogether we thus find a rather good explanation for the hyperfine structure of the negative-parity Λ states in the $1\hbar\omega$ shell due to instanton effects. The only striking exception is the $\Lambda\frac{1}{2}^-(1405,****)$: although 't Hooft's force provides an explanation of the relatively low energy of the dominantly flavor singlet states below the dominantly flavor octet states, the instanton-induced interaction[3], even if treated fully relativistically, cannot explain the exceptionally large splitting between the "spin-orbit partners" $\Lambda\frac{1}{2}^-(1405,****)$ and $\Lambda\frac{3}{2}^-(1520,****)$. Both states are roughly degenerate with a mass close to the $\Lambda\frac{3}{2}^-(1520,****)$. This shortcoming is observed in *all* other constituent quark models for baryons as well and remains one of the outstanding problems. It is worthwhile to comment here on this somewhat puzzling state. In view of the otherwise very consistent description of hyperfine structures in the $1\hbar\omega$ and $2\hbar\omega$ bands, we believe that the too high predicted mass does not really reflect a fundamental flaw in our model but rather the fact that other dynamical effects that are specific to that state are presently not taken into account in our model. There is still controversy about the physical nature of the $\Lambda\frac{1}{2}^-(1405,****)$ and its role in the $\bar{K}N$ interaction at low energies. A review of this discussion is given by Dalitz [25] in the latest edition of the *Review of Particle Physics*. The mass splitting of $\Lambda\frac{1}{2}^-(1405)$ and $\Lambda\frac{3}{2}^-(1520)$ is often interpreted as a possible hint for the relevance of spin-orbit forces in baryon spectroscopy. In our opinion such an interpretation is rather questionable. The splitting between these states is exceptionally large and otherwise the light-baryon spectra show hardly any evidence for strong spin-orbit effects. This was just the reason why we have chosen those confinement Dirac structures which induce only moderate spin-orbit effects. Larger spin-orbit interactions would generally spoil the agreement for the spectrum in other sectors. Another extreme possibility discussed in the literature is that the $\Lambda\frac{1}{2}^-(1405)$, which is lying about 30 MeV below the $N\bar{K}$ threshold, might be an unstable $N\bar{K}$ bound state. But, such an interpretation requires the observation of another state lying close to the $\Lambda\frac{3}{2}^-(1520)$ MeV which then completes the $\Lambda\frac{1}{2}^-$ three-quark states of the $1\hbar\omega$ shell. However, this energy region is already well explored by $N\bar{K}$ scattering experiments with no sign of such a resonance [25]. The most appropriate dynamical explanation for the low position $\Lambda\frac{1}{2}^-(1405)$ seems to be a strong coupling of the bare three-quark state to virtual meson-baryon ($\bar{K}N$) decay channels due to its proximity to $\bar{K}N$ threshold. A confirmation of this conjecture on the basis of our covariant model requires the calculation of the $\bar{K}N$ decay amplitude of the model state $[\Lambda\frac{1}{2}^-]_1(1524)$, which then should be exceptionally large. But a really quantitative statement would require a fully dynamical treatment of various external meson-baryon decay channels in general. Such investigations have been made in non-relativistic quark models [27], showing indeed a natural shift of the lowest $\Lambda\frac{1}{2}^-$three-quark state towards the $\bar{K}N$ threshold. An incorporation of these effects in our fully relativistic Bethe-Salpeter framework, however, seems presently to be technically too much involved.

[3] We should add a remark here concerning the genuine three-body force of the instanton-induced interaction: In the literature one sometimes finds the statement that this force, which only acts in the *uds* singlet states, should additionally affect the $\Lambda\frac{1}{2}^-(1405)$. However, as discussed in ref. [5], this statement is not correct: The three-body force can be shown to act only on flavor-antisymmetric, spatial-symmetric three-quark states. There are, however, *no physical* three-quark states (baryons) with this property, since these are color-antisymmetric and finally the Pauli principle can only be satisfied by spin-antisymmetric three-quark wave functions, which do not exist. Hence this three-body force does not contribute to physical color singlet, but only to color octet or decuplet three-quark states.

2.2.4 Beyond the $2\hbar\omega$ band

The high energy part of the positive- and negative-parity Λ spectrum beyond the mass region of the $2\hbar\omega$ and $1\hbar\omega$ shell is experimentally hardly explored. Here the Particle Data Group states only three further resonances with established quantum numbers. In the negative-parity sector these are the well-established four-star resonance $\Lambda\frac{7}{2}^-(2100,****)$ and the one-star resonance $\Lambda\frac{3}{2}^-(2325,*)$ for which evidence, however, is very poor. According to its spin $J^\pi = \frac{7}{2}^-$ the $\Lambda\frac{7}{2}^-(2100,****)$ has to be assigned to the $3\hbar\omega$ band, but its position is comparatively

Table 5. Calculated positions of the lightest few Λ states assigned to the negative-parity $3\hbar\omega$ shell. Notation as in table 1.

State		J^π	Rating	Experiment [MeV] [24]	Mass [MeV] in model $\mathcal{A}$	Mass [MeV] in model $\mathcal{B}$
	S_{01}	$\frac{1}{2}^-$			$[\Lambda\frac{1}{2}^-]_4(2011)$	$[\Lambda\frac{1}{2}^-]_4(2173)$
					$[\Lambda\frac{1}{2}^-]_5(2076)$	$[\Lambda\frac{1}{2}^-]_5(2249)$
					$[\Lambda\frac{1}{2}^-]_6(2117)$	$[\Lambda\frac{1}{2}^-]_6(2308)$
					$[\Lambda\frac{1}{2}^-]_7(2263)$	$[\Lambda\frac{1}{2}^-]_7(2399)$
					$[\Lambda\frac{1}{2}^-]_8(2310)$	$[\Lambda\frac{1}{2}^-]_8(2406)$
					$[\Lambda\frac{3}{2}^-]_4(1987)$	$[\Lambda\frac{3}{2}^-]_4(2152)$
					$[\Lambda\frac{3}{2}^-]_5(2090)$	$[\Lambda\frac{3}{2}^-]_5(2212)$
					$[\Lambda\frac{3}{2}^-]_6(2147)$	$[\Lambda\frac{3}{2}^-]_6(2316)$
					$[\Lambda\frac{3}{2}^-]_7(2259)$	$[\Lambda\frac{3}{2}^-]_7(2366)$
					$[\Lambda\frac{3}{2}^-]_8(2275)$	$[\Lambda\frac{3}{2}^-]_8(2384)$
$\Lambda(2325)$	D_{03}	$\frac{3}{2}^-$	*	2307–2372	$[\Lambda\frac{3}{2}^-]_9(2313)$	$[\Lambda\frac{3}{2}^-]_9(2400)$
					$[\Lambda\frac{3}{2}^-]_{10}(2314)$	$[\Lambda\frac{3}{2}^-]_{10}(2422)$
	D_{05}	$\frac{5}{2}^-$			$[\Lambda\frac{5}{2}^-]_2(2080)$	$[\Lambda\frac{5}{2}^-]_2(2207)$
					$[\Lambda\frac{5}{2}^-]_3(2179)$	$[\Lambda\frac{5}{2}^-]_3(2297)$
					$[\Lambda\frac{5}{2}^-]_4(2287)$	$[\Lambda\frac{5}{2}^-]_4(2375)$
					$[\Lambda\frac{5}{2}^-]_5(2314)$	$[\Lambda\frac{5}{2}^-]_5(2417)$
$\Lambda(2100)$	G_{07}	$\frac{7}{2}^-$	****	2090–2110	$[\Lambda\frac{7}{2}^-]_1(2090)$	$[\Lambda\frac{7}{2}^-]_1(2185)$
					$[\Lambda\frac{7}{2}^-]_2(2227)$	$[\Lambda\frac{7}{2}^-]_2(2286)$
					$[\Lambda\frac{7}{2}^-]_3(2327)$	$[\Lambda\frac{7}{2}^-]_3(2405)$
					$[\Lambda\frac{7}{2}^-]_4(2380)$	$[\Lambda\frac{7}{2}^-]_4(2429)$
	G_{09}	$\frac{9}{2}^-$			$[\Lambda\frac{9}{2}^-]_1(2370)$	$[\Lambda\frac{9}{2}^-]_1(2400)$
					$[\Lambda\frac{9}{2}^-]_2(2437)$	$[\Lambda\frac{9}{2}^-]_2(2450)$

low and nearly degenerate with the first $\Lambda\frac{7}{2}^+$-resonance $\Lambda\frac{7}{2}^+(2020,*)$ in the upper part of the positive-parity $2\hbar\omega$ shell. In the positive-parity sector the well-established three-star resonance $\Lambda\frac{9}{2}^+(2350,***)$ is seen experimentally in the H_{09} partial wave and due to its spin and position this state is assigned to the $4\hbar\omega$ band. Apart from a bump $\Lambda?^?(2585,**)$ with undefined spin and parity, no resonances have been observed so far which could be assigned to the higher $5\hbar\omega$ and $6\hbar\omega$ shells. Our predictions of model $\mathcal{A}$ and $\mathcal{B}$ for the lightest few states in the $3\hbar\omega$ and $4\hbar\omega$ bands are summarized in tables 5 and 6, respectively. Again let us restrict our detailed discussion to model $\mathcal{A}$. As can be seen in fig. 2 and tables 5 and 6, model $\mathcal{A}$ predicts the first excitations in the $\Lambda\frac{7}{2}^-$ and $\Lambda\frac{9}{2}^+$ sectors in excellent agreement with the measured positions of the well-established resonances observed in these sectors. The predicted masses for the first-excited state in $\Lambda\frac{7}{2}^-$ at 2090 MeV and for the first excitation in $\Lambda\frac{9}{2}^+$ at 2340 MeV are in both cases very close to the reported resonance positions of $\Lambda\frac{7}{2}^-(2100,****)$ and $\Lambda\frac{9}{2}^+(2350,***)$, respectively. According to fig. 1, we would expect that the $\Lambda\frac{9}{2}^+(2350,***)$ is the octet partner of $N\frac{9}{2}^+(2220,****)$. In fact, the model state associated to the $\Lambda\frac{9}{2}^+(2350,***)$ turns out to be dominantly flavor octet ($\sim$ 45% ^{2}8[56] and $\sim$ 32% ^{2}8[70]) with an additional moderate admixture ($\sim$ 22%) of a flavor singlet ^{2}1[70] configuration. The model state associated to the $\Lambda\frac{7}{2}^-(2100,****)$ shows almost equally big flavor octet ($\sim$ 16% ^{2}8[56] and $\sim$ 31% ^{2}8[70]) and flavor singlet ($\sim$ 51% ^{2}1[70]) contributions. Unfortunately, the lack of data allows no detailed investigation of the instanton-induced hyperfine structures in $3\hbar\omega$ and $4\hbar\omega$ shells in comparison with experiment as was possible in the lower-lying $1\hbar\omega$ and $2\hbar\omega$ shells. Nevertheless, the remarkably good predictions of the two single resonances $\Lambda\frac{7}{2}^-(2100,****)$ and $\Lambda\frac{9}{2}^+(2350,***)$ already clearly demonstrate the importance of instanton-induced effects also in this higher mass region of the Λ spectrum, since 't Hooft's force nicely explains the comparatively low positions of these states. This is convincingly illustrated in figs. 4 and 5. 't Hooft's interaction shifts both associated model states relatively strongly downward by roughly 200 MeV with respect to the other states and hence these become well isolated. As can be seen in figs. 4 and 5, this mass shift originates for both states merely from an attractive non-strange scalar diquark correlation, while the non-strange–strange diquark contributions is negligible. Once again we observe the remarkable feature that the shift of the states is exactly the right size to match the experimentally measured positions just when the 't Hooft couplings g_{nn} and g_{ns} are fixed to reproduce the ground-state hyperfine splittings. Otherwise, 't Hooft's force causes in the $3\hbar\omega$ and $4\hbar\omega$ shells in general quite similar effects as in the lower-lying $1\hbar\omega$ and $2\hbar\omega$ shells as can be seen in figs. 4 and 5. Therefore it is worthwhile to comment at this stage

Table 6. Calculated positions of the lightest few Λ states assigned to the positive-parity $4\hbar\omega$ shell. Notation as in table 1.

Experimental state [24]	PW	J^π	Rating	Mass range [MeV] [24]	Model state in model $\mathcal{A}$	Model state in model $\mathcal{B}$
	P_{01}	$\frac{1}{2}^+$			$[\Lambda\frac{1}{2}^+]_8(2156)$	$[\Lambda\frac{1}{2}^+]_8(2374)$
					$[\Lambda\frac{1}{2}^+]_9(2223)$	$[\Lambda\frac{1}{2}^+]_9(2452)$
					$[\Lambda\frac{1}{2}^+]_{10}(2345)$	$[\Lambda\frac{1}{2}^+]_{10}(2516)$
	P_{03}	$\frac{3}{2}^+$			$[\Lambda\frac{3}{2}^+]_8(2278)$	$[\Lambda\frac{3}{2}^+]_8(2430)$
					$[\Lambda\frac{3}{2}^+]_9(2382)$	$[\Lambda\frac{3}{2}^+]_9(2509)$
					$[\Lambda\frac{3}{2}^+]_{10}(2408)$	$[\Lambda\frac{3}{2}^+]_{10}(2558)$
	F_{05}	$\frac{5}{2}^+$			$[\Lambda\frac{5}{2}^+]_6(2270)$	$[\Lambda\frac{5}{2}^+]_6(2407)$
					$[\Lambda\frac{5}{2}^+]_7(2375)$	$[\Lambda\frac{5}{2}^+]_7(2469)$
					$[\Lambda\frac{5}{2}^+]_8(2436)$	$[\Lambda\frac{5}{2}^+]_8(2556)$
					$[\Lambda\frac{5}{2}^+]_9(2494)$	$[\Lambda\frac{5}{2}^+]_9(2595)$
	F_{07}	$\frac{7}{2}^+$			$[\Lambda\frac{7}{2}^+]_2(2331)$	$[\Lambda\frac{7}{2}^+]_2(2449)$
					$[\Lambda\frac{7}{2}^+]_3(2431)$	$[\Lambda\frac{7}{2}^+]_3(2539)$
					$[\Lambda\frac{7}{2}^+]_4(2533)$	$[\Lambda\frac{7}{2}^+]_4(2611)$
					$[\Lambda\frac{7}{2}^+]_5(2556)$	$[\Lambda\frac{7}{2}^+]_5(2632)$
$\Lambda(2350)$	H_{09}	$\frac{9}{2}^+$	***	2340–2370	$[\Lambda\frac{9}{2}^+]_1(2340)$	$[\Lambda\frac{9}{2}^+]_1(2433)$
					$[\Lambda\frac{9}{2}^+]_2(2479)$	$[\Lambda\frac{9}{2}^+]_2(2536)$
					$[\Lambda\frac{9}{2}^+]_3(2565)$	$[\Lambda\frac{9}{2}^+]_3(2637)$
					$[\Lambda\frac{9}{2}^+]_4(2608)$	$[\Lambda\frac{9}{2}^+]_4(2649)$
	$H_{0\,11}$	$\frac{11}{2}^+$			$[\Lambda\frac{11}{2}^+]_1(2601)$	$[\Lambda\frac{11}{2}^+]_1(2632)$
					$[\Lambda\frac{11}{2}^+]_2(2677)$	$[\Lambda\frac{11}{2}^+]_2(2689)$

on the instanton-induced hyperfine structures of the shells in general.

2.2.5 Instanton-induced hyperfine structures and approximate parity doublets

In the foregoing discussion we convincingly demonstrated that 't Hooft's force with its couplings g_{nn} and g_{ns} fixed from the ground-state baryons excellently explains the most prominent features in the single even- and odd-parity bands of the experimental Λ spectrum. Here let us summarize how 't Hooft's force globally reorganizes the pure confinement Λ spectrum. The systematics is essentially the same as already exposed in the detailed discussion of the nucleon spectrum in ref. [5]. Without residual instanton force the three-body confinement arranges the Λ spectrum into alternating even- and odd-parity bands, where in each band the states are clustered in rather narrow energy ranges. Due to the strong selection rules of 't Hooft's force a particular set of states in each $N\hbar\omega$ shell, namely those states which are dominantly ^{2}8[56], ^{2}8[70] or ^{2}1[70], are selectively lowered relative to the bulk of dominantly ^{4}8[70], ^{2}8[20], and ^{4}1[70] states, which essentially remain unaffected. In particular, the states of the shell with maximally possible total spin $J_{\max}(N) = N + \frac{3}{2}$ which possess an internal spin-quartet ($S = 3/2$) function in order to achieve this maximal total spin, remain unshifted. Thus each $N\hbar\omega$ shell systematically splits into an upper part with total spins up to $J_{\max}(N)$ and a lower part with total spins up to $J_{\max}(N)-1$. With the couplings fixed from the ground states the lower part comes to lie fairly in between the upper parts of the two adjacent $N\hbar\omega$ and $(N-2)\hbar\omega$ shells with the same parity and thus nearly degenerate with the unshifted part of the $(N-1)\hbar\omega$ shell with opposite parity. Concerning the lower part of the shells, the main difference to the nucleon spectrum is firstly that in general more states are shifted downwards due to the additional flavor singlet ^{2}1[70] configuration, and secondly that both types of diquarks, non-strange and non-strange–strange, emerge. In the Λ spectrum we thus observe in figs. 4 and 5 the lowered part of the shells actually separating into two further parts. The excited states with dominant non-strange diquark contribution are generally more strongly lowered than those with dominant non-strange–strange diquark contribution. This level ordering is qualitatively understandable in the following manner. Firstly, the scalar non-strange diquark correlation is stronger than the non-strange–strange correlation due to $g_{nn} > g_{ns}$. Apart from that, the second, still more important effect is due to the different kinematics of the two distinct diquark plus quark systems. In a strongly simplified, nonrelativistic picture with harmonic three-body confinement forces (ρ- plus λ-oscillator) one can approximately consider these states as two-particle bound states of a scalar diquark with mass M_D and a quark with mass m_q, *i.e.* as non-strange diquark plus strange quark (M_{nn}, m_s) or as non-strange–strange diquark plus non-strange quark (M_{ns}, m_n). Diquark and quark move in a two-body confining potential which then is given by the λ-oscillator alone.

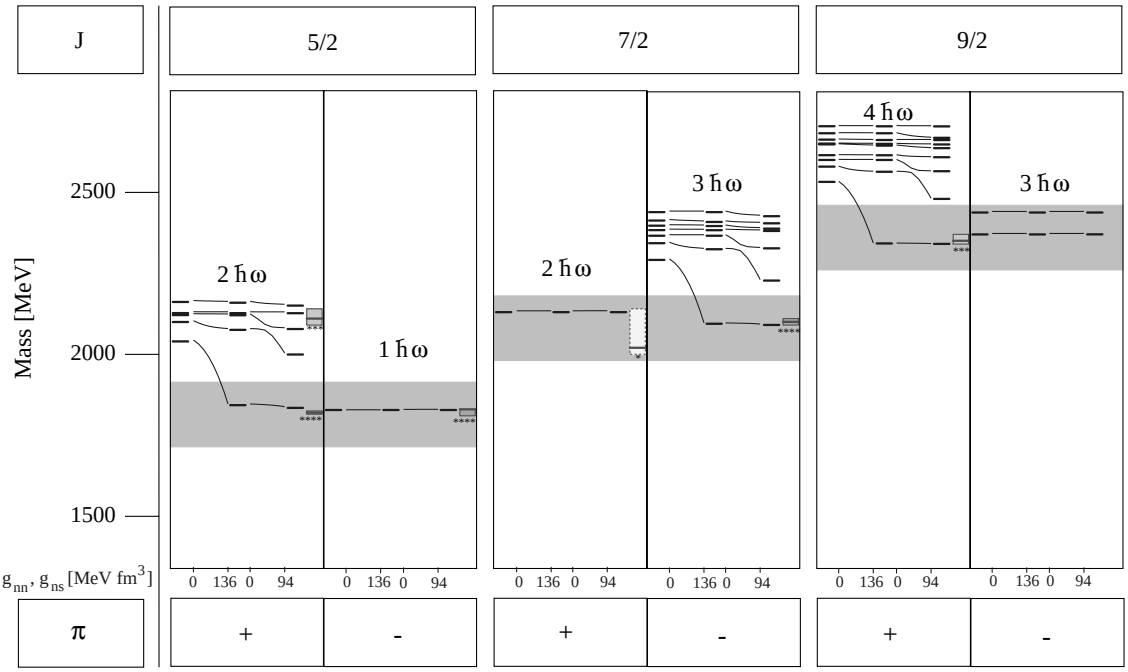

Fig. 6. Instanton-induced generation of approximate parity doublets of lowest-lying Λ states in the sectors with $J = \frac{5}{2}$, $\frac{7}{2}$ and $\frac{9}{2}$ (in model $\mathcal{A}$).

The two distinct diquark-quark systems form oscillator shells with *different* mass gaps $\hbar\omega_{(nn)s}$ and $\hbar\omega_{(ns)n}$, where the frequencies $\omega_{Dq} \sim (\frac{M_D+m_q}{M_D m_q})^{\frac{1}{2}}$ are proportional to the square root of the inverse reduced diquark-quark masses. Assuming weakly bound diquarks, *i.e.* $M_{nn} \approx 2m_n$ and $M_{ns} \approx m_n + m_s$, one finds $\omega_{(nn)s} \approx \omega_{(ns)n}(\frac{m_n+m_s}{2m_n})^{\frac{1}{2}}$, thus in fact $\hbar\omega_{(nn)s} < \hbar\omega_{(ns)n}$. Hence this level ordering is predominantly a flavor $SU(3)$ symmetry breaking effect from the quark mass difference $m_s > m_n$.

Similar to the nucleon spectrum the overlapping positive- and negative-parity bands lead to approximate parity doublets. Figure 6 shows how 't Hooft's force induces such approximates doublets for the lowest-excited states in the sectors with total spin $J = \frac{5}{2}$, $\frac{7}{2}$, and $\frac{9}{2}$. The lowest states in $\frac{5}{2}^-$, $\frac{7}{2}^+$, $\frac{9}{2}^-$ are those with the maximum total spin in the $1\hbar\omega$, $2\hbar\omega$, and $3\hbar\omega$ bands, respectively, and thus are determined by confinement alone. In the corresponding sectors $\frac{5}{2}^+$, $\frac{7}{2}^-$, $\frac{9}{2}^+$ with the same spin but opposite parity there are always exactly two[4] states of the higher-lying $2\hbar\omega$, $3\hbar\omega$, and $4\hbar\omega$ shells which are selectively lowered by 't Hooft's force and thus become well isolated from the other states. It is quite remarkable that the shift of the lowest excitations (with the non-strange diquark contribution) once again is such that these in fact become degenerate with the unshifted first-excited states of opposite parity. The experimentally best established parity doublet in the Λ spectrum, which nicely confirms this scenario, is that of the two four-star resonances $\Lambda\frac{5}{2}^+(1820,****)$ and $\Lambda\frac{5}{2}^-(1830,****)$ in the $2\hbar\omega$ and $1\hbar\omega$ shell, respectively. It is the counterpart to the well-established parity doublet structure $N\frac{5}{2}^+(1680,****) - N\frac{5}{2}^-(1675,****)$ in the nucleon spectrum (see ref. [5]). The two single resonances $\Lambda\frac{9}{2}^+(2350,***)$ and $\Lambda\frac{7}{2}^-(2100,****)$ observed in the high-energy region of the Λ spectrum are just the states with maximally possible total spin $J = J_{\max}(N) - 1$ in the lowered substructures of the $N = 4$ and $N = 3$ shells, respectively. In the $\Lambda\frac{9}{2}^+$ sector the situation is similar to the corresponding $N\frac{9}{2}^+$ nucleon sector, where this mass shift of the lowest state turned out to be important for generating the striking parity doublet structure $N\frac{9}{2}^+(2220,****)$–$N\frac{9}{2}^-(2250,****)$ in the upper part of the nucleon spectrum [5]. The counterpart to the doublet partner $N\frac{9}{2}^-(2250,****)$ of $N\frac{9}{2}^+(2220,****)$ has not yet been observed in the $\Lambda\frac{9}{2}^-$ sector. But it is interesting that our model predicts the lowest state in this sector at 2370 MeV, indeed approximately degenerate to the $\Lambda\frac{9}{2}^+(2350,***)$. In the sectors with spin $J = \frac{7}{2}$ the same mechanism can nicely explain the parity doublet $\Lambda\frac{7}{2}^+(2020,*)$–$\Lambda\frac{7}{2}^-(2100,****)$ observed experimentally. Here 't Hooft's force induces a strong attractive scalar non-strange diquark correlation in the $\Lambda\frac{7}{2}^-$ state shifting this $3\hbar\omega$ state down to 2090 MeV, deeply enough to match the well-established $\Lambda\frac{7}{2}^-(2100,****)$ and thus to become nearly degenerate to the unaffected $\Lambda\frac{7}{2}^+$ state in the $2\hbar\omega$ shell predicted

[4] One state with a non-strange diquark contribution and another with a non-strange–strange diquark contribution.

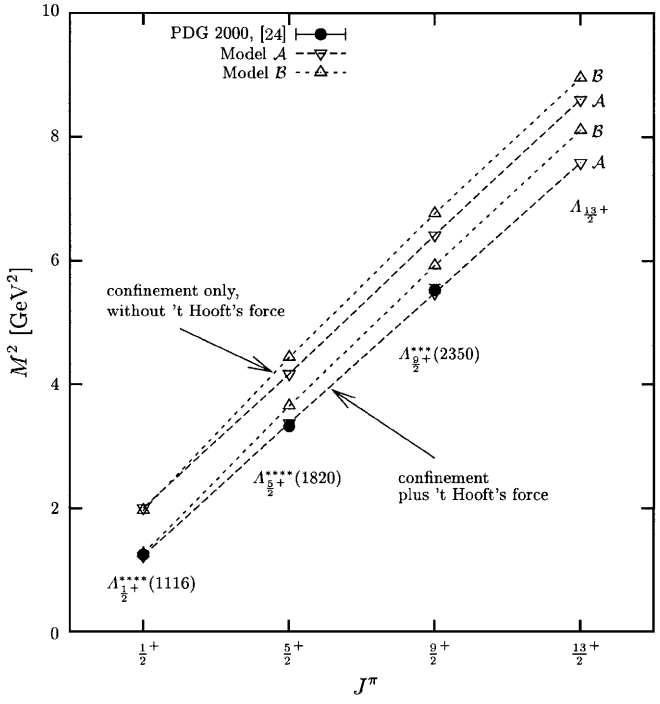

Fig. 7. Chew-Frautschi plot (M^2 *vs.* J) of the positive-parity Λ Regge trajectory $\Lambda\frac{1}{2}^+$, $\Lambda\frac{5}{2}^+$, $\Lambda\frac{9}{2}^+$, $\Lambda\frac{13}{2}^+$, ..., in the models $\mathcal{A}$ and $\mathcal{B}$ (lower curves) compared to experimental masses from the Particle Data Group (see [24]). The upper curves show the trajectories without influence of 't Hooft's instanton-induced interaction.

at 2130 MeV. It is interesting to compare this nice result to that of the corresponding nucleon sectors $N\frac{7}{2}^\pm$. In ref. [5] we showed that 't Hooft's force induced in the same manner the degeneracy of the lowest $N\frac{7}{2}^\pm$ nucleon states. In particular, we likewise found a similar strong downward shift of the $N\frac{7}{2}^-$ state. However, the currently available experimental data in $N\frac{7}{2}^\pm$ do not show a clear parity doublet structure according to the comparatively high position of the $N\frac{7}{2}^-(2190,****)$ with respect to the $N\frac{7}{2}^+(1990,**)$. While in the $\Lambda\frac{7}{2}^-$ sector the instanton-induced effect is able to explain the low-lying $\Lambda\frac{7}{2}^-(2100,****)$, in the $N\frac{7}{2}^-$ sector the same effect shifts the first state predicted far below the $N\frac{7}{2}^-(2190,****)$. In view of the otherwise striking similarities between the nucleon and Λ states that *all* can be simultaneously explained by 't Hooft's force in both flavor sectors, this discrepancy in the $N\frac{7}{2}^-$ sector is rather surprising. We therefore consider the remarkably good prediction for the low-lying $\Lambda\frac{7}{2}^-(2100,****)$ as a further strong support for our conjecture in ref. [5] that there might be a $N\frac{7}{2}^-$ state below the $N\frac{7}{2}^-(2190,****)$ at roughly 2015 MeV which is the expected parity doublet partner to $N\frac{7}{2}^+(1990,**)$.

Note that the lowest states in the sectors $J^\pi = \frac{5}{2}^+$ and $\frac{9}{2}^+$ belong to the positive-parity Λ Regge trajectory. Since in our model both states are quite strongly lowered by the instanton interaction as the ground state, it is again interesting to investigate how far 't Hooft's force influences the linear Regge characteristics $M^2 \sim J$ observed empirically for the Regge states $\Lambda\frac{1}{2}^+(1116,****)$, $\Lambda\frac{5}{2}^+(1820,****)$, and $\Lambda\frac{9}{2}^+(2350,***)$.

2.2.6 The positive-parity Λ Regge trajectory

Figure 7 depicts the Chew-Frautschi plot (M^2 *vs.* J) of the positive-parity Λ Regge trajectory in both confinement models $\mathcal{A}$ and $\mathcal{B}$ in comparison to the states $\Lambda\frac{1}{2}^+(1116,****)$, $\Lambda\frac{5}{2}^+(1820,****)$, and $\Lambda\frac{9}{2}^+(2350,***)$ observed experimentally. To illustrate the influence of 't Hooft's force we displayed in addition the trajectory as determined by the confinement force alone.

In consistence with the well-described Δ-trajectory which is determined by the string-like confinement alone [5], the flavor-independent confinement force produces likewise a linear characteristics for the pure confinement Λ trajectories. In model $\mathcal{A}$ this trajectory already shows the quantitatively correct slope, whereas the slope in model $\mathcal{B}$ turns out too large right from start. Similar to the nucleon Regge trajectory we observe once more the remarkable and non-trivial feature of 't Hooft's force to be compatible with the linear Regge characteristics. Again the downward shift of the Regge states, which is largest for the ground states and moderate for the higher states, is such that it preserves the linear behavior $M^2 \sim J$ with almost the same slope as in the pure confinement case. In model $\mathcal{A}$ the equally large shift of all trajectory members in the mass square M^2 leads simultaneously to an excellent agreement with the observed states $\Lambda\frac{1}{2}^+(1116,****)$, $\Lambda\frac{5}{2}^+(1820,****)$, and $\Lambda\frac{9}{2}^+(2350,***)$ and also the next (still "missing") member predicted in $\Lambda\frac{13}{2}^+$ at 2754 MeV lies fairly well on this linear trajectory. In model $\mathcal{B}$, however, the slope remains too big to account for the observed states. In table 7 the predicted positions for the Λ Regge states are once more explicitly summarized in comparison to the experimental findings.

This result once again illustrates the importance of instanton effects in the higher mass regions of baryon spectra. In particular, it demonstrates that our string-like, flavor-independent confinement ansatz $\mathcal{A}$ with its parameters a (offset) and b (slope) fixed entirely from the phenomenology of the *non-strange* Δ spectrum works equally well also in the strange flavor sector. In this respect model $\mathcal{B}$, however, strongly fails: although the confinement ansatz $\mathcal{B}$ could equally well as model $\mathcal{A}$ account for the non-strange nucleon and Δ Regge trajectories, it produces here, in the strange Λ sector, a wrong slope for the trajectory. At the end of this section we shall now briefly comment on the shortcomings of model $\mathcal{B}$ in general.

2.2.7 Shortcomings of model $\mathcal{B}$

In accordance with our results for the nucleon spectrum in ref. [5], also the Λ spectrum is consistently better described in model $\mathcal{A}$ than in model $\mathcal{B}$. For this reason our

Table 7. Position of states belonging to the positive-parity Λ Regge trajectory calculated in the models $\mathcal{A}$ and $\mathcal{B}$ in comparison to the experimental resonance positions [24]. For a graphical presentation see fig. 7.

Regge state	Rating	J^π	Experimental Mass [MeV] [24]	Mass [MeV] Model $\mathcal{A}$	Mass [MeV] Model $\mathcal{B}$
$\Lambda(1116)$	****	$\frac{1}{2}^+$	1116	1108	1123
$\Lambda(1820)$	****	$\frac{5}{2}^+$	1815–1825	1834	1909
$\Lambda(2350)$	***	$\frac{9}{2}^+$	2340–2370	2340	2433
"missing"		$\frac{13}{2}^+$		2754	2848

preceding detailed discussion of the Λ spectrum has been restricted mainly to the results of model $\mathcal{A}$. But for the sake of completeness we should conclude our investigations of the Λ spectrum by briefly summarizing the main shortcomings of model $\mathcal{B}$. In the Λ sector the discrepancies are even more distinctive than in the nucleon sector. As mentioned, model $\mathcal{B}$ already fails in describing the Λ Regge trajectory. The slope of the trajectory turns out too large. This is quite in contrast to the non-strange sectors, where Δ and nucleon trajectories still could be quantitatively explained also by model $\mathcal{B}$ [5].

Figure 8 shows for model $\mathcal{B}$ the influence of 't Hooft's force on the positive- and negative-parity Λ states in analogy to the corresponding effects of model $\mathcal{A}$ in figs. 4 and 5. Looking at the pure confinement spectra on the left in each column, we find the centroids of the $2\hbar\omega$, $3\hbar\omega$, and $4\hbar\omega$ band structures generally positioned higher than in model $\mathcal{A}$. Moreover, we again observe the confinement Dirac structure of model $\mathcal{B}$ inducing different spin-orbit effects than that of model $\mathcal{A}$. Similar to the nucleon sector this leads to different intra-band splittings, level orderings and configuration mixings in each shell which finally implies a different effect of 't Hooft's force on the states. All in all, the 't Hooft couplings g_{nn} and g_{ns} as chosen to reproduce the positions of flavor octet ground states (here the $\Lambda(1116, ****)$) are not sufficiently large to account for the masses of several comparatively low-lying states in each shell. In this respect, the largest discrepancies to experiment show up in the $\Lambda\frac{1}{2}^+$ sector, where the first scalar/isoscalar excitation predicted appears far above the low-lying Roper-type resonance $\Lambda\frac{1}{2}^+(1600, ***)$. In the $\Lambda\frac{1}{2}^-$ the interplay of 't Hooft's residual interaction with the relativistic effects of the confinement force even produces a completely different hyperfine structure of the three $1\hbar\omega$ states. Here the two first states predicted agree with the second and third resonances observed, while there is no state that could be associated with the low-lying $\Lambda\frac{1}{2}^-(1405, ****)$. Instead, the third $1\hbar\omega$ state is predicted at roughly 2 GeV due to a strong upward shift of this state by the attractive part of 't Hooft's force that acts in the pseudo-scalar diquark channel. It is interesting that this result would indeed allow for the alternative interpretation of $\Lambda\frac{1}{2}^-(1405, ****)$ as an additional $\bar{K}N$ bound state below the $\bar{K}N$ threshold, since all other states of the $1\hbar\omega$ shell are reasonably well reproduced. But in view of the otherwise rather poor results of model $\mathcal{B}$ we do not take this alternative seriously.

2.3 Summary for the Λ spectrum

To summarize our discussion of the Λ sector, we presented our results of models $\mathcal{A}$ and $\mathcal{B}$ for the complete Λ-resonance spectrum. With the parameters being fixed all calculated states were true parameter-free predictions which we compared with the presently available experimental data. In fact, we found excellent agreement between our predictions of model $\mathcal{A}$ and the positions of the hitherto experimentally observed resonances in the Λ sector. Moreover, we again analyzed in detail the role of 't Hooft's residual force for the hyperfine structures of the excited Λ spectrum and similar to the nucleon spectrum, we could convincingly demonstrate that also in the strange Λ sector instanton-induced effects in fact provide a consistent and uniform explanation for almost all prominent features in the lower as well as in the higher mass region of the spectrum. Once the 't Hooft couplings are fixed to account for the correct position of the octet-ground states (here the Λ ground state), several excited states can be simultaneously well described, most of these even in completely quantitative agreement:

- We found an excellent description of the states $\Lambda\frac{1}{2}^+(1116, ****)$, $\Lambda\frac{5}{2}^+(1820, ****)$ and $\Lambda\frac{9}{2}^+(2350, ***)$ belonging to the positive-parity Λ Regge trajectory. The model yields the correct empirical Regge characteristics $M^2 \sim J$ with the quantitatively right slope of the trajectory. Once more we could demonstrate the non-trivial property of 't Hooft's force to be compatible with the observed linear Regge characteristics.
- The hyperfine intra-band structure of the positive-parity $2\hbar\omega$ shell could be nicely reproduced. As in the $2\hbar\omega$ shell of the nucleon spectrum the analogous pattern of four comparatively low-lying states is explained due to a selective lowering by 't Hooft's force: Similar to the Roper state model $\mathcal{A}$ likewise accounts for the strikingly low position of the strange partner of the Roper resonance, the $\Lambda\frac{1}{2}^+(1600, ***)$. Moreover, also the model states associated to the three other low-lying resonances $\Lambda\frac{1}{2}^+(1810, ***)$, $\Lambda\frac{3}{2}^+(1890, ****)$, and $\Lambda\frac{5}{2}^+(1820, ****)$ are predicted close to the experimental resonance positions.
- The intra-band structure of the negative-parity $1\hbar\omega$ shell could be likewise explained by 't Hooft's force. In the upper part of this shell the model states fit quantitatively the structure of the four well-established states $\Lambda\frac{1}{2}^-(1670, ****)$, $\Lambda\frac{1}{2}^-(1800, ***)$,

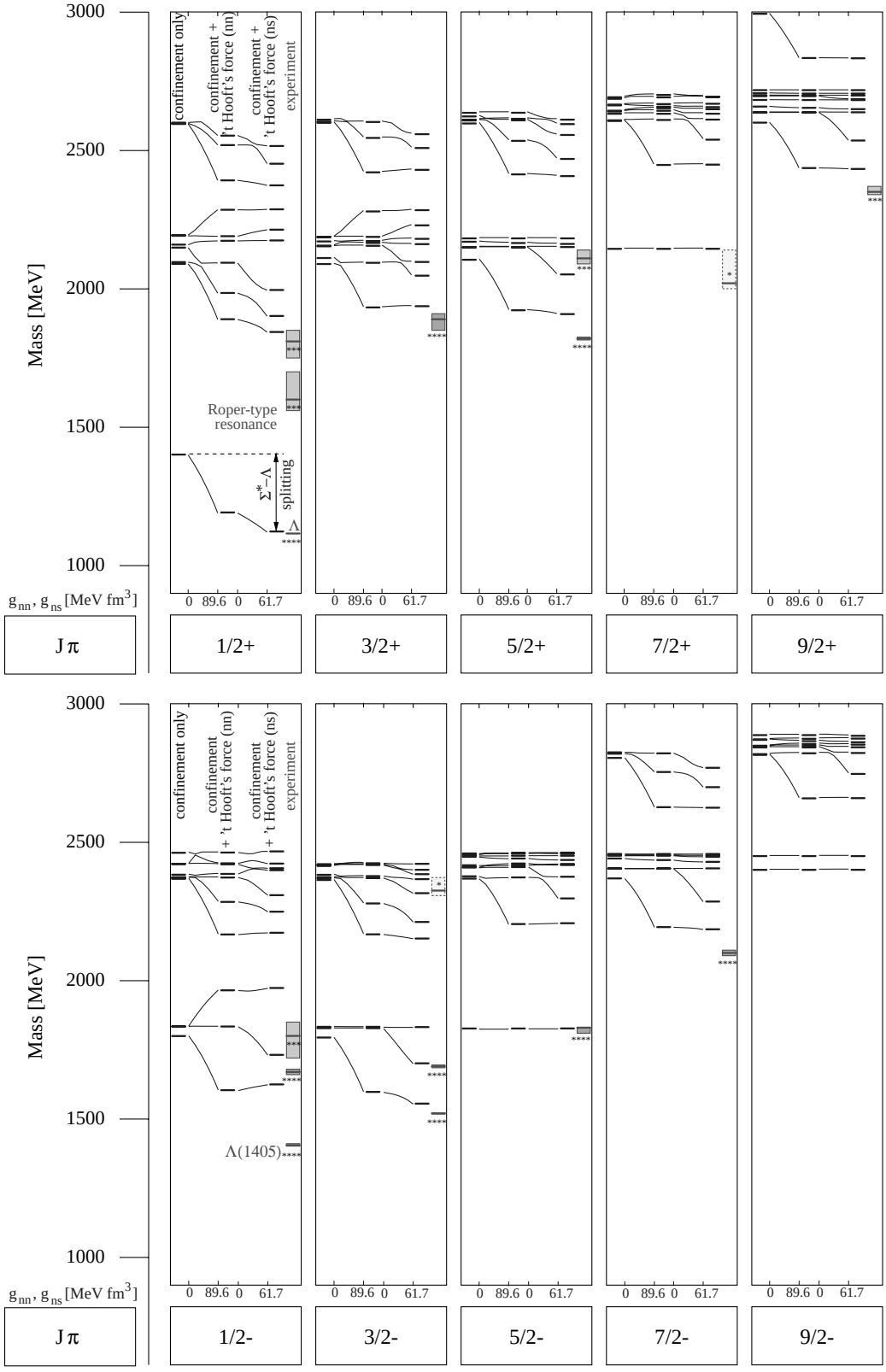

Fig. 8. Influence of the instanton-induced interaction on the energy levels of the positive-parity (above) and negative-parity (below) Λ states in model $\mathcal{B}$. The curves illustrate the variation of energy levels with increasing 't Hooft couplings g_{nn} and g_{ns} which are finally fixed to $g_{nn} = 89.6$ MeV fm^3 and $g_{ns} = 61.7$ MeV fm^3.

$\Lambda\frac{3}{2}^-(1690,****)$, and $\Lambda\frac{5}{2}^-(1830,****)$. These states in fact turned out to be dominantly flavor octet and hence could be identified as the octet counterparts of the $1\hbar\omega$ nucleon states. Moreover 't Hooft's force provides an explanation for the position of the dominantly flavor singlet states below the dominantly flavor octet states. The position of the $\Lambda\frac{3}{2}^-(1520,****)$ could be nicely explained, however, the first $\Lambda\frac{1}{2}^-$ state turned out to be degenerate with the $\Lambda\frac{3}{2}^-(1520,****)$ and thus the notorious problem in quark models to explain the exceptionally large splitting between the $\Lambda\frac{1}{2}^-(1405,****)$ and $\Lambda\frac{3}{2}^-(1520,****)$ unfortunately remains unresolved also in our fully relativistic approach.

– Due to 't Hooft's force we again found overlapping substructures of shells with opposite parity leading to the occurrence of approximately degenerate states with the same spin but opposite parity in the same manner as in the nucleon spectrum. In this way our model is able to account for approximate parity doublets observed in the Λ spectrum, *e.g.* $\Lambda\frac{5}{2}^+(1820,****)$–$\Lambda\frac{5}{2}^-(1830,****)$ and $\Lambda\frac{7}{2}^+(2020,*)$–$\Lambda\frac{7}{2}^-(2100,****)$.

Concerning the results of model $\mathcal{B}$ we found similar shortcomings as discussed in detail for the nucleon spectrum in ref. [5]. But, in addition, the centroids of the band-structures are generally predicted too high showing that the confinement ansatz $\mathcal{B}$ works even less well in this strange flavor sector.

At the end of this section we should finally mention that the fully relativistic treatment of the quark dynamics within our covariant Salpeter framework of model $\mathcal{A}$ leads again to large improvements of the results as compared to the corresponding non-relativistic quark model of [28, 29] which employed instanton-induced forces as well. Although similar effects of 't Hooft's force likewise emerged in this non-relativistic version, the lowering of particular Λ states due to the scalar diquark correlations were in general too small to account quantitatively for prominent features as, *e.g.*, the low position of the Roper partner $\Lambda\frac{3}{2}^+(1600,***)$. Positive-parity excited states tended to be too massive by roughly 200 MeV. All in all the results of refs. [28,29] for the Λ spectrum are rather similar to those of our inferior model $\mathcal{B}$.

Let us now continue our investigations with the discussion of the strange Σ-baryons ($S^*=-1$, $T=1$), where in contrast to the Λ states 't Hooft's force acts only in the non-strange–strange diquark channel but is absent for the flavor-symmetric ($T=1$) non-strange diquarks.

3 The Σ-resonance spectrum

In this section we will discuss our predictions for the excited Σ-baryons with strangeness $S^*=-1$ and isospin $T=1$ and compare our results with the corresponding experimental data quoted by the Particle Data Group [24]. Again let us start with some general remarks concerning the effects of 't Hooft's force expected in this flavor sector.

3.1 Remarks — Implications of 't Hooft's force and the experimental situation

The Σ-baryons have the same flavor content of two non-strange quarks and one strange quark as the Λ-baryons. But in contrast to the Λ states the non-strange quarks form symmetric isovector ($T=1$) quark pairs and therefore 't Hooft's force does not act in the non-strange diquark channel but exclusively in the flavor-antisymmetric non-strange–strange diquark channel. For the Σ-baryons the flavor wave functions can be combined to the mixed symmetric octet representations $\Sigma_{\mathbf{8}}$ corresponding to the non-strange N states and to the totally symmetric flavor decuplet representations $\Sigma_{\mathbf{10}}$ which correspond to the non-strange Δ states. The positive and negative energy components of the Salpeter amplitude $\Phi^{\Sigma}_{J^\pi}$ describing an excited Σ state with spin and parity J^π are obtained by the embedding map (see ref. [4])

$$\Phi^{\Sigma}_{J^\pi} \;=\; T^{+++}\varphi^{\Sigma}_{J^\pi} \;+\; T^{---}\varphi^{\Sigma}_{J^{-\pi}} \tag{5}$$

of totally S_3-symmetric Pauli spinors $\varphi^{\Sigma}_{J^\pi}$ and $\varphi^{\Sigma}_{J^{-\pi}}$, which then in general can be decomposed into the following six different spin-flavor $SU(6)$-configurations:

$$\begin{aligned}|\varphi^{\Sigma}_{J^\pm}\rangle = \;& |\Sigma\; J^\pm,\; {}^2\!8[56]\rangle \;+\; |\Sigma\; J^\pm,\; {}^2\!8[70]\rangle \\ &+ |\Sigma\; J^\pm,\; {}^4\!8[70]\rangle \;+\; |\Sigma\; J^\pm,\; {}^2\!8[20]\rangle \\ &+ |\Sigma\; J^\pm,\; {}^4\!10[56]\rangle \;+\; |\Sigma\; J^\pm,\; {}^2\!10[70]\rangle,\end{aligned} \tag{6}$$

with the four flavor octet contributions

$$|\Sigma\; J^\pm,\; {}^2\!8[56]\rangle :=$$
$$\sum_L \left[|\psi^{L\,\pm}_{\mathcal{S}}\rangle \otimes \frac{1}{\sqrt{2}} \left(|\chi^{\frac{1}{2}}_{\mathcal{M}_\mathcal{A}}\rangle \otimes |\phi^{\Sigma}_{\mathcal{M}_\mathcal{A}}\rangle + |\chi^{\frac{1}{2}}_{\mathcal{M}_\mathcal{S}}\rangle \otimes |\phi^{\Sigma}_{\mathcal{M}_\mathcal{S}}\rangle \right) \right]^J,$$

$$|\Sigma\; J^\pm,\; {}^2\!8[70]\rangle :=$$
$$\sum_L \left[\frac{1}{2}\, |\psi^{L\,\pm}_{\mathcal{M}_\mathcal{A}}\rangle \otimes \left(|\chi^{\frac{1}{2}}_{\mathcal{M}_\mathcal{A}}\rangle \otimes |\phi^{\Sigma}_{\mathcal{M}_\mathcal{S}}\rangle + |\chi^{\frac{1}{2}}_{\mathcal{M}_\mathcal{S}}\rangle \otimes |\phi^{\Sigma}_{\mathcal{M}_\mathcal{A}}\rangle \right) + \frac{1}{2}\, |\psi^{L\,\pm}_{\mathcal{M}_\mathcal{S}}\rangle \otimes \left(|\chi^{\frac{1}{2}}_{\mathcal{M}_\mathcal{A}}\rangle \otimes |\phi^{\Sigma}_{\mathcal{M}_\mathcal{S}}\rangle - |\chi^{\frac{1}{2}}_{\mathcal{M}_\mathcal{S}}\rangle \otimes |\phi^{\Sigma}_{\mathcal{M}_\mathcal{A}}\rangle \right) \right]^J,$$

$$|\Sigma\; J^\pm,\; {}^4\!8[70]\rangle := \sum_L \left[\frac{1}{\sqrt{2}} \left(|\psi^{L\,\pm}_{\mathcal{M}_\mathcal{A}}\rangle \otimes |\chi^{\frac{3}{2}}_{\mathcal{S}}\rangle \otimes |\phi^{\Sigma}_{\mathcal{M}_\mathcal{A}}\rangle - |\psi^{L\,\pm}_{\mathcal{M}_\mathcal{S}}\rangle \otimes |\chi^{\frac{3}{2}}_{\mathcal{S}}\rangle \otimes |\phi^{\Sigma}_{\mathcal{M}_\mathcal{S}}\rangle \right) \right]^J,$$

$$|\Sigma\; J^\pm,\; {}^2\!8[20]\rangle :=$$
$$\sum_L \left[|\psi^{L\,\pm}_{\mathcal{A}}\rangle \otimes \frac{1}{\sqrt{2}} \left(|\chi^{\frac{1}{2}}_{\mathcal{M}_\mathcal{A}}\rangle \otimes |\phi^{\Sigma}_{\mathcal{M}_\mathcal{S}}\rangle - |\chi^{\frac{1}{2}}_{\mathcal{M}_\mathcal{S}}\rangle \otimes |\phi^{\Sigma}_{\mathcal{M}_\mathcal{A}}\rangle \right) \right]^J, \tag{7}$$

and the two flavor decuplet contributions

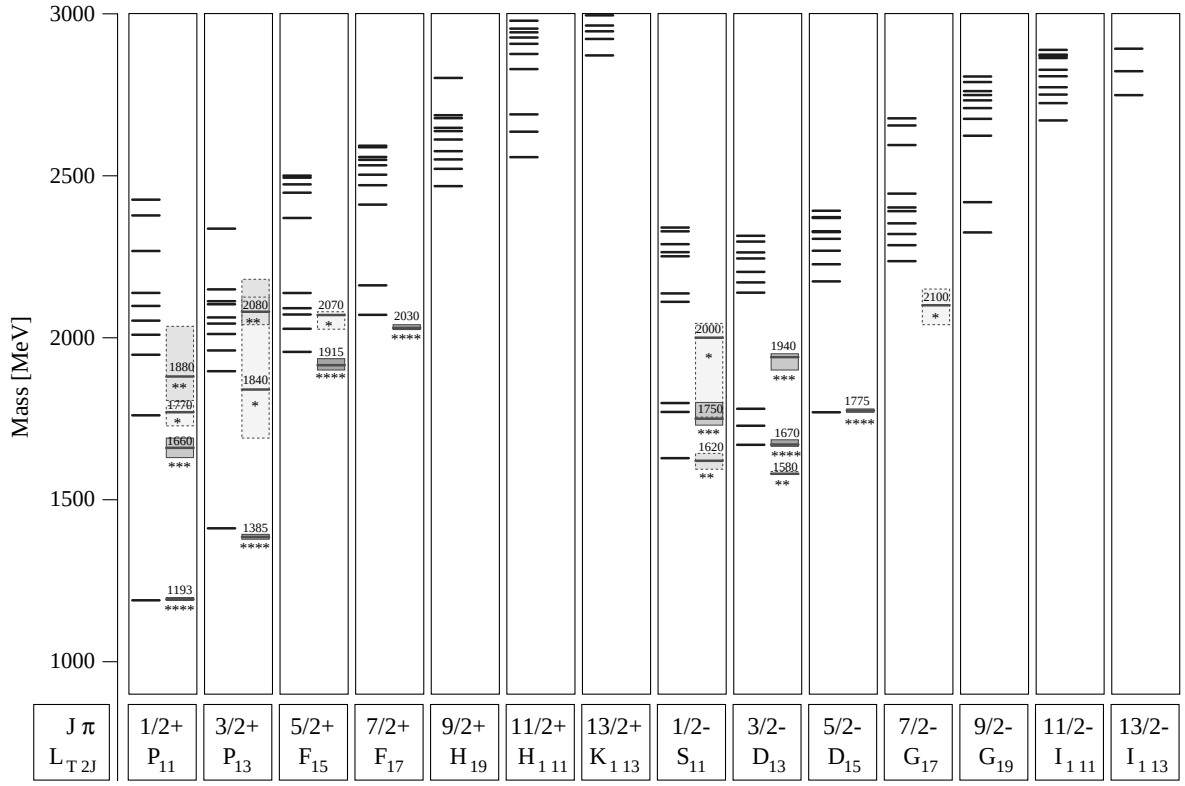

Fig. 9. The predicted positive- and negative-parity *Σ-resonance spectrum* with isospin $T = 1$ and strangeness $S^* = -1$ in *model* $\mathcal{A}$ (left part of each column) in comparison to the experimental spectrum taken from Particle Data Group [24] (right part of each column). The resonances are classified by the total spin J and parity π. The experimental resonance position is indicated by a bar, the corresponding uncertainty by the shaded box, which is darker for better-established resonances; the status of each resonance is additionally indicated by stars.

$$|\Sigma\ J^{\pm},\ {}^4 10[56]\rangle := \sum_L \left[|\psi_{\mathcal{S}}^{L\ \pm}\rangle \otimes |\chi_{\mathcal{S}}^{\frac{3}{2}}\rangle \right]^J \otimes |\phi_{\mathcal{S}}^{\Sigma}\rangle,$$

$$|\Sigma\ J^{\pm},\ {}^2 10[70]\rangle :=$$

$$\sum_L \left[\frac{1}{\sqrt{2}} \left(|\psi_{\mathcal{M}_S}^{L\ \pm}\rangle \otimes |\chi_{\mathcal{M}_S}^{\frac{1}{2}}\rangle + |\psi_{\mathcal{M}_A}^{L\pm}\rangle \otimes |\chi_{\mathcal{M}_A}^{\frac{1}{2}}\rangle \right) \right]^J \otimes |\phi_{\mathcal{S}}^{\Sigma}\rangle. \tag{8}$$

Here we used the same notation for the spatial, spin and flavor wave functions as in the preceding section. For each shell the constituent quark model thus predicts the same number of states as in the combined spectrum of N and Δ states. Due to the flavor-$SU(3)$ symmetry breaking quark mass difference $m_s - m_n > 0$, the decuplet and octet states mix. Since the instanton induced force acts on flavor-antisymmetric quark pairs only, it does not affect the totally symmetric flavor decuplet contributions ${}^4 10[56]$ and ${}^2 10[70]$ (similar to the non-strange Δ states). But 't Hooft's force again affects the flavor octet contributions in the same manner as for the nucleon states: From the strong selection rules of 't Hooft's force the states with dominant ${}^4 8[70]$ and ${}^2 8[20]$ spin-flavor $SU(6)$ contributions are expected to be hardly influenced, whereas the dominantly ${}^2 8[56]$ and ${}^2 8[70]$ states shift downward due to the attractive scalar non-strange–strange diquark correlation within these states. Apart from the mixing of flavor-octet and flavor-decuplet configurations owing to the flavor-$SU(3)$ symmetry breaking effects from the mass difference of the non-strange and strange quark masses, we nonetheless anticipate a spectrum of overlapping dominantly flavor-decuplet and dominantly flavor-octet states, which by themselves form similar intra-band structures as their corresponding counterparts in the non-strange Δ and N spectra, respectively. In particular, we expect 't Hooft's force generating hyperfine splittings of the dominantly octet states with the same systematics as observed for the nucleon states (and the dominantly flavor-octet Λ states). But note in this respect the following substantial differences to the N and Λ spectra: The instanton-induced hyperfine splittings, which here arise solely from the non-strange–strange diquark correlation, are expected to be considerably smaller and therefore, these structures generally might be hidden according to the overlapping flavor-decuplet states.

This might be the reason why also the experimental situation concerning the intra-band splittings is rather unclear and inconclusive. In contrast to the N and Λ sectors, the Σ sector lacks well-established experimental

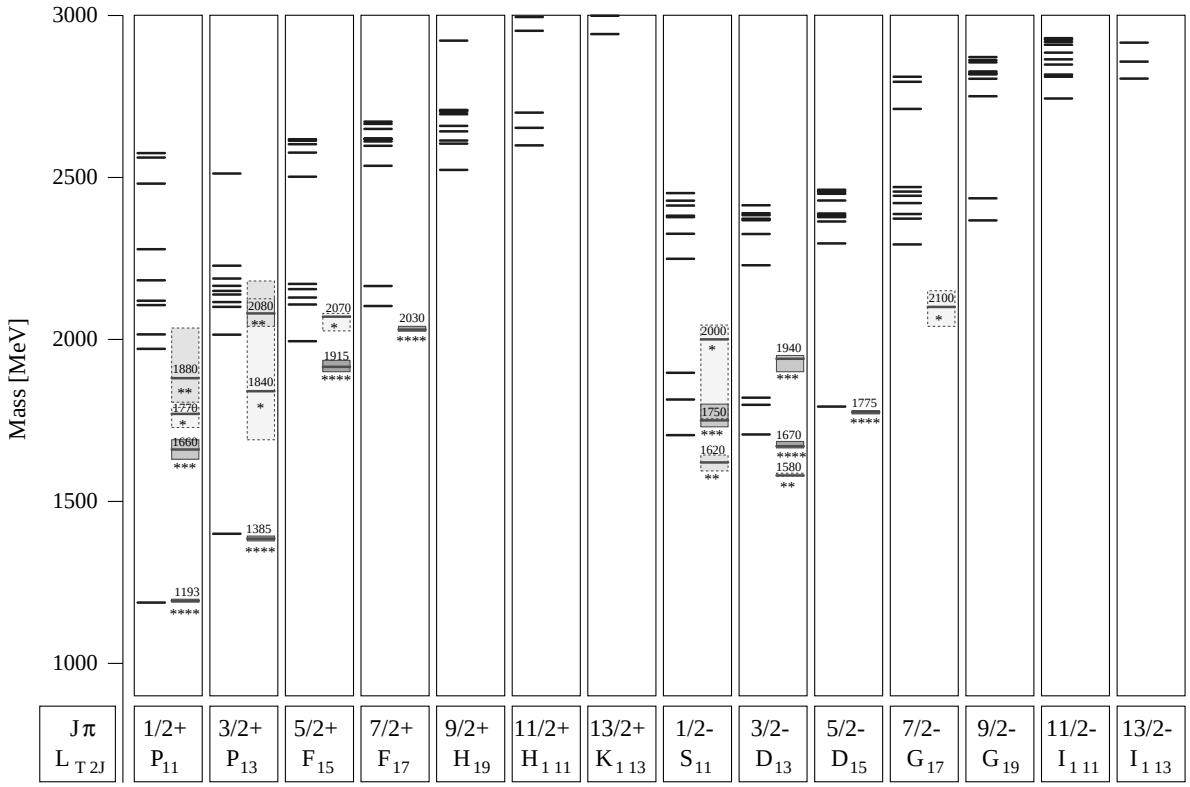

Fig. 10. The predicted positive- and negative-parity *Σ-resonance spectrum* with isospin $T = 1$ and strangeness $S^* = -1$ in *model* $\mathcal{B}$ (left part of each column) in comparison to the experimental spectrum taken from Particle Data Group [24] (right part of each column). The resonances are classified by the total spin J and parity π. See also caption to fig. 9.

data. Many resonances in the lower energy regions of the $1\hbar\omega$ and $2\hbar\omega$ bands are only poorly established. The clearest evidence for a hyperfine structure with an equivalent in the N and Λ spectrum is the low-lying three-star resonance $\Sigma\frac{1}{2}^+(1660, ***)$ as the counterpart to the Roper resonance $N\frac{1}{2}^+(1440, ****)$ and its partner $\Lambda\frac{1}{2}^+(1600, ***)$. Altogether there are (apart from the $\Sigma\frac{1}{2}^+$ and $\Sigma^*\frac{3}{2}^+$ ground states) only four well-established resonances with four-star rating, *i.e.* the $\Sigma\frac{5}{2}^+(1915, ****)$ and the $\Sigma\frac{7}{2}^+(2030, ****)$ in the positive-parity sector, as well as the $\Sigma\frac{3}{2}^-(1670, ****)$ and the $\Sigma\frac{5}{2}^-(1775, ****)$ in the negative-parity sector. It should be noted here that, unlike the N and Λ sector, the two lowest states in the $J^\pi = \frac{5}{2}^\pm$ sectors do *not* form a parity doublet structure and moreover, there are no strong evidences for parity doublets in general.

3.2 Discussion of the complete Σ spectrum

Figures 9 and 10 show our predictions for the Σ spectrum in models $\mathcal{A}$ and $\mathcal{B}$, respectively. These are compared with currently available experimental data as quoted by the Particle Data Group [24]. As before, the states depicted in each column are classified by their total spin and parity J^π. For each sector the predictions for at most ten radial excitations are shown on the left-hand side of each column. The experimental Σ-resonance positions are displayed on the right, where we use the same notation concerning the status and the uncertainty of each resonance as before. For both parities figs. 9 and 10 show our predictions for spins up to $J = \frac{13}{2}$. In addition, the calculated masses of positive- and negative-parity states are given explicitly in tables 8, 10, and 12.

3.2.1 Positive-parity excited Σ states

All observed positive-parity excited Σ-baryons quoted by the Particle Data Group [24] lie in the energy region between 1600 and 2100 MeV and possess total spins from $J^\pi = \frac{1}{2}^+$ to $\frac{7}{2}^+$. Hence, they all should belong to the positive-parity $2\hbar\omega$ band. There are no candidates with established quantum numbers for the higher-lying $4\hbar\omega$ or even $6\hbar\omega$ bands. Our predictions in models $\mathcal{A}$ and $\mathcal{B}$ for Σ states of the $2\hbar\omega$ shell are summarized in table 8, where the assignment to observed states again is made according to a comparison of the predicted and experimentally determined resonance positions.

Unfortunately, the assignment here is far less clear than for the corresponding Δ, N, and Λ states due to the lack of well-established experimental data in this flavor sector. Although even more states are expected, less states have been seen by experiments up to now and the quality

Table 8. Calculated positions of Σ states assigned to the positive-parity $2\hbar\omega$ shell in comparison to the corresponding experimental mass values taken from [24]. Notation as in table 1.

Experimental state [24]	PW	J^π	Rating	Mass range [MeV] [24]	Model state in model $\mathcal{A}$	Model state in model $\mathcal{B}$
$\Sigma(1660)$	P_{11}	$\frac{1}{2}^+$	***	1630–1690	$[\Sigma\frac{1}{2}^+]_2(1760)$	$[\Sigma\frac{1}{2}^+]_2(1971)$
$\Sigma(1770)$	P_{11}	$\frac{1}{2}^+$	*	1728–1790		
$\Sigma(1880)$	P_{11}	$\frac{1}{2}^+$	**	1806–2035	$[\Sigma\frac{1}{2}^+]_3(1947)$	$[\Sigma\frac{1}{2}^+]_3(2015)$
					$[\Sigma\frac{1}{2}^+]_4(2009)$	$[\Sigma\frac{1}{2}^+]_4(2106)$
					$[\Sigma\frac{1}{2}^+]_5(2052)$	$[\Sigma\frac{1}{2}^+]_5(2119)$
					$[\Sigma\frac{1}{2}^+]_6(2098)$	$[\Sigma\frac{1}{2}^+]_6(2182)$
					$[\Sigma\frac{1}{2}^+]_7(2138)$	$[\Sigma\frac{1}{2}^+]_7(2278)$
$\Sigma(1840)$	P_{13}	$\frac{3}{2}^+$	*	1690–2125	$[\Sigma\frac{3}{2}^+]_2(1896)$	$[\Sigma\frac{3}{2}^+]_2(2014)$
					$[\Sigma\frac{3}{2}^+]_3(1961)$	$[\Sigma\frac{3}{2}^+]_3(2100)$
					$[\Sigma\frac{3}{2}^+]_4(2011)$	$[\Sigma\frac{3}{2}^+]_4(2115)$
					$[\Sigma\frac{3}{2}^+]_5(2044)$	$[\Sigma\frac{3}{2}^+]_5(2138)$
$\Sigma(2080)$	P_{13}	$\frac{3}{2}^+$	**	2040–2180	$[\Sigma\frac{3}{2}^+]_6(2062)$	$[\Sigma\frac{3}{2}^+]_6(2149)$
					$[\Sigma\frac{3}{2}^+]_7(2103)$	$[\Sigma\frac{3}{2}^+]_7(2165)$
					$[\Sigma\frac{3}{2}^+]_8(2112)$	$[\Sigma\frac{3}{2}^+]_8(2188)$
					$[\Sigma\frac{3}{2}^+]_9(2149)$	$[\Sigma\frac{3}{2}^+]_9(2227)$
$\Sigma(1915)$	F_{15}	$\frac{5}{2}^+$	****	1900–1935	$[\Sigma\frac{5}{2}^+]_1(1956)$	$[\Sigma\frac{5}{2}^+]_1(1994)$
					$[\Sigma\frac{5}{2}^+]_2(2027)$	$[\Sigma\frac{5}{2}^+]_2(2107)$
$\Sigma(2070)$	F_{15}	$\frac{5}{2}^+$	*	2026–2080	$[\Sigma\frac{5}{2}^+]_3(2071)$	$[\Sigma\frac{5}{2}^+]_3(2129)$
					$[\Sigma\frac{5}{2}^+]_4(2091)$	$[\Sigma\frac{5}{2}^+]_4(2155)$
					$[\Sigma\frac{5}{2}^+]_5(2138)$	$[\Sigma\frac{5}{2}^+]_5(2171)$
$\Sigma(2030)$	F_{17}	$\frac{7}{2}^+$	****	2025–2040	$[\Sigma\frac{7}{2}^+]_1(2070)$	$[\Sigma\frac{7}{2}^+]_1(2103)$
					$[\Sigma\frac{7}{2}^+]_2(2161)$	$[\Sigma\frac{7}{2}^+]_2(2165)$

of data is even worse. Actually, only three states are established. These are the two well-established four-star resonances $\Sigma\frac{5}{2}^+(1915,****)$ and $\Sigma\frac{7}{2}^+(2030,****)$ and the three-star Roper-type resonance $\Sigma\frac{1}{2}^+(1660,***)$. The few remaining resonances have only one- and two-star ratings. Consequently, apart from the Roper-type resonance, the experimental situation concerning the intra-band splittings of the $2\hbar\omega$ band is rather unclear and less apparent than in the nucleon and Λ sector. But, in fact this is what we would anticipate from the much weaker effects of the instanton-induced force in this flavor sector, where 't Hooft's force acts exclusively in the scalar non-strange–strange diquark channel with the weaker coupling g_{ns}. In the Λ sector, where both types of diquarks occur, we could nicely demonstrate the fact that owing to flavor-$SU(3)$ symmetry breaking effects the influence of non-strange–strange diquark correlations on the energy levels is significantly weaker than that arising from correlations in the scalar non-strange diquark sector. Consequently, those particular Σ states that are lowered by 't Hooft's force do not become as clearly isolated from the majority of unaffected, strongly clustered states as the corresponding states in the nucleon and Λ spectra. Moreover, the spectrum of unaffected energy levels is even richer according to the additional flavor-decuplet states in the Σ sector Therefore, we expect the hyperfine structures of the Σ spectrum much more difficult to resolve experimentally and from this point of view the inferior quality of experimental data seems not surprising. The significantly weaker effect of 't Hooft's force on the positive-parity excited Σ states in model $\mathcal{A}$ is convincingly demonstrated in fig. 11.

The figure shows for each total spin J the behavior of Σ energy levels as a function of the 't Hooft coupling g_{ns}. The leftmost spectrum in each column is that obtained with the confinement force of model $\mathcal{A}$ alone. Then the 't Hooft coupling g_{ns} is gradually increased up to its value $g_{ns} = 94$ MeV fm^3 adjusted to reproduce the hyperon splittings $\Sigma^* - \Sigma - \Lambda$ and $\Xi^* - \Xi$. The right part of each column then depicts the resulting spectrum obtained with the full dynamics in comparison to the experimental data. Indeed, we again observe the same systematics as found already in the nucleon and Λ sectors (here compare to ref. [5] and fig. 4), namely the downward mass shift of exactly four dominantly ^{2}8[56] or ^{2}8[70] states of the $2\hbar\omega$ shell in the sectors $J^\pi = \frac{1}{2}^+$, $\frac{3}{2}^+$, and $\frac{5}{2}^+$. In analogy to the N and Λ sectors, the largest effect is found for the Roper-like state in the $J^\pi = \frac{1}{2}^+$ sector, whereas the almost equally large downward mass shift of the three other states is comparatively weak. On the one hand, the weaker instanton-induced hyperfine splittings are sufficiently large to explain quantitatively some of the observed structures along with the well-reproduced $\Sigma\frac{3}{2}^+(1385,****)$–$\Sigma\frac{1}{2}^+(1193,****)$ ground-state splitting. This is nicely confirmed by the correctly

Table 9. Configuration mixing of Σ ground states and the positive-parity excited Σ states assigned to the $2\hbar\omega$ band in model $\mathcal{A}$. For explanation see also caption of table 2.

J^π	Model state	pos.	^{2}8[56]	^{2}8[70]	^{4}8[70]	^{2}8[20]	^{4}10[56]	^{2}10[70]
	in model $\mathcal{A}$	neg.	^{2}8[56]	^{2}8[70]	^{4}8[70]	^{2}8[20]	^{4}10[56]	^{2}10[70]
$\frac{1}{2}^+$	$[\Sigma\frac{1}{2}^+]_1(1190)$	98.7	**94.6**	3.9	0.0	0.0	0.0	0.1
	ground state Σ	1.3	0.4	0.6	0.2	0.0	0.0	0.0
$\frac{1}{2}^+$	$[\Sigma\frac{1}{2}^+]_2(1760)$	98.8	**96.1**	2.3	0.0	0.1	0.0	0.2
		1.2	0.3	0.6	0.3	0.0	0.0	0.0
	$[\Sigma\frac{1}{2}^+]_3(1947)$	99.1	6.9	**88.4**	0.9	0.3	0.0	2.5
		0.9	0.2	0.3	0.3	0.1	0.0	0.0
	$[\Sigma\frac{1}{2}^+]_4(2009)$	99.0	0.0	0.2	8.4	0.1	**89.9**	0.4
		1.0	0.0	0.0	0.1	0.0	0.5	0.3
	$[\Sigma\frac{1}{2}^+]_5(2052)$	99.2	0.8	1.8	1.2	1.9	0.2	**93.2**
		0.8	0.0	0.0	0.0	0.0	0.2	0.5
	$[\Sigma\frac{1}{2}^+]_6(2098)$	99.2	0.2	1.1	**88.3**	0.4	8.5	0.6
		0.8	0.0	0.0	0.7	0.0	0.0	0.0
	$[\Sigma\frac{1}{2}^+]_7(2138)$	98.9	0.3	0.8	0.8	**95.2**	0.0	1.9
		1.1	0.0	0.4	0.5	0.1	0.0	0.0
$\frac{3}{2}^+$	$[\Sigma\frac{3}{2}^+]_1(1412)$	99.4	0.0	0.0	0.5	0.0	**98.9**	0.0
	ground state Σ^*	0.6	0.0	0.0	0.0	0.0	0.3	0.2
$\frac{3}{2}^+$	$[\Sigma\frac{3}{2}^+]_2(1896)$	98.8	**73.9**	22.2	0.6	0.1	0.0	2.0
		1.2	0.4	0.3	0.5	0.0	0.0	0.0
	$[\Sigma\frac{3}{2}^+]_3(1961)$	99.1	0.0	0.0	5.1	0.1	**93.9**	0.1
		0.9	0.0	0.0	0.1	0.0	0.5	0.3
	$[\Sigma\frac{3}{2}^+]_4(2011)$	99.0	1.5	1.5	17.3	1.4	**73.4**	4.0
		1.0	0.0	0.1	0.2	0.0	0.5	0.2
	$[\Sigma\frac{3}{2}^+]_5(2044)$	99.0	2.4	18.9	28.0	10.2	7.1	**32.5**
		1.0	0.0	0.3	0.3	0.0	0.0	0.4
	$[\Sigma\frac{3}{2}^+]_6(2062)$	99.1	4.6	19.5	**61.6**	2.4	6.0	5.0
		0.9	0.1	0.1	0.5	0.0	0.0	0.1
	$[\Sigma\frac{3}{2}^+]_7(2103)$	99.1	10.2	37.0	**40.8**	1.4	0.8	8.8
		0.9	0.0	0.3	0.4	0.0	0.0	0.1
	$[\Sigma\frac{3}{2}^+]_8(2112)$	99.1	4.0	1.7	25.0	5.9	15.9	**46.6**
		0.9	0.0	0.1	0.2	0.0	0.1	0.5
	$[\Sigma\frac{3}{2}^+]_9(2149)$	99.0	0.3	0.5	19.8	**77.1**	1.2	0.2
		1.0	0.0	0.4	0.5	0.1	0.0	0.0
$\frac{5}{2}^+$	$[\Sigma\frac{5}{2}^+]_1(1956)$	98.7	**77.8**	18.2	0.2	0.0	0.0	2.5
		1.3	0.4	0.4	0.4	0.1	0.0	0.0
	$[\Sigma\frac{5}{2}^+]_2(2027)$	99.0	2.9	7.8	16.3	0.0	**65.9**	6.0
		1.0	0.0	0.1	0.1	0.1	0.5	0.2
	$[\Sigma\frac{5}{2}^+]_3(2071)$	98.9	14.0	**72.0**	7.6	0.0	4.9	0.4
		1.1	0.5	0.3	0.1	0.1	0.0	0.0
	$[\Sigma\frac{5}{2}^+]_4(2091)$	99.1	0.1	2.4	**53.9**	0.0	5.2	37.5
		0.9	0.0	0.2	0.2	0.2	0.3	0.1
	$[\Sigma\frac{5}{2}^+]_5(2138)$	99.1	2.0	0.3	21.4	0.0	22.8	**52.7**
		0.9	0.0	0.1	0.1	0.0	0.4	0.3
$\frac{7}{2}^+$	$[\Sigma\frac{7}{2}^+]_1(2070)$	99.0	0.0	0.0	29.4	0.0	**69.6**	0.0
		1.0	0.0	0.0	0.2	0.0	0.4	0.2
	$[\Sigma\frac{7}{2}^+]_2(2161)$	99.2	0.0	0.0	**70.0**	0.0	29.2	0.0
		0.8	0.1	0.1	0.4	0.1	0.1	0.1

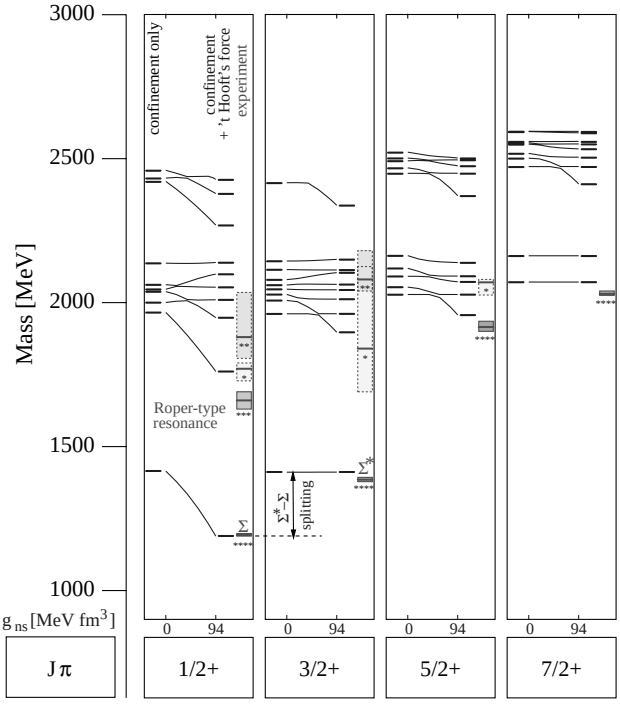

Fig. 11. Instanton-induced hyperfine splittings of the positive-parity Σ states in model $\mathcal{A}$. On the left in each column the spectrum from confinement alone is shown. The curves show the change of the spectrum as a function of the 't Hooft coupling g_{ns} which finally is fixed (right spectrum) from the hyperon splittings $\Sigma^* - \Sigma - \Lambda$ and $\Xi^* - \Xi$. The rightmost spectrum shows for comparison the experimental data with their uncertainties.

described mass splitting between the two well-established resonances $\Sigma\frac{5}{2}^+(1915,****)$ and $\Sigma\frac{7}{2}^+(2030,****)$. But on the other hand, the separation of the lowered states relative to the bulk of unaffected states in fact is far less clear than in the N and Λ sectors. While in the $2\hbar\omega$ band of the N and Λ spectrum the mass gap between the two split shell structures amounts to roughly 200 MeV, it is here mostly not even 100 MeV. Indeed, this might explain the experimentally badly resolved structures especially in the $\frac{3}{2}^+$ sector. In the following discussion we shall investigate the situation for each spin sector $J^\pi = \frac{1}{2}^+$, $\frac{3}{2}^+$, $\frac{5}{2}^+$, and $\frac{7}{2}^+$ separately. We restrict this detailed discussion to the more realistic model $\mathcal{A}$. The contributions of the different spin-flavor $SU(6)$-configurations to each $2\hbar\omega$ state in model $\mathcal{A}$ are additionally tabulated in table 9. This information will be useful to identify hyperfine structures of Σ states with corresponding structures in the Δ, N, and Λ sectors.

For the $\Sigma\frac{7}{2}^+$ sector with maximal total spin $J = \frac{7}{2}$ in the $2\hbar\omega$ band our model predicts two states: the lowest at 2070 MeV and another, roughly 90 MeV higher, at 2161 MeV. Both states are totally unaffected by 't Hooft's force and hence are determined by the confinement kernel alone, as illustrated in fig. 11. Although being predicted slightly too heavy by roughly 30-40 MeV, the lower-mass resonance can rather clearly be associated with the well-established four-star resonance $\Sigma\frac{7}{2}^+(2030,****)$. It is dominantly a ^{4}10[56] state ($\sim 70\%$) with a 30% admixture of a ^{4}8[70] configuration and thus $\Sigma\frac{7}{2}^+(2030,****)$ may be viewed as the flavor decuplet counterpart to the $\Delta\frac{7}{2}^+(1950,****)$ in the corresponding $\Delta\frac{7}{2}^+$ sector. The second excited state turns out to be dominantly ^{4}8[70] ($\sim 70\%$) with a 30% admixture of ^{4}10[56]. This state, which corresponds to the $\Lambda\frac{7}{2}^+(2020,*)$ and the $N\frac{7}{2}^+(1990,**)$ in the Λ and nucleon spectrum, respectively, is still missing in the experimental Σ spectrum.

In the $\Sigma\frac{5}{2}^+$ sector we predict the existence of five $2\hbar\omega$ states. Similar to the lowest states predicted in the $N\frac{5}{2}^+$ and $\Lambda\frac{5}{2}^+$ sectors, the lowest $\Sigma\frac{5}{2}^+$ state exhibits a dominant ^{2}8[56] contribution ($\sim 79\%$) with additional admixture ($\sim 19\%$) of ^{2}8[70]. As shown in fig. 11, this state similarly reveals a downward mass shift by 't Hooft's force of roughly 100 MeV and thus becomes the lowest state predicted at 1956 MeV which may be clearly associated with the four-star resonance $\Sigma\frac{5}{2}^+(1915,****)$. Thus, we identify this resonance as the counterpart to the Regge states $N\frac{5}{2}^+(1680,****)$ and $\Lambda\frac{5}{2}^+(1820,****)$ in the N and Λ spectrum. The mass difference to the first excitation predicted in $\Sigma\frac{7}{2}^+$ amounts to 114 MeV such that the experimental mass splitting of 115 MeV between the $\Sigma\frac{5}{2}^+(1915,****)$ and the $\Sigma\frac{7}{2}^+(2030,****)$ is quite well explained by 't Hooft's force. The remaining four states in $\Sigma\frac{3}{2}^+$ are virtually not affected by 't Hooft's force and lie in a mass range between 2000 and 2140 MeV, *i.e.* around the one-star resonance $\Sigma\frac{5}{2}^+(2070,*)$ observed as second structure in the F_{15} partial wave.

The $\Sigma\frac{3}{2}^+$ sector is rather poorly explored. Only two poorly established structures have been resolved in the P_{13} partial wave, one in a region around 1840 MeV, which is the one-star $\Sigma\frac{3}{2}^+(1840,*)$, and another one, the slightly better established two-star resonance $\Sigma\frac{3}{2}^+(2080,**)$. The observed situation roughly corresponds to that predicted for the eight states expected in our model $\mathcal{A}$. Two of the eight states are rather low-lying at 1896 and 1961 MeV and possibly correspond to the $\Sigma\frac{3}{2}^+(1840,*)$. In analogy to the $\Sigma\frac{5}{2}^+$ sector, the lowest-lying state at 1896 MeV is predicted to be dominantly ^{2}8[56] ($\sim 75\%$) and hence its low position arises from a downward mass shift by 't Hooft's force as depicted in fig. 11. This state is the expected flavor octet partner of the first excitations in the corresponding $N\frac{3}{2}^+$ and $\Lambda\frac{3}{2}^+$ sectors, *i.e.* the $N\frac{3}{2}^+(1720,****)$ and the $\Lambda\frac{3}{2}^+(1890,****)$. The second state, predicted at 1961 MeV, is dominantly ^{4}10[56] ($\sim 95\%$) and hence remains totally unaffected by 't Hooft's force. But, similar to its $\Delta\frac{3}{2}^+$ counterpart, its comparatively low position arises due to rather strong relativistic effects induced from the Dirac structure of the

confinement kernel $\mathcal{A}$ (here we refer to the discussion of the Δ spectrum in ref. [5]). The remaining six states cluster in a rather narrow mass range between 2010 and 2150 MeV roughly corresponding to the range of possible values quoted for the second resonance $\Sigma\frac{3}{2}^+(2080,**)$.

Finally, let us focus on the $\Sigma\frac{1}{2}^+$ sector with the scalar/isoscalar excitations of the $\Sigma\frac{1}{2}^+$ ground state. Similar to the $N\frac{1}{2}^+$ sector two states are selectively lowered from the other members of the $2\hbar\omega$ band, as demonstrated in fig. 11. In fact, the systematics is exactly the same as in the corresponding nucleon sector. Again, the almost pure (96%) $^28[56]$ Roper-like state, which is already the lowest state in the pure confinement spectrum, shows the strongest downward mass shift in fig. 11. Similar to the corresponding N and Λ Roper states, this mass shift of roughly 200 MeV is as large as that of the $\Sigma\frac{1}{2}^+$ ground state. Hence this clearly isolated state becomes the lowest radial excitation at 1760 MeV, and, although being predicted roughly 100 MeV too high, this state should be associated with the $\Sigma\frac{1}{2}^+(1660,***)$, the counterpart to Roper resonance $N\frac{1}{2}^+(1440,****)$. The second radial excitation, which is dominantly a $^28[70]$ state, shows a moderate mass shift of roughly 100 MeV and finally is predicted at 1947 MeV within the error range of the two-star resonance $\Sigma\frac{1}{2}^+(1880,**)$. Hence this resonance is the expected counterpart to the low-lying nucleon resonance $N\frac{1}{2}^+(1710,***)$. There is a further comparatively low-lying structure observed experimentally in the P_{11} partial wave. This is the only poorly established one-star resonance $\Sigma\frac{1}{2}^+(1770,*)$ which, however, does absolutely not fit in the systematics observed so far in the N and Λ sector. Note, however, that this poorly established structure rests solely on one partial wave analysis which is in disagreement with most other analyses (see ref. [24]). Therefore, the existence of this third low-lying structure is highly questionable and will presumably be disproved by future experiments. The remaining four $2\hbar\omega$ states expected in this sector form a pattern of more or less equidistant states in a region between 2000 and 2140 where so far no structure has been experimentally resolved.

3.2.2 Negative-parity excited Σ states

Let us now turn to the discussion of negative-parity states, where most of the resonances observed so far should belong to the $1\hbar\omega$ band with spins $J^\pi = \frac{1}{2}^-$, $\frac{3}{2}^-$, and $\frac{5}{2}^-$. There is only one resonance with higher spin $J^\pi = \frac{7}{2}^-$, the $\Lambda\frac{7}{2}^-(2100,*)$ which definitely cannot be a member of the $1\hbar\omega$ shell. However, its evidence is only poor. Table 10 shows the predicted masses in models $\mathcal{A}$ and $\mathcal{B}$ for the negative-parity states expected in the $1\hbar\omega$ band. Where possible, the assignment of model states to resonances observed is made according to a comparison of calculated and measured resonance positions.

Again let us restrict our detailed discussion to the better results of model $\mathcal{A}$ depicted in fig. 9. Table 11 explicitly shows to what extent the different spin-flavor $SU(6)$ configurations are contributing in model $\mathcal{A}$ to each state of the $1\hbar\omega$ band.

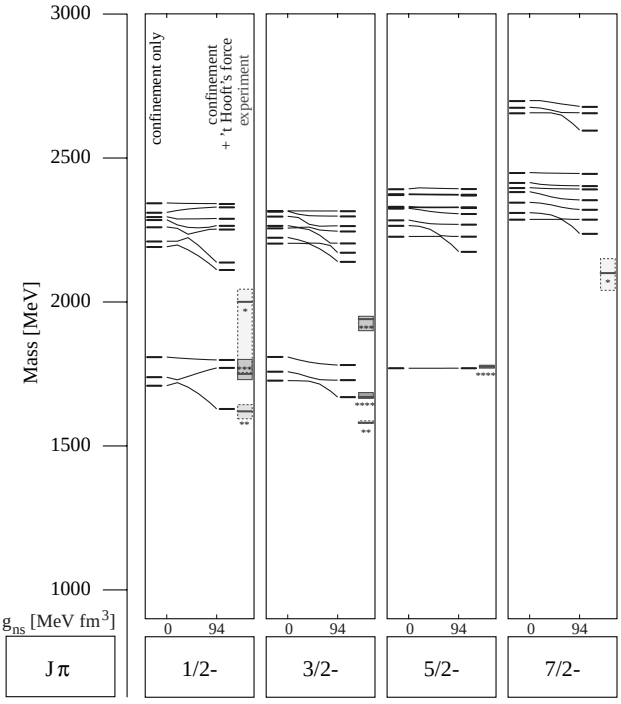

Fig. 12. Instanton-induced hyperfine splittings of the positive-parity Σ states in model $\mathcal{A}$. See caption of fig. 11 for further explanations.

Unlike the situation for the corresponding negative-parity nucleon and Λ-resonances, where a unique one-to-one correspondence between our predictions and the observed states was readily apparent, the experimental situation here is still quite inconclusive. Apart from the two four-star states $\Sigma\frac{3}{2}^-(1670,****)$ and $\Sigma\frac{5}{2}^-(1775,****)$, most of the PDG quoted states [24] are not established and quark models for baryons [30–32,28] in general have difficulties to account for some of the less well-established structures, *e.g.* the poorly determined two-star resonance $\Sigma\frac{3}{2}^-(1580,**)$. In fact, as can be seen in fig. 9 and in table 10, our model as well can only partially explain the experimental features of the negative-parity Σ sector. Note, however, that the best established four-star states $\Sigma\frac{3}{2}^-(1670,****)$ and $\Sigma\frac{5}{2}^-(1775,****)$ are quite well described. Figure 12 illustrates the effect of the instanton-induced interaction on the energy levels of several negative-parity Σ states in model $\mathcal{A}$. As before, the figure demonstrates the change of the spectrum with increasing 't Hooft coupling g_{ns} which finally is fixed to account for the flavor octet ground-state hyperons. Note that the effects of 't Hooft's force are again significantly smaller than in the corresponding nucleon and Λ sectors. But they are sufficiently large to provide a quantitatively correct explanation for at least some of the observed hyperfine splittings in the $1\hbar\omega$ shell, as, *e.g.*, that of the two best-established states $\Sigma\frac{3}{2}^-(1670,****)$ and $\Sigma\frac{5}{2}^-(1775,****)$.

Table 10. Calculated positions of Σ states assigned to the negative-parity $1\hbar\omega$ shell in comparison to the corresponding experimental mass values taken from [24]. Notation as in table 1.

Experimental state [24]	PW	J^π	Rating	Mass range [MeV] [24]	Model state in model $\mathcal{A}$	Model state in model $\mathcal{B}$
$\Sigma(1620)$	S_{11}	$\frac{1}{2}^-$	**	1594–1643	$[\Sigma\frac{1}{2}^-]_1(1628)$	$[\Sigma\frac{1}{2}^-]_1(1704)$
$\Sigma(1750)$	S_{11}	$\frac{1}{2}^-$	***	1730–1800	$[\Sigma\frac{1}{2}^-]_2(1771)$ $[\Sigma\frac{1}{2}^-]_3(1798)$	$[\Sigma\frac{1}{2}^-]_2(1814)$
$\Sigma(2000)$	S_{11}	$\frac{1}{2}^-$	*	1755–2044		$[\Sigma\frac{1}{2}^-]_3(1897)$
$\Sigma(1580)$	D_{13}	$\frac{3}{2}^-$	**	1578–1587		
$\Sigma(1670)$	D_{13}	$\frac{3}{2}^-$	****	1665–1685	$[\Sigma\frac{3}{2}^-]_1(1669)$	$[\Sigma\frac{3}{2}^-]_1(1706)$
					$[\Sigma\frac{3}{2}^-]_2(1728)$	$[\Sigma\frac{3}{2}^-]_2(1798)$
					$[\Sigma\frac{3}{2}^-]_3(1781)$	$[\Sigma\frac{3}{2}^-]_3(1820)$
$\Sigma(1940)$	D_{13}	$\frac{3}{2}^-$	***	1900–1950		
$\Sigma(1775)$	D_{15}	$\frac{5}{2}^-$	****	1770–1780	$[\Sigma\frac{5}{2}^-]_1(1770)$	$[\Sigma\frac{5}{2}^-]_1(1792)$

Table 11. Configuration mixing of negative-parity Σ states in model $\mathcal{A}$ assigned to the $1\hbar\omega$ band. For explanation see also caption of table 4.

J^π	Model state in model $\mathcal{A}$	pos. neg.	^{2}8[56] ^{2}8[56]	^{2}8[70] ^{2}8[70]	^{4}8[70] ^{4}8[70]	^{2}8[20] ^{2}8[20]	^{4}10[56] ^{4}10[56]	^{2}10[70] ^{2}10[70]
$\frac{1}{2}^-$	$[\Sigma\frac{1}{2}^-]_1(1628)$	98.6 1.4	5.4 0.7	**87.4** 0.3	2.3 0.1	0.1 0.3	0.0 0.0	3.4 0.0
	$[\Sigma\frac{1}{2}^-]_2(1771)$	99.3 0.7	0.2 0.0	2.9 0.0	**94.6** 0.5	0.2 0.1	0.3 0.0	1.1 0.0
	$[\Sigma\frac{1}{2}^-]_3(1798)$	99.2 0.8	0.1 0.0	2.8 0.0	1.7 0.0	0.3 0.0	0.0 0.4	**94.4** 0.3
$\frac{3}{2}^-$	$[\Sigma\frac{3}{2}^-]_1(1669)$	98.9 1.1	5.1 0.2	**89.0** 0.3	1.2 0.4	0.1 0.2	0.0 0.0	3.4 0.0
	$[\Sigma\frac{3}{2}^-]_2(1728)$	99.2 0.8	0.1 0.1	0.1 0.2	**82.7** 0.3	0.1 0.1	0.2 0.0	16.0 0.1
	$[\Sigma\frac{3}{2}^-]_3(1781)$	99.2 0.8	0.2 0.0	4.4 0.1	15.0 0.1	0.2 0.0	0.0 0.1	**79.3** 0.5
$\frac{5}{2}^-$	$[\Sigma\frac{5}{2}^-]_1(1770)$	99.2 0.8	0.0 0.0	0.0 0.2	**99.0** 0.5	0.0 0.1	0.2 0.0	0.0 0.0

In the following discussion we will investigate in detail the situation for each spin sector $\frac{1}{2}^-$, $\frac{3}{2}^-$, and $\frac{5}{2}^-$ in turn:

In the $\Sigma\frac{5}{2}^-$ sector our model $\mathcal{A}$ predicts a single $1\hbar\omega$ state at 1770 MeV which accurately accounts for the single four-star resonance $\Sigma\frac{5}{2}^-(1775,****)$ observed in the D_{15} partial wave. Due to its maximally possible spin $J=\frac{5}{2}$ this state, which is predicted to be purely ^{4}8[70], remains totally unaffected by 't Hooft's force as illustrated in fig. 12. This state is the flavor octet partner of the $\Lambda\frac{5}{2}^-(1830,****)$ and the $N\frac{5}{2}^-(1675,****)$ in the Λ and nucleon spectrum, respectively. It is quite interesting to compare this result with that in the corresponding $\Lambda\frac{5}{2}^-$ sector where our model likewise predicted a purely ^{4}8[70] state in the $1\hbar\omega$ shell at 1828 MeV that exactly matches the measured position of the $\Lambda\frac{5}{2}^-(1830,****)$. But note the significant mass difference of ~ 55 MeV between the $\Lambda\frac{5}{2}^-(1830,****)$ and the $\Sigma\frac{5}{2}^-(1775,****)$ although both states have exactly the same flavor content of two non-strange and one strange quark. This mass splitting is roughly of the same order of magnitude as the $\Sigma-\Lambda$ ground-state splitting which amounts to ~ 75 MeV, but it shows the reversed order; see fig. 13 where the mass splittings between these Σ and Λ states (model $\mathcal{A}$ and experiment) is graphically illustrated. Due to the accurate predictions for both $J^\pi=\frac{5}{2}^-$ resonances this mass splitting is remarkably well reproduced with 58 MeV in our model $\mathcal{A}$. But, unlike the $\Sigma-\Lambda$ ground-state splitting which originates from 't Hooft's interaction due to the different 't Hooft couplings $g_{nn}>g_{ns}$, the reversed $\Lambda\frac{5}{2}^-$–$\Sigma\frac{5}{2}^-$ splitting is not an instanton-induced effect, since both $J^\pi=\frac{5}{2}^-$ states are entirely determined by the confinement potential alone. It is a spin-independent effect arising due to the flavor $SU(3)$ breaking from the non-strange and strange quark mass difference. This effect is qualitatively understandable considering once again the naive non-relativistic oscillator model, where the coordinates are chosen such that the two non-strange quarks

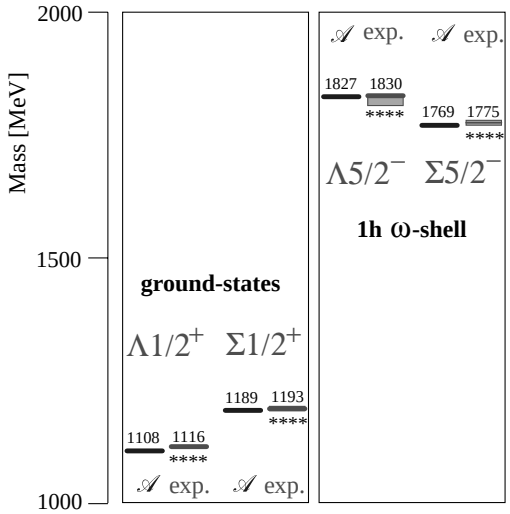

Fig. 13. Mass splittings between Λ and Σ states. See the text for further explanation.

move in the ρ-oscillator and the strange quark moves relative to the non-strange quark pair in the λ-oscillator (see [30,26]). Then, due to the heavier strange quark mass, the λ-frequency ω_λ is smaller than the ρ-frequency ω_ρ, namely $\omega_\lambda = \omega_\rho\,(\frac{2m_n+m_s}{3m_s})^{\frac{1}{2}} < \omega_\rho$. Owing to Pauli's principle, the total $L = 1$ wave functions must be symmetric under exchange of the two non-strange quarks. Both states, $\Lambda\frac{5}{2}^-$ and $\Sigma\frac{5}{2}^-$, contain a spin-quartet wave function which is symmetric under interchange of any two quarks. But the crucial difference between the two states is their distinct isospin: the flavor wave function of $\Lambda\frac{5}{2}^-$ $(T = 0)$ is antisymmetric while that of $\Sigma\frac{5}{2}^-$ $(T = 1)$ is symmetric under exchange of the two non-strange quarks. To achieve total symmetry the $\Lambda\frac{5}{2}^-$ must be orbitally excited in the odd ρ-coordinate, whereas $\Sigma\frac{5}{2}^-$ has to be orbitally excited in the even λ-coordinate. Since the ρ-oscillator has the higher frequency, the $\Lambda\frac{5}{2}^-$ thus is heavier than the $\Sigma\frac{5}{2}^-$. The accurate prediction of this mass difference in our model shows that the quark mass difference $m_s - m_n$ fixed from the ground-state decuplet in fact is correctly affecting the energy levels of the first excited $\Lambda\frac{5}{2}^-$ and $\Sigma\frac{5}{2}^-$ states. Moreover, it provides good support for our confinement force which is chosen flavor independent. Finally, it should be noted here that, in nice agreement with our predictions, the lowest $\Sigma\frac{5}{2}^+$ state does *not* form an approximate parity doublet structure together with the lowest excitation in $\Sigma\frac{5}{2}^-$. In this respect the Σ spectrum differs significantly from the nucleon and Λ spectrum which both reveal a well-established parity doublet structure formed by the lowest excitations in $N\frac{5}{2}^\pm$ and $\Lambda\frac{5}{2}^\pm$, respectively. In the $N\frac{5}{2}^+$ and $\Lambda\frac{5}{2}^+$ sectors the effect of a strong scalar *non-strange* diquark correlation was sufficiently large to lower the first excitations deeply enough to become nearly degenerate with the lowest excitations $N\frac{5}{2}^-$ and $\Lambda\frac{5}{2}^-$, respectively. In accordance with the experimental findings $(\Sigma\frac{5}{2}^+(1915,****) \leftrightarrow \Sigma\frac{5}{2}^-(1775,****))$, the effect of the scalar *non-strange–strange* diquark correlation in the corresponding lowest $\Sigma\frac{5}{2}^+$ state is, however, too weak to generate likewise a degeneracy for the lowest $\Sigma\frac{5}{2}^\pm$ states.

In the $\Sigma\frac{3}{2}^-$ sector the currently available data of altogether three observed resonances significantly disagree with our predictions for the three states expected in the $1\hbar\omega$ shell. However, the best established of these states, the four-star resonance $\Sigma\frac{3}{2}^-(1670,****)$, is exactly reproduced by the lowest state predicted in this sector at 1669 MeV. This state turns out to be dominantly $^2 8[70]$ $(\sim 90\%)$ and, as shown in fig. 12, it is slightly lowered by 't Hooft's interaction. Hence, it is the counterpart of $\Lambda\frac{3}{2}^-(1690,****)$ and $N\frac{3}{2}^-(1520,****)$ in the Λ and nucleon spectrum, respectively. In addition to the $\Sigma\frac{3}{2}^-(1670,****)$ there are two further D_{13} resonances extracted from experiment, one poorly established two-star resonance $\Sigma\frac{3}{2}^-(1580,**)$ lying even below the $\Sigma\frac{3}{2}^-(1670,****)$, and another with three-star rating, the $\Sigma\frac{3}{2}^-(1940,***)$, which lies exceptionally high at almost 2 GeV. However, the two remaining $\Sigma\frac{3}{2}^-$ states predicted in the $1\hbar\omega$ band by no means can account for these two states observed. Our result is quite similar to that of other constituent quark models [30,31]. The calculation with model $\mathcal{A}$ yields two rather close states at 1728 and 1781 MeV. The first one is dominantly $(\sim 83\%)$ a $^4 8[70]$ state and is the expected flavor octet partner of the $N\frac{3}{2}^-(1700,***)$. The second, dominantly $^2 10[70]$ state $(\sim 80\%)$ is the expected flavor decuplet counterpart of the $\Delta(1700,****)$. The rather puzzling experimental situation of the $1\hbar\omega$ states in the $\Sigma\frac{3}{2}^-$ sector does absolutely not fit in the systematics observed in the N and Δ sector and in general is completely incomprehensible in a potential model framework. Concerning the $\Sigma\frac{3}{2}^-(1940,***)$ one could speculate whether it is a member of the $3\hbar\omega$ band (see table 12). But even then the measured position remains puzzling. Although 't Hooft's force selectively lowers two states of $3\hbar\omega$ band (see fig. 12), the shift is much too weak to account for this state. The lowest $\Sigma\frac{3}{2}^-$ state of the $3\hbar\omega$ shell is predicted at 2139 MeV but the $\Sigma\frac{3}{2}^-(1940,***)$ lies exactly in between this lowest predicted $3\hbar\omega$ state and the highest predicted $1\hbar\omega$ state. It is worthwhile to mention here that not all analyses of $\bar{K}N$ scattering data require this state (see [24] and references therein). The evidence for the poorly determined $\Sigma\frac{3}{2}^-(1580,**)$ in any case is not compulsory. Thus, except for the well-established $\Sigma\frac{3}{2}^-(1670,****)$, the experimental situation in $\Sigma\frac{3}{2}^-$ is quite inconclusive and a verification of these rather old data by new experiments would be highly desirable.

The situation appears slightly better for the $\Sigma\frac{1}{2}^-$ sector. The lowest state predicted at 1628 MeV nicely coincides with the $\Sigma\frac{1}{2}^-(1620,**)$. This state may be viewed as the flavor octet partner of the Λ- and nucleon states

Table 12. Calculated positions of the lightest few Σ states assigned to the negative-parity $3\hbar\omega$ shell in comparison to the corresponding experimental mass values taken from [24]. Notation as in table 1.

Experimental state [24]	PW	J^π	Rating	Mass range [MeV] [24]	Model state in model $\mathcal{A}$	Model state in model $\mathcal{B}$
$\Sigma(2000)$	S_{11}	$\frac{1}{2}^-$	*	1755–2044		
					$[\Sigma\frac{1}{2}^-]_4(2111)$	$[\Sigma\frac{1}{2}^-]_4(2249)$
					$[\Sigma\frac{1}{2}^-]_5(2136)$	$[\Sigma\frac{1}{2}^-]_5(2326)$
					$[\Sigma\frac{1}{2}^-]_6(2251)$	$[\Sigma\frac{1}{2}^-]_6(2377)$
					$[\Sigma\frac{1}{2}^-]_7(2264)$	$[\Sigma\frac{1}{2}^-]_7(2382)$
					$[\Sigma\frac{1}{2}^-]_8(2288)$	$[\Sigma\frac{1}{2}^-]_8(2413)$
$\Sigma(1940)$	D_{13}	$\frac{3}{2}^-$	***	1900–1950		
					$[\Sigma\frac{3}{2}^-]_4(2139)$	$[\Sigma\frac{3}{2}^-]_4(2229)$
					$[\Sigma\frac{3}{2}^-]_5(2171)$	$[\Sigma\frac{3}{2}^-]_5(2325)$
					$[\Sigma\frac{3}{2}^-]_6(2203)$	$[\Sigma\frac{3}{2}^-]_6(2368)$
					$[\Sigma\frac{3}{2}^-]_7(2244)$	$[\Sigma\frac{3}{2}^-]_7(2372)$
					$[\Sigma\frac{3}{2}^-]_8(2263)$	$[\Sigma\frac{3}{2}^-]_8(2383)$
	D_{15}	$\frac{5}{2}^-$			$[\Sigma\frac{5}{2}^-]_2(2174)$	$[\Sigma\frac{5}{2}^-]_2(2296)$
					$[\Sigma\frac{5}{2}^-]_3(2226)$	$[\Sigma\frac{5}{2}^-]_3(2364)$
					$[\Sigma\frac{5}{2}^-]_4(2268)$	$[\Sigma\frac{5}{2}^-]_4(2377)$
					$[\Sigma\frac{5}{2}^-]_5(2305)$	$[\Sigma\frac{5}{2}^-]_5(2382)$
$\Sigma(2100)$	G_{17}	$\frac{7}{2}^-$	*	2040–2150		
					$[\Sigma\frac{7}{2}^-]_1(2236)$	$[\Sigma\frac{7}{2}^-]_1(2293)$
					$[\Sigma\frac{7}{2}^-]_2(2285)$	$[\Sigma\frac{7}{2}^-]_2(2373)$
					$[\Sigma\frac{7}{2}^-]_3(2320)$	$[\Sigma\frac{7}{2}^-]_3(2387)$
					$[\Sigma\frac{7}{2}^-]_4(2353)$	$[\Sigma\frac{7}{2}^-]_4(2420)$
	G_{19}	$\frac{9}{2}^-$			$[\Sigma\frac{9}{2}^-]_1(2325)$	$[\Sigma\frac{9}{2}^-]_1(2367)$
					$[\Sigma\frac{9}{2}^-]_2(2418)$	$[\Sigma\frac{9}{2}^-]_2(2435)$

$\Lambda\frac{1}{2}^-(1670,****)$ and $N\frac{1}{2}^-(1535,****)$ since it likewise exhibits a dominant ^{2}8[70] contribution ($\sim$ 88%). Similar to its N and Λ counterparts this state is lowered by 't Hooft's force (see fig. 12), here by roughly 80 MeV which is just the right size to correctly reproduce the position of the $\Sigma\frac{1}{2}^-(1620,**)$ within its experimental uncertainties. We can reproduce as well the more established three-star state $\Sigma\frac{1}{2}^-(1750,***)$, but our model predicts within its range of possible values two close states at 1771 and 1798 MeV although so far only one state is experimentally resolved in this mass region of the S_{11} partial wave. But there is another very poorly determined structure seen in the S_{11} partial wave, the one-star $\Sigma\frac{1}{2}^-(2000,*)$, whose large range of possible values even overlaps with that of the $\Sigma\frac{1}{2}^-(1750,***)$. The first of the two close states predicted turns out to be a dominantly ^{4}8[70] state ($\sim$ 95%). It corresponds to the $N\frac{1}{2}^-(1650,****)$ and the $\Lambda\frac{1}{2}^-(1800,***)$ in the N and Λ spectrum and similarly shows an upwards mass shift due to the repulsive action of 't Hooft's force in the pseudo-scalar diquark channel. In this way the instanton force provides a good explanation for the mass splitting between the $\Sigma\frac{1}{2}^-(1620,**)$ and the $\Sigma\frac{1}{2}^-(1750,***)$, as shown in fig. 12. The second state predicted close to the $\Sigma\frac{1}{2}^-(1750,***)$ is hardly influenced by 't Hooft's force, since it consists of an almost pure ^{2}10[70] configuration. This state is the expected flavor decuplet partner of the Δ-resonance $\Delta\frac{1}{2}^-(1620,****)$.

Finally, there remains to comment on the negative-parity states of the $3\hbar\omega$ band. Our predictions for the lightest few states in this shell are summarized in table 12.

All states predicted in this band structure lie beyond 2100 MeV. Concerning the instanton-induced hyperfine structures (see fig. 12), we should note that 't Hooft's force selectively lowers a group of six (dominantly ^{2}8[56] and ^{2}8[70]) states in the sectors with spins J from $\frac{1}{2}$ to $\frac{7}{2}$. In fact, we find the same systematics observed for the corresponding group of six states in the nucleon $3\hbar\omega$ band [5]. But once again the mass shift here is rather small and only the two lowered states in the $J^\pi = \frac{1}{2}^-$ sector become significantly isolated from the other $3\hbar\omega$ states. In the $\Sigma\frac{1}{2}^-$ and $\Sigma\frac{3}{2}^-$ the downward mass shift cannot account for the positions of the rather poorly established resonance $\Sigma\frac{1}{2}^-(2000,*)$ and the $\Sigma\frac{3}{2}^-(1940,***)$ which already could not be associated with states predicted in the $1\hbar\omega$ shell. The one-star state $\Sigma\frac{7}{2}^-(2100,*)$ is the only effect seen in the G_{17} partial wave. According to its total spin $J = \frac{7}{2}$ this state definitely cannot belong to the $1\hbar\omega$ shell, but must be, if we take it seriously, a member of the $3\hbar\omega$ band. Our model has the same problems to

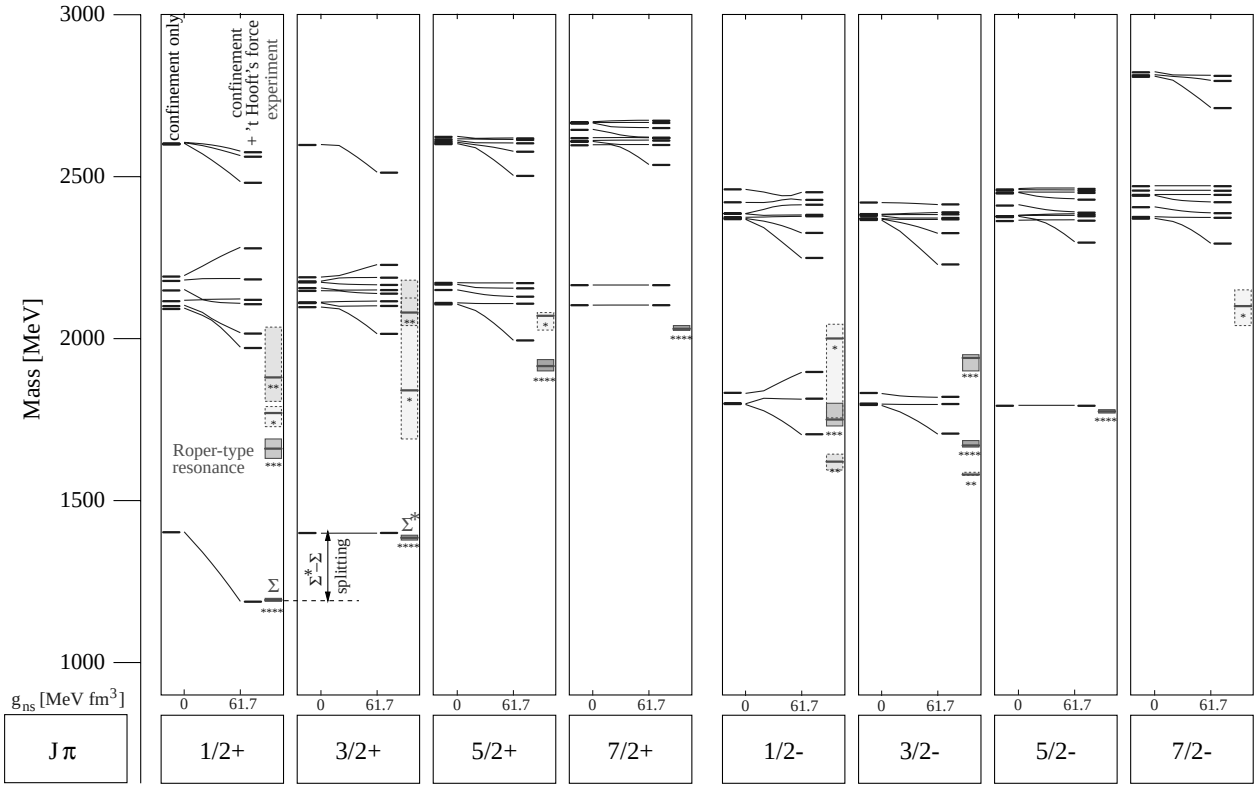

Fig. 14. Influence of the instanton-induced interaction on the energy levels of the positive-parity (left) and negative-parity (right) Σ states in model $\mathcal{B}$. The curves illustrate the variation of energy levels with increasing 't Hooft coupling g_{ns} which is finally fixed to account for the hyperon splittings $\Sigma^* - \Sigma - \Lambda$ and $\Xi^* - \Xi$.

explain this structure as all other constituent quark models. The downward mass shift of the dominantly $^2 8[70]$ state in the $\Sigma\frac{7}{2}^-$ sector is much too small to explain the puzzling low position of the $\Sigma\frac{7}{2}^-(2100,*)$. Its position predicted at 2236 MeV is far above the PDG quoted position for the $\Sigma\frac{7}{2}^-(2100,*)$. We should note in this respect that the corresponding lowest excitation in $\Lambda\frac{7}{2}^-$ is observed at the same resonance position, but remember that the well-established $\Lambda\frac{7}{2}^-(2100,****)$ could be explained due to the much stronger effect of a scalar *non-strange* diquark correlation. We thus do not worry about this poorly established one-star resonance whose existence is highly questionable anyway.

3.2.3 Comment on the results of model $\mathcal{B}$

So far we discussed entirely the predictions of model $\mathcal{A}$ which in the course of our previous investigations of the N and Λ spectra turned out to achieve significantly better agreement with the phenomenology than model $\mathcal{B}$. For the sake of completeness we will conclude the discussion of the Σ sector briefly commenting on the results of model $\mathcal{B}$. Comparing the predicted Σ spectra of models $\mathcal{A}$ and $\mathcal{B}$ in figs. 9 and 10, respectively, the superior predictive power of model $\mathcal{A}$ to that of model $\mathcal{B}$ is once again confirmed. The Σ spectrum predicted in model $\mathcal{B}$ reveals essentially the same shortcomings that could be already exposed in the discussion of the nucleon and Λ spectra. Similar to the Λ spectrum the centroids of the $1\hbar\omega$ and $2\hbar\omega$ band structures again are predicted too high compared to that of the observed states.

Figure 14 displays for model $\mathcal{B}$ the effect of 't Hooft's force on the energy levels of the positive- and negative-parity Σ states. In comparison to the corresponding figs. 11 and 12 of model $\mathcal{A}$, we find once again that the interplay of 't Hooft's residual interaction with the relativistic effects of the confinement kernel $\mathcal{B}$ induces hyperfine structures which differ significantly from those induced in model $\mathcal{A}$. Similar to the $N\frac{1}{2}^+$ and $\Lambda\frac{1}{2}^+$ sector the largest discrepancies between both models show up in the $\Sigma\frac{1}{2}^+$ sector, where the instanton force in model $\mathcal{B}$ cannot account for the low position of the Roper-type resonance $\Sigma\frac{1}{2}^+(1660,***)$.

3.3 Summary for the Σ spectrum

To summarize the discussion of this section, we presented the predicted Σ spectra of both model versions in comparison with the rather scarce currently available experimental data. Model $\mathcal{A}$ provides a good description for all well-established four-star resonances in the positive-

and negative-parity sectors. Studying the influence of 't Hooft's residual force, which here exclusively acts in the scalar non-strange–strange diquark channel, we found significantly smaller effects than in the Λ and N sectors, where the much stronger effects of the non-strange diquark correlation emerged. This is consistent with the in fact smaller hyperfine splittings observed in this flavor sector and in particular it nicely explains the absence of approximate parity doublet structures, for which there is (in contrast to the N and Λ sectors) hardly any evidence in the experimental Σ spectrum. Along with the well-reproduced $\Sigma\frac{3}{2}^+(1385,****)$–$\Sigma\frac{1}{2}^+(1193,****)$ ground-state splitting, 't Hooft's force in general provides again a rather good description of the observed intra-band structures as far as they are experimentally resolved by the partly inconclusive data. In particular, we found a strong lowering of the lowest $\Sigma\frac{1}{2}^+$ excitation corresponding to the low-lying $\Sigma\frac{1}{2}^+(1660,***)$, the counterpart of the Roper resonance. Finally, we should mention that once again our fully relativistic approach (model $\mathcal{A}$) shows significant improvements relative to the corresponding non-relativistic model of Blask *et al.* [28,29].

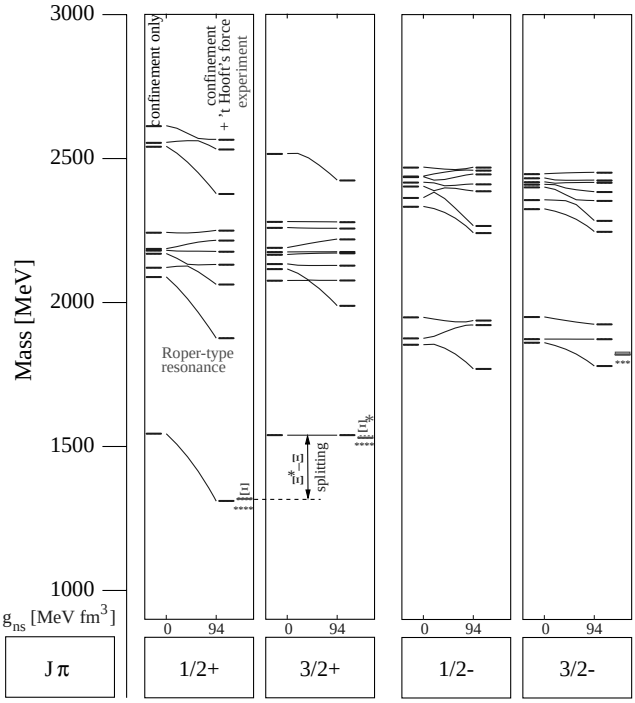

Fig. 15. Instanton-induced hyperfine splittings of the positive- (left) and negative-parity (right) Ξ states in model $\mathcal{A}$. On the left in each column the spectrum from confinement alone is shown. The curves show the change of the spectrum as a function of the 't Hooft coupling g_{ns} which finally is fixed (right spectrum) from the hyperon splittings $\Sigma^*-\Sigma-\Lambda$ and $\Xi^*-\Xi$. The rightmost spectrum shows for comparison the experimental data.

4 The Ξ-resonance spectrum

In this section we present our predictions for the excited Ξ-baryons with strangeness $S^*=-2$ and isospin $T=\frac{1}{2}$. Our results in this flavor sector are almost entirely predictive, due to the lack of experimental data. Not much is known about Ξ-resonances since no direct formation is possible and the Ξ-baryons can only be produced as a part of a final state which in general is topologically complicated and difficult to study. Moreover, the production cross-sections are rather small [24]. Apart from the well-established ground states $\Xi\frac{1}{2}^+(1318,****)$ and $\Xi\frac{3}{2}^+(1530,****)$ there is only one single negative-parity excited state whose quantum numbers are established, *i.e.* the three-star resonance $\Xi\frac{3}{2}^-(1820,***)$. There are further evidences for Ξ-resonances (even with a three-star rating), but in all cases spin and parity of these states are completely undetermined [24].

There is not much to say about the structures expected in this flavor sector: There are exactly the same degrees of freedom as in the Σ sector discussed in the preceding section. The octet and decuplet flavor wave function corresponding to that in the Σ sector only differ by the interchange $|n\rangle \leftrightarrow |s\rangle$ of the non-strange and strange quark flavors and the Salpeter amplitudes $\Phi^{\Xi}_{J^\pi}$ of excited Ξ states with spin and parity J^π are obtained by the embedding map (see ref. [4])

$$\Phi^{\Xi}_{J^\pi} \;=\; T^{+++}\varphi^{\Xi}_{J^\pi} \;+\; T^{---}\varphi^{\Xi}_{J^{-\pi}} \qquad (9)$$

of Pauli spinors $\varphi^{\Xi}_{J^\pi}$ and $\varphi^{\Xi}_{J^{-\pi}}$ which, analogous to the Σ states, decompose into the spin-flavor $SU(6)$-configurations

$$\begin{aligned}|\varphi^{\Xi}_{J^\pm}\rangle = {}& |\Xi\ J^\pm,\ {}^2\!8[56]\rangle \;+\; |\Xi\ J^\pm,\ {}^2\!8[70]\rangle \\ & + |\Xi\ J^\pm,\ {}^4\!8[70]\rangle \;+\; |\Xi\ J^\pm,\ {}^2\!8[20]\rangle \\ & + |\Xi\ J^\pm,\ {}^4\!10[56]\rangle \;+\; |\Xi\ J^\pm,\ {}^2\!10[70]\rangle, \qquad (10)\end{aligned}$$

with the flavor-octet and decuplet contributions

$$|\Xi\ J^\pm,\ {}^2\!8[56]\rangle := \sum_L \left[|\psi^{L\,\pm}_{\mathcal{S}}\rangle\otimes\frac{1}{\sqrt{2}}\left(|\chi^{\frac{1}{2}}_{\mathcal{M}_\mathcal{A}}\rangle\otimes|\phi^{\Xi}_{\mathcal{M}_\mathcal{A}}\rangle+|\chi^{\frac{1}{2}}_{\mathcal{M}_\mathcal{S}}\rangle\otimes|\phi^{\Xi}_{\mathcal{M}_\mathcal{S}}\rangle\right)\right]^J,$$

$$\begin{aligned}|\Xi\ J^\pm,\ {}^2\!8[70]\rangle := {}& \sum_L \left[\frac{1}{2}\,|\psi^{L\,\pm}_{\mathcal{M}_\mathcal{A}}\rangle\otimes\left(|\chi^{\frac{1}{2}}_{\mathcal{M}_\mathcal{A}}\rangle\otimes|\phi^{\Xi}_{\mathcal{M}_\mathcal{S}}\rangle + |\chi^{\frac{1}{2}}_{\mathcal{M}_\mathcal{S}}\rangle\otimes|\phi^{\Xi}_{\mathcal{M}_\mathcal{A}}\rangle\right)\right. \\ & \left. +\frac{1}{2}\,|\psi^{L\,\pm}_{\mathcal{M}_\mathcal{S}}\rangle\otimes\left(|\chi^{\frac{1}{2}}_{\mathcal{M}_\mathcal{A}}\rangle\otimes|\phi^{\Xi}_{\mathcal{M}_\mathcal{A}}\rangle - |\chi^{\frac{1}{2}}_{\mathcal{M}_\mathcal{S}}\rangle\otimes|\phi^{\Xi}_{\mathcal{M}_\mathcal{S}}\rangle\right)\right]^J,\end{aligned}$$

Table 13. Calculated positions of Ξ states assigned to the negative-parity $1\hbar\omega$ shell. Notation as in table 1.

Experimental state [24]	PW	J^π	Rating	Mass range [MeV] [24]	Model state in model $\mathcal{A}$	Model state in model $\mathcal{B}$
	S_{11}	$\frac{1}{2}^-$			$[\Xi\frac{1}{2}^-]_1(1770)$	$[\Xi\frac{1}{2}^-]_1(1855)$
					$[\Xi\frac{1}{2}^-]_2(1922)$	$[\Xi\frac{1}{2}^-]_2(1976)$
					$[\Xi\frac{1}{2}^-]_3(1938)$	$[\Xi\frac{1}{2}^-]_3(2112)$
$\Xi(1820)$	D_{13}	$\frac{3}{2}^-$	***	1818–1828	$[\Xi\frac{3}{2}^-]_1(1780)$	$[\Xi\frac{3}{2}^-]_1(1868)$
					$[\Xi\frac{3}{2}^-]_2(1873)$	$[\Xi\frac{3}{2}^-]_2(1979)$
					$[\Xi\frac{3}{2}^-]_3(1924)$	$[\Xi\frac{3}{2}^-]_3(1994)$
	D_{15}	$\frac{5}{2}^-$			$[\Xi\frac{5}{2}^-]_1(1955)$	$[\Xi\frac{5}{2}^-]_1(1991)$

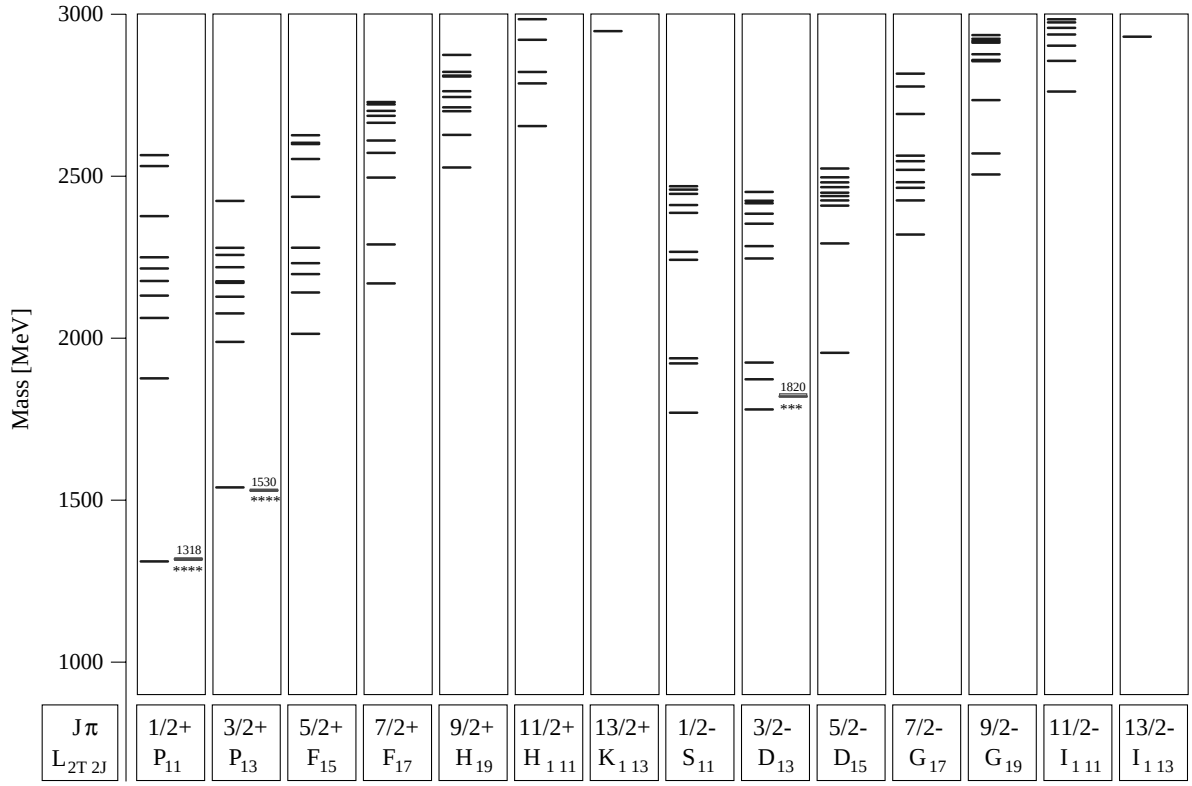

Fig. 16. The predicted positive- and negative-parity *Ξ-resonance spectrum* with isospin $T = \frac{1}{2}$ and strangeness $S^* = -2$ in *model $\mathcal{A}$* (left part of each column) in comparison to the experimental spectrum taken from Particle Data Group [24] (right part of each column). The resonances are classified by the total spin J and parity π. The experimental resonance position is indicated by a bar, the corresponding uncertainty by the shaded box; the status of each resonance is indicated by stars. At most ten radial excitations are shown in each column.

$$|\Xi\ J^\pm,\ {}^4 8[70]\rangle := \sum_L \left[\frac{1}{\sqrt{2}}\Big(|\psi^{L\,\pm}_{\mathcal{M}_\mathcal{A}}\rangle\otimes|\chi^{\frac{3}{2}}_{\mathcal{S}}\rangle\otimes|\phi^{\Xi}_{\mathcal{M}_\mathcal{A}}\rangle - |\psi^{L\,\pm}_{\mathcal{M}_\mathcal{S}}\rangle\otimes|\chi^{\frac{3}{2}}_{\mathcal{S}}\rangle\otimes|\phi^{\Xi}_{\mathcal{M}_\mathcal{S}}\rangle\Big)\right]^J,$$

$$|\Xi\ J^\pm,\ {}^2 8[20]\rangle := \sum_L \left[|\psi^{L\,\pm}_{\mathcal{A}}\rangle\otimes\frac{1}{\sqrt{2}}\Big(|\chi^{\frac{1}{2}}_{\mathcal{M}_\mathcal{A}}\rangle\otimes|\phi^{\Xi}_{\mathcal{M}_\mathcal{S}}\rangle - |\chi^{\frac{1}{2}}_{\mathcal{M}_\mathcal{S}}\rangle\otimes|\phi^{\Xi}_{\mathcal{M}_\mathcal{A}}\rangle\Big)\right]^J,$$

$$|\Xi\ J^\pm,\ {}^4 10[56]\rangle := \sum_L \left[|\psi^{L\,\pm}_{\mathcal{S}}\rangle\otimes|\chi^{\frac{3}{2}}_{\mathcal{S}}\rangle\right]^J\otimes|\phi^{\Xi}_{\mathcal{S}}\rangle,$$

$$|\Xi\ J^\pm,\ {}^2 10[70]\rangle := \sum_L \left[\frac{1}{\sqrt{2}}\Big(|\psi^{L\,\pm}_{\mathcal{M}_\mathcal{S}}\rangle\otimes|\chi^{\frac{1}{2}}_{\mathcal{M}_\mathcal{S}}\rangle + |\psi^{L\,\pm}_{\mathcal{M}_\mathcal{A}}\rangle\otimes|\chi^{\frac{1}{2}}_{\mathcal{M}_\mathcal{A}}\rangle\Big)\right]^J\otimes|\phi^{\Xi}_{\mathcal{S}}\rangle. \tag{11}$$

Again 't Hooft's force acts here for non-strange–strange quark pairs which are antisymmetric in flavor thus

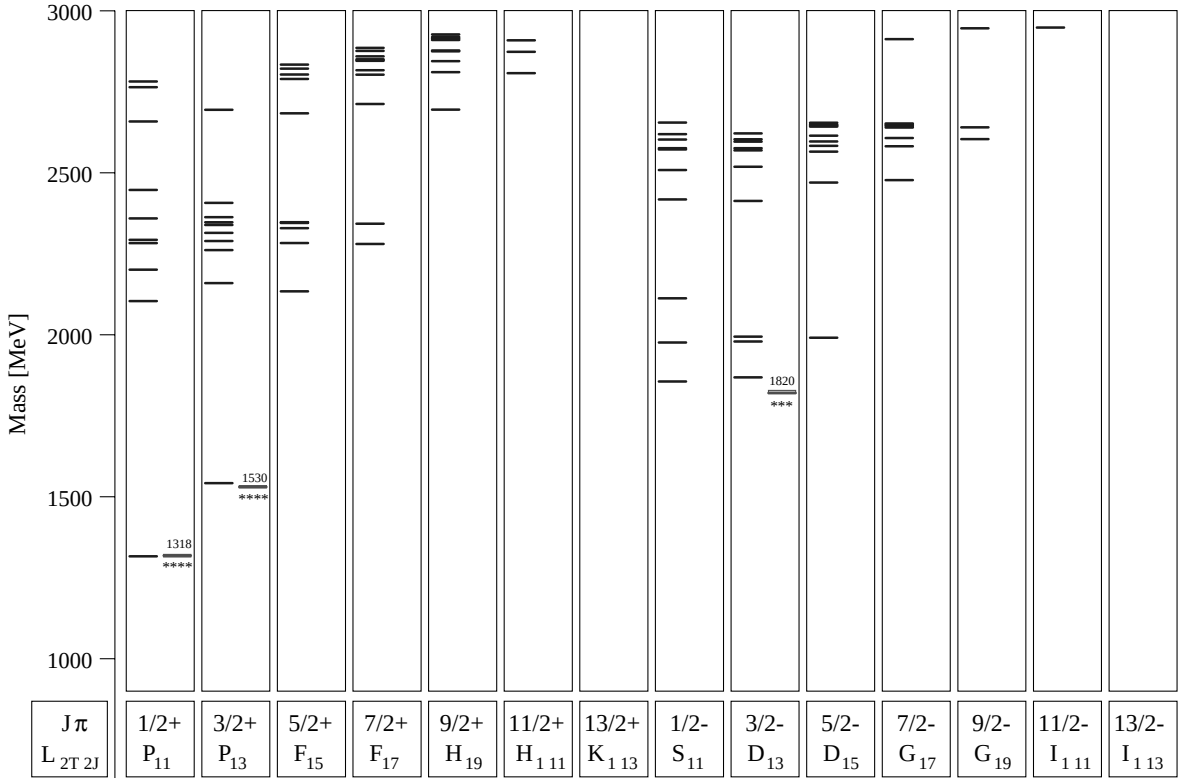

Fig. 17. The predicted positive- and negative-parity *Ξ-resonance spectrum* with isospin $T = \frac{1}{2}$ and strangeness $S^* = -2$ in *model* $\mathcal{B}$ (left part of each column) in comparison to the experimental spectrum taken from Particle Data Group [24] (right part of each column). The resonances are classified by the total spin J and parity π. See also caption to fig. 16.

Table 14. Calculated positions of Ξ states assigned to the positive-parity $2\hbar\omega$ shell. Notation as in table 1.

Experimental state [24]	PW	J^π	Rating	Mass range [MeV] [24]	Model state in model $\mathcal{A}$	Model state in model $\mathcal{B}$
	P_{11}	$\frac{1}{2}^+$			$[\Xi\frac{1}{2}^+]_2(1876)$	$[\Xi\frac{1}{2}^+]_2(2104)$
					$[\Xi\frac{1}{2}^+]_3(2062)$	$[\Xi\frac{1}{2}^+]_3(2201)$
					$[\Xi\frac{1}{2}^+]_4(2131)$	$[\Xi\frac{1}{2}^+]_4(2283)$
					$[\Xi\frac{1}{2}^+]_5(2176)$	$[\Xi\frac{1}{2}^+]_5(2293)$
					$[\Xi\frac{1}{2}^+]_6(2215)$	$[\Xi\frac{1}{2}^+]_6(2359)$
					$[\Xi\frac{1}{2}^+]_7(2249)$	$[\Xi\frac{1}{2}^+]_7(2446)$
	P_{13}	$\frac{3}{2}^+$			$[\Xi\frac{3}{2}^+]_2(1988)$	$[\Xi\frac{3}{2}^+]_2(2159)$
					$[\Xi\frac{3}{2}^+]_3(2076)$	$[\Xi\frac{3}{2}^+]_3(2261)$
					$[\Xi\frac{3}{2}^+]_4(2128)$	$[\Xi\frac{3}{2}^+]_4(2289)$
					$[\Xi\frac{3}{2}^+]_5(2170)$	$[\Xi\frac{3}{2}^+]_5(2314)$
					$[\Xi\frac{3}{2}^+]_6(2175)$	$[\Xi\frac{3}{2}^+]_6(2338)$
					$[\Xi\frac{3}{2}^+]_7(2219)$	$[\Xi\frac{3}{2}^+]_7(2347)$
					$[\Xi\frac{3}{2}^+]_8(2257)$	$[\Xi\frac{3}{2}^+]_8(2363)$
					$[\Xi\frac{3}{2}^+]_9(2279)$	$[\Xi\frac{3}{2}^+]_9(2407)$
	F_{15}	$\frac{5}{2}^+$			$[\Xi\frac{5}{2}^+]_1(2013)$	$[\Xi\frac{5}{2}^+]_1(2134)$
					$[\Xi\frac{5}{2}^+]_2(2141)$	$[\Xi\frac{5}{2}^+]_2(2283)$
					$[\Xi\frac{5}{2}^+]_3(2197)$	$[\Xi\frac{5}{2}^+]_3(2329)$
					$[\Xi\frac{5}{2}^+]_4(2231)$	$[\Xi\frac{5}{2}^+]_4(2345)$
					$[\Xi\frac{5}{2}^+]_5(2279)$	$[\Xi\frac{5}{2}^+]_5(2347)$
	F_{17}	$\frac{7}{2}^+$			$[\Xi\frac{7}{2}^+]_1(2169)$	$[\Xi\frac{7}{2}^+]_1(2280)$
					$[\Xi\frac{7}{2}^+]_2(2289)$	$[\Xi\frac{7}{2}^+]_2(2342)$

Table 15. Calculated positions of the lightest few Ξ states assigned to the negative-parity $3\hbar\omega$ shell. Notation as in table 1.

Experimental state [24]	PW	J^π	Rating	Mass range [MeV] [24]	Model state in model $\mathcal{A}$	Model state in model $\mathcal{B}$
	S_{11}	$\frac{1}{2}^-$			$[\Xi\frac{1}{2}^-]_4(2241)$	$[\Xi\frac{1}{2}^-]_4(2417)$
					$[\Xi\frac{1}{2}^-]_5(2266)$	$[\Xi\frac{1}{2}^-]_5(2508)$
					$[\Xi\frac{1}{2}^-]_6(2387)$	$[\Xi\frac{1}{2}^-]_6(2571)$
					$[\Xi\frac{1}{2}^-]_7(2411)$	$[\Xi\frac{1}{2}^-]_7(2575)$
					$[\Xi\frac{1}{2}^-]_8(2445)$	$[\Xi\frac{1}{2}^-]_8(2602)$
	D_{13}	$\frac{3}{2}^-$			$[\Xi\frac{3}{2}^-]_4(2246)$	$[\Xi\frac{3}{2}^-]_4(2413)$
					$[\Xi\frac{3}{2}^-]_5(2284)$	$[\Xi\frac{3}{2}^-]_5(2518)$
					$[\Xi\frac{3}{2}^-]_6(2353)$	$[\Xi\frac{3}{2}^-]_6(2569)$
					$[\Xi\frac{3}{2}^-]_7(2384)$	$[\Xi\frac{3}{2}^-]_7(2576)$
					$[\Xi\frac{3}{2}^-]_8(2416)$	$[\Xi\frac{3}{2}^-]_8(2596)$
	D_{15}	$\frac{5}{2}^-$			$[\Xi\frac{5}{2}^-]_2(2292)$	$[\Xi\frac{5}{2}^-]_2(2469)$
					$[\Xi\frac{5}{2}^-]_3(2409)$	$[\Xi\frac{5}{2}^-]_3(2565)$
					$[\Xi\frac{5}{2}^-]_4(2425)$	$[\Xi\frac{5}{2}^-]_4(2583)$
					$[\Xi\frac{5}{2}^-]_5(2438)$	$[\Xi\frac{5}{2}^-]_5(2596)$
	G_{17}	$\frac{7}{2}^-$			$[\Xi\frac{7}{2}^-]_1(2320)$	$[\Xi\frac{7}{2}^-]_1(2477)$
					$[\Xi\frac{7}{2}^-]_2(2425)$	$[\Xi\frac{7}{2}^-]_2(2581)$
					$[\Xi\frac{7}{2}^-]_3(2464)$	$[\Xi\frac{7}{2}^-]_3(2607)$
					$[\Xi\frac{7}{2}^-]_4(2481)$	$[\Xi\frac{7}{2}^-]_4(2639)$
	G_{19}	$\frac{9}{2}^-$			$[\Xi\frac{9}{2}^-]_1(2505)$	$[\Xi\frac{9}{2}^-]_1(2604)$
					$[\Xi\frac{9}{2}^-]_2(2570)$	$[\Xi\frac{9}{2}^-]_2(2640)$

Table 16. Calculated positions of Ω states assigned to the negative-parity $1\hbar\omega$ shell. Notation as in table 1.

Experimental state [24]	PW	J^π	Rating	Mass range [MeV] [24]	Model state in model $\mathcal{A}$	Model state in model $\mathcal{B}$
	S_{31}	$\frac{1}{2}^-$			$[\Omega\frac{1}{2}^-]_1(1992)$	$[\Omega\frac{1}{2}^-]_1(2108)$
	D_{33}	$\frac{3}{2}^-$			$[\Omega\frac{3}{2}^-]_1(1976)$	$[\Omega\frac{3}{2}^-]_1(2110)$

Table 17. Calculated positions of Ω states assigned to the positive-parity $2\hbar\omega$ shell. Notation as in table 1.

Experimental state [24]	PW	J^π	Rating	Mass range [MeV] [24]	Model state in model $\mathcal{A}$	Model state in model $\mathcal{B}$
	P_{31}	$\frac{1}{2}^+$			$[\Omega\frac{1}{2}^+]_1(2232)$	$[\Omega\frac{1}{2}^+]_1(2442)$
					$[\Omega\frac{1}{2}^+]_1(2256)$	$[\Omega\frac{1}{2}^+]_1(2462)$
	P_{33}	$\frac{3}{2}^+$			$[\Omega\frac{3}{2}^+]_2(2177)$	$[\Omega\frac{3}{2}^+]_2(2461)$
					$[\Omega\frac{3}{2}^+]_3(2236)$	$[\Omega\frac{3}{2}^+]_3(2466)$
					$[\Omega\frac{3}{2}^+]_4(2287)$	$[\Omega\frac{3}{2}^+]_4(2497)$
	F_{35}	$\frac{5}{2}^+$			$[\Omega\frac{5}{2}^+]_1(2253)$	$[\Omega\frac{5}{2}^+]_1(2460)$
					$[\Omega\frac{5}{2}^+]_2(2312)$	$[\Omega\frac{5}{2}^+]_2(2493)$
	F_{37}	$\frac{7}{2}^+$			$[\Omega\frac{7}{2}^+]_1(2292)$	$[\Omega\frac{7}{2}^+]_1(2458)$

affecting the states in the same manner as in the Σ sector. Apart from slightly different spin-orbit effects and the overall higher mass positions of states due to bigger strangeness content, the predicted structures of the Ξ spectrum as well as the configuration mixing of states is thus very similar to the Σ sector. In particular, 't Hooft's force generates quite the same hyperfine structures, as shown in fig. 15 for model $\mathcal{A}$ (compare to the corresponding figs. 11 and 12 for the Σ sector).

In this respect it is worth noting that along with the downward mass shift of the $\Xi\frac{1}{2}^+$ ground state, which nicely explains the $\Xi\frac{3}{2}^+(1530,****)$–$\Xi\frac{1}{2}^+(1318,****)$ ground-state splitting, we observe again an equally large (roughly 200 MeV) selective lowering of the lowest positive-parity excited state with the same quantum numbers $J^\pi = \frac{1}{2}^+$. This state, which we predict to occur at 1876 MeV in model $\mathcal{A}$, can be viewed as the Roper-type analog of the Ξ-resonances. Also in the negative-parity sector the instanton-induced effects are quite the same as in the Σ spectrum. Thus, all our remarks concerning the structure of the positive- and negative-parity Σ spectrum basically hold also for the excited states predicted in the Ξ sector.

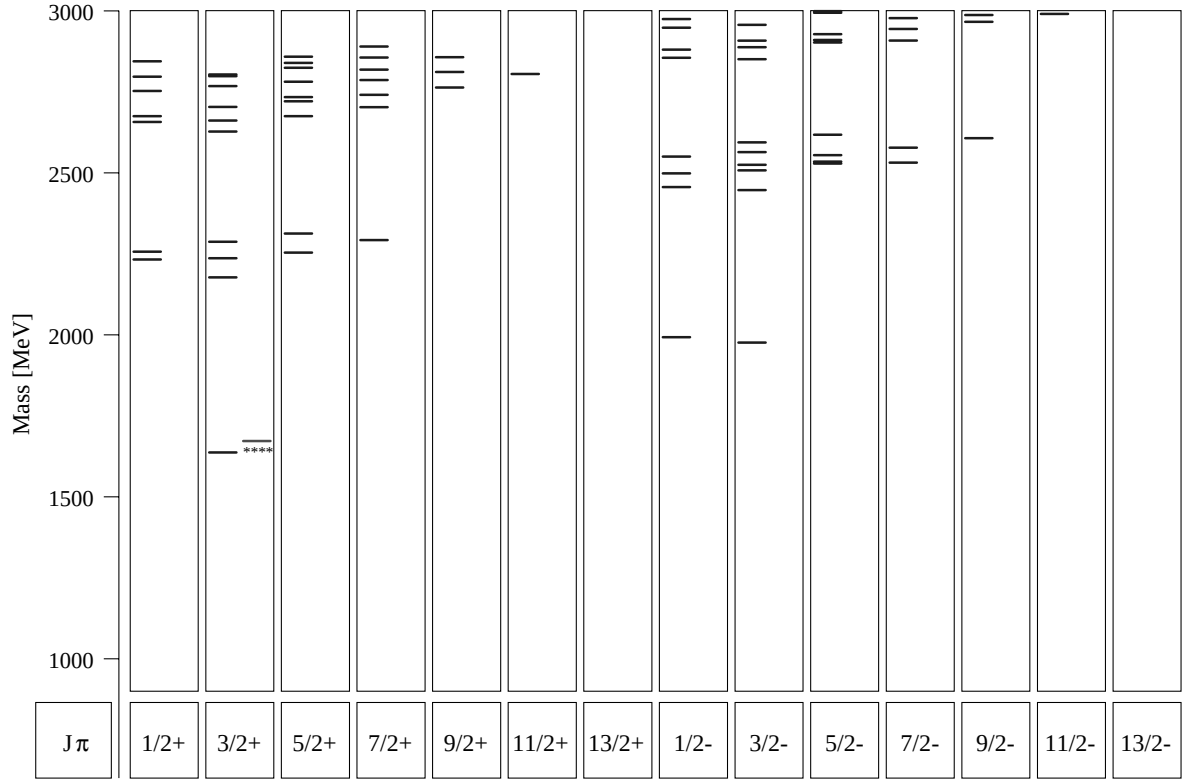

Fig. 18. The predicted positive- and negative-parity *Ω-baryon spectrum* with isospin $T = 0$ and strangeness $S^* = -3$ in *model* $\mathcal{A}$ (left part of each column) in comparison to experimental data [24] (right part of the column). The resonances are classified by the total spin J and parity π. At most ten radial excitations are shown in each column.

Our predictions for the Ξ-resonances with spin and parity J^π up to $\frac{13}{2}^\pm$ are graphically displayed in figs. 16 and 17. In addition, the positions of $1\hbar\omega$ and $2\hbar\omega$ states and the lightest few $3\hbar\omega$ states are explicitly tabulated in tables 13, 14 and 15. According to our previous results in the other flavor sectors, we expect the predictions of model $\mathcal{A}$ to be most reliable, but for the sake of completeness we also present those of model $\mathcal{B}$.

As mentioned before, there is little information on the excited states available at the moment. The $\Xi\frac{3}{2}^-(1820, ***)$ is the only excited resonance with established spin and parity. We associate this resonance with the lowest $\Xi\frac{3}{2}^-$ state predicted close to the $\Xi\frac{3}{2}^-(1820, ***)$ at 1780 MeV (in model $\mathcal{A}$, see table 13). Concerning the other states quoted by the PDG [24], whose spins and parities are unknown so far, we should note that a speculative assignment to model states in general is ambiguous and inconclusive. New experimental efforts to shed light into this poorly explored flavor sector would be highly desirable.

5 The Ω spectrum

Finally, let us conclude our discussion of the light-baryon spectrum by presenting our predictions for the Ω-baryons with strangeness $S^* = -3$ and isospin $T = 0$. Almost nothing is known experimentally about the excited Ω spectrum even 35 years after the unambiguous discovery of the Ω^- ground state in 1964. Apart from the ground state only three excitations with $S^* = -3$ have been found [24], but all of them without established spin and parity: $\Omega?^?(2250, ***)$, $\Omega?^?(2380, ***)$, and $\Omega?^?(2470, ***)$. But note that even the quantum numbers of the $\Omega\frac{3}{2}^+(1672, ****)$ have not actually been measured but follow from the assignment to the ground-state decuplet.

Similar to the Δ sector, in our approach also the Ω states are determined by the three-body confinement force alone, since 't Hooft's force does not act on their common totally symmetric flavor-decuplet wave function, which differs to that of the Δ states only by the replacement $|n\rangle \to |s\rangle$ of all non-strange flavors by the heavier strange quark flavors. Thus, apart from the overall higher positions and slightly smaller spin-orbit effects the predicted structures are essentially the same as in the Δ spectrum. Our predictions for the Ω-baryons are depicted in figs. 18 and 19 for model $\mathcal{A}$ and $\mathcal{B}$, respectively, where again those of version $\mathcal{A}$ should be most reliable. The calculated masses for the $1\hbar\omega$, $2\hbar\omega$ and $3\hbar\omega$ states are explicitly summarized in tables 16, 17 and 18, respectively. Note that the three excited states observed roughly fit the structures predicted, but a possible spin assignment would be rather ambiguous.

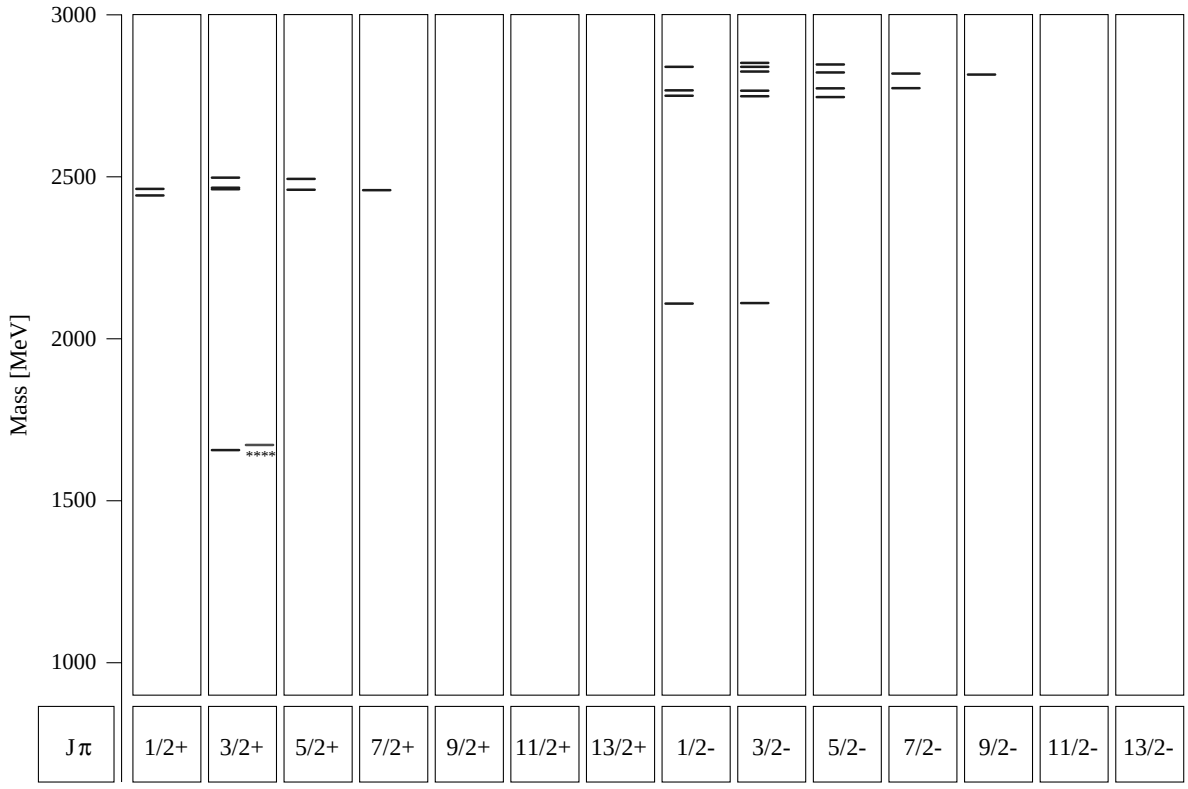

Fig. 19. The predicted positive- and negative-parity *Ω-baryon spectrum* with isospin $T = 0$ and strangeness $S^* = -3$ in *model* $\mathcal{B}$ (left part of each column) in comparison to experimental data [24] (right part of the column). The resonances are classified by the total spin J and parity π. At most ten radial excitations are shown in each column.

6 Summary and conclusion

Extending our previous work [5] on non-strange baryons we have presented in this paper a calculation of the strange-baryon spectrum together with a detailed comparison with experiment. Within a relativistic quark model with instantaneous forces we are able to describe the known Regge trajectories and the hyperfine structure in detail. 't Hooft's instanton-induced interaction played a central role, but it was also crucial to establish a suitable confinement interaction (model $\mathcal{A}$) and, in particular, the Dirac structure of this force. In comparison with non-relativistic or "relativized" quark models, the phenomenological success of the present relativistic model is remarkable; our earlier paper [5] and the present work demonstrate that the complete known light-baryon spectrum with roughly 100 resonance masses [24] can be uniformly described with the help of seven model parameters.

Our model potentials are purely phenomenological as far as confinement is concerned. The residual interaction has a QCD background in 't Hooft's instanton-induced quark force; our paper, however, only tests the operator structure of this force, in particular, the flavor dependence. For purpose, we only determine the strengths by a fit to the baryon spectrum. In the appendix we present a poor-man's consistency check: by fixing a common cutoff for instanton sizes we could roughly reproduce the quark model masses and couplings under the assumptions of spontaneous chiral symmetry breaking. This is certainly only a first step towards a more complete incorporation of instanton effects [17–23].

Based on the Bethe-Salpeter amplitudes electro-weak decays and formfactors were already computed [33] in the Mandelstam formalism [34]. The results will soon be published as well as some calculations of heavy flavored (charm and bottom) baryons, where as a new feature, the importance of one-gluon exchange cannot be ruled out. Work on the perturbative calculation of strong baryon decays [34] is more difficult but in progress.

We have profited very much from scientific discussions with V.V. Anisovich, G.E. Brown, E. Klempt, K. Kretzschmar, A. Sarantsev and E.V. Shuryak to whom we want to express our gratitude. We also thank the Deutsche Forschungsgemeinschaft (DFG) for financial support.

Appendix A. Checking the consistency with QCD relations

So far, the effective constituent quark masses m_n, m_s and the effective 't Hooft coupling strengths g_{nn} and g_{ns} together with the effective range λ of the regularized instanton-induced four-fermion interaction have been treated as free parameters of our two models $\mathcal{A}$ and $\mathcal{B}$.

Table 18. Calculated positions of negative-parity Ω states in the $3\hbar\omega$ shell. Notation as in table 1.

Experimental state [24]	PW	J^π	Rating	Mass range [MeV] [24]	Model state in model $\mathcal{A}$	Model state in model $\mathcal{B}$
	S_{31}	$\frac{1}{2}^-$			$[\Omega\frac{1}{2}^-]_2(2456)$	$[\Omega\frac{1}{2}^-]_2(2750)$
					$[\Omega\frac{1}{2}^-]_3(2498)$	$[\Omega\frac{1}{2}^-]_3(2766)$
					$[\Omega\frac{1}{2}^-]_4(2550)$	$[\Omega\frac{1}{2}^-]_4(2839)$
	D_{33}	$\frac{3}{2}^-$			$[\Omega\frac{3}{2}^-]_2(2446)$	$[\Omega\frac{3}{2}^-]_2(2748)$
					$[\Omega\frac{3}{2}^-]_3(2507)$	$[\Omega\frac{3}{2}^-]_3(2765)$
					$[\Omega\frac{3}{2}^-]_4(2524)$	$[\Omega\frac{3}{2}^-]_4(2824)$
					$[\Omega\frac{3}{2}^-]_5(2564)$	$[\Omega\frac{3}{2}^-]_5(2839)$
					$[\Omega\frac{3}{2}^-]_6(2594)$	$[\Omega\frac{3}{2}^-]_6(2851)$
	D_{35}	$\frac{5}{2}^-$			$[\Omega\frac{5}{2}^-]_1(2528)$	$[\Omega\frac{5}{2}^-]_1(2746)$
					$[\Omega\frac{5}{2}^-]_2(2534)$	$[\Omega\frac{5}{2}^-]_2(2772)$
					$[\Omega\frac{5}{2}^-]_3(2554)$	$[\Omega\frac{5}{2}^-]_3(2822)$
					$[\Omega\frac{5}{2}^-]_4(2617)$	$[\Omega\frac{5}{2}^-]_4(2846)$
	G_{37}	$\frac{7}{2}^-$			$[\Omega\frac{7}{2}^-]_1(2531)$	$[\Omega\frac{7}{2}^-]_1(2773)$
					$[\Omega\frac{7}{2}^-]_2(2577)$	$[\Omega\frac{7}{2}^-]_2(2818)$
	G_{39}	$\frac{9}{2}^-$			$[\Omega\frac{9}{2}^-]_1(2606)$	$[\Omega\frac{9}{2}^-]_1(2815)$

They have been adjusted to fit the experimental spectra. To be more precise, the parameters g_{nn}, g_{ns} and λ of the 't Hooft interaction have been fixed to the values given in ref. [5] in order to reproduce the correct hyperfine structure of the octet and decuplet ground-state baryons, *i.e.* the mass splittings $N-\Delta$, $\Sigma^*-\Sigma$, $\Xi^*-\Xi$ and $\Sigma-\Lambda$ and as a very nice feature of model $\mathcal{A}$ it turned out that at the same time the effect of 't Hooft's force with these values fixed could even account also for substantial structures of the excited baryon spectra such as, *e.g.*, the low position of the Roper resonance and its strange partners or the appearance of approximately degenerate parity doublets in the experimental nucleon and Λ spectrum. Thus we could impressively demonstrate the possibility that besides a proper confinement mechanism (as given by model $\mathcal{A}$), instanton-induced interactions indeed may play the essential role in the determination of the spectra of light-flavored baryons. An additional nice feature of the instanton force is that it intrinsically provides a constituent quark mass generation via the Nambu mechanism and hence it appears even natural to work directly with constituent quark masses m_n and m_s as done in the present framework. In order to confirm this picture of light baryons, it is important to investigate whether our phenomenologically adjusted parameters g_{nn}, g_{ns}, λ, m_n and m_s are really consistent with the theory of instantons and its relation to QCD as discussed in detail in ref [5]. There we have shown that due to the process of chiral symmetry breaking 't Hooft's instanton-induced interaction leads to relations for the effective constituent quark masses m_n, m_s and the effective 't Hooft coupling constants g_{nn}, g_{ns}. The QCD relations have been derived by normal ordering of the original instanton-induced six-quark vertex [10] with respect to the true physical QCD vacuum which exhibits the non-vanishing quark condensates $\langle\overline{\Psi}_n\Psi_n\rangle$ and $\langle\overline{\Psi}_s\Psi_s\rangle$ for non-strange and strange quark fields, respectively. They are functions of the critical maximum instanton size ρ_c, whose value we expect to be in rough qualitative[5] agreement with the effective range $\lambda = 0.4$ fm of the regularized instanton force in our model. Let us briefly recall these ρ_c-dependent relations of ref. [5]:

– The Wick contraction of two fermion lines gives the *effective constituent quark masses* (if possible contributions from the confinement force are excluded)

$$\begin{aligned} m_n(\rho_c) &:= m_n^0 + \int_0^{\rho_c} \mathrm{d}\rho\, \frac{d_0(\rho)}{\rho^5}\ \frac{4}{3}\pi^2\rho^3 \\ &\quad\times\Big(m_n^0\rho - \frac{2}{3}\pi^2\rho^3\ \langle\overline{\Psi}_n\Psi_n\rangle\Big)\ \Big(m_s^0\rho - \frac{2}{3}\pi^2\rho^3\ \langle\overline{\Psi}_s\Psi_s\rangle\Big), \\ m_s(\rho_c) &:= m_s^0 + \int_0^{\rho_c} \mathrm{d}\rho\, \frac{d_0(\rho)}{\rho^5}\ \frac{4}{3}\pi^2\rho^3 \\ &\quad\times\Big(m_n^0\rho - \frac{2}{3}\pi^2\rho^3\ \langle\overline{\Psi}_n\Psi_n\rangle\Big)^2. \quad \text{(A.1)} \end{aligned}$$

– The Wick contraction of a single fermion line gives the *effective 't Hooft couplings*

$$\begin{aligned} g_{nn}(\rho_c) &:= \frac{3}{8}\int_0^{\rho_c} \mathrm{d}\rho\, \frac{d_0(\rho)}{\rho^5}\left(\frac{4}{3}\pi^2\rho^3\right)^2 \\ &\quad\times\Big(m_s^0\rho - \frac{2}{3}\pi^2\rho^3\ \langle\overline{\Psi}_s\Psi_s\rangle\Big), \\ g_{ns}(\rho_c) &:= \frac{3}{8}\int_0^{\rho_c} \mathrm{d}\rho\, \frac{d_0(\rho)}{\rho^5}\left(\frac{4}{3}\pi^2\rho^3\right)^2 \\ &\quad\times\Big(m_n^0\rho - \frac{2}{3}\pi^2\rho^3\langle\overline{\Psi}_n\Psi_n\rangle\Big). \quad \text{(A.2)} \end{aligned}$$

[5] Note that the regularization procedure in the 't Hooft kernel is rather arbitrary. The meaning of the effective range strongly depends on the regularizing function chosen. Thus only a rough correspondence between the effective range of the 't Hooft interaction and the effective instanton size may be expected.

Table 19. Phenomenological standard values of QCD parameters, compare to ref. [36]

Current quark masses	non-strange	m_n^0	9	MeV
	strange	m_s^0	150	MeV
Quark condensates	non-strange	$\langle\overline{\Psi}_n\Psi_n\rangle$	-225^3	MeV^3
	strange	$\langle\overline{\Psi}_s\Psi_s\rangle$	0.8	$\langle\overline{\Psi}_n\Psi_n\rangle$
QCD scale parameter		$\Lambda_{\rm QCD}$	200	MeV

Here the instanton density $d_0(\rho)$ for three colors and three flavors reads

$$d_0(\rho) = 3.63 \cdot 10^{-3} \left(\frac{8\pi^2}{g^2(\rho)}\right)^6 \exp\left(-\frac{8\pi^2}{g^2(\rho)}\right), \quad \text{(A.3)}$$

where $g(\rho)$ is the ρ-dependent running coupling constant, which in two-loop accuracy is given by [35]

$$\frac{8\pi^2}{g^2(\rho)} = 9\ln\left(\frac{1}{\rho\ \Lambda_{\rm QCD}}\right) + \frac{32}{9}\ln\left[\ln\left(\frac{1}{\rho\ \Lambda_{\rm QCD}}\right)\right]. \quad \text{(A.4)}$$

In this way the parameters m_n, m_s, g_{nn} and g_{ns}, which we fixed from a fit to the phenomenology of the experimental light-baryon spectrum, are related to standard QCD parameters, *i.e.* the current quark masses m_n^0 and m_s^0, the quark condensates $\langle\overline{\Psi}_n\Psi_n\rangle$ and $\langle\overline{\Psi}_s\Psi_s\rangle$ and the QCD scale parameter $\Lambda_{\rm QCD}$. Typical phenomenological values of these QCD parameters taken from [36] are listed in table 19.

It is now quite interesting to study to what extent these expressions for the coupling constants (A.2) and the constituent quark masses (A.1) are consistent with the phenomenologically determined values in our covariant Salpeter-equation–based quark model. In other words, the question is whether there is a common uniform instanton cutoff ρ_c which approximately agrees with the effective range $\lambda = 0.4$ fm of our model, such that the corresponding constituent quark masses $m_n(\rho_c)$, $m_s(\rho_c)$ and couplings $g_{nn}(\rho_c)$, $g_{ns}(\rho_c)$ obtained by the gap equations with the standard QCD values given in table 19 are in fair agreement with our phenomenologically fixed values. We restrict here our discussion to the confinement model $\mathcal{A}$, which in connection with 't Hooft's force yields consistently better results for the excited baryon spectrum than model $\mathcal{B}$ and hence seems to be the more realistic model. The corresponding situation is presented in fig. 20.

The plotted curves show the constituent quark masses (dash-dotted curve) and 't Hooft couplings (dashed curve) as a function of the critical instanton size ρ_c in two-loop approximation. They have been calculated with the QCD parameters given in table 19. The horizontal lines represent the corresponding fitted values in model $\mathcal{A}$. Apart from the strange quark mass m_s, we indeed find that the two fitted coupling strengths $g_{nn} = 136$ MeV fm^3 and $g_{ns} = 94$ MeV fm^3 together with the fitted non-strange quark mass $m_n = 330$ MeV can be nicely reproduced by the gap equations with an approximately uniform critical instanton size $\rho_c \simeq 0.44$ fm, which is in a satisfactory

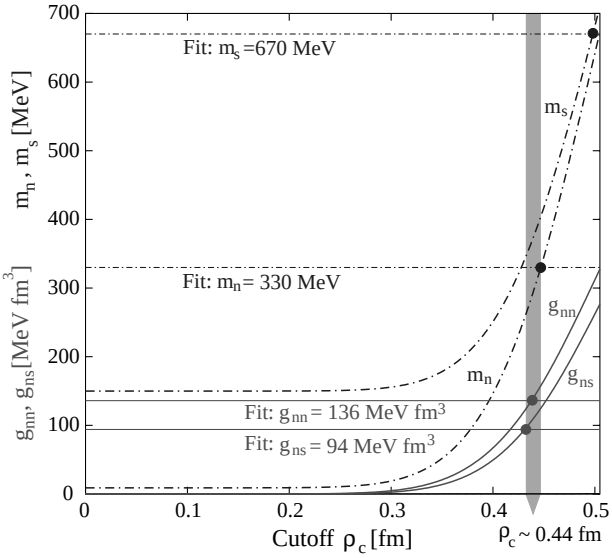

Fig. 20. The effective non-strange, strange constituent quark masses m_n, m_s (dash-dotted lines) and the effective coupling constants g_{nn}, g_{ns} (dashed lines) as functions of the critical maximum instanton size ρ_c due to eqs. (A.1) and (A.2), respectively. The calculation has been performed in two-loop approximation using the standard QCD parameters given in table 19. The horizontal lines represent the corresponding phenomenologically adjusted values of model $\mathcal{A}$.

Table 20. Empirically fitted 't Hooft couplings and constituent quark masses of model $\mathcal{A}$ (right column) in comparison with the corresponding gap equation results (left column) with $\rho_c \simeq 0.44$ fm (compare to fig. 20). The calculations have been performed in two-loop approximation with the standard QCD parameters given in table 19.

Gap equations		Empirical fit	(model $\mathcal{A}$)
$\rho_c = 0.44$	fm	$\lambda = 0.4$	fm
$g_{nn} = 141$	MeV fm^3	$g_{nn} = 136$	MeV fm^3
$g_{ns} = 110$	MeV fm^3	$g_{ns} = 94$	MeV fm^3
$m_n = 297$	MeV	$m_n = 330$	MeV
$m_s = 375$	MeV	$m_s = 630$	MeV

qualitative agreement with the effective range $\lambda = 0.4$ fm of the 't Hooft interaction. This value $\rho_c \simeq 0.44$ fm also conforms qualitatively with recent lattice investigations [37–39] on the topological structure of the QCD vacuum which in fact predict a strong suppression of tunneling events for larger instanton sizes $\rho > 0.45$ fm. Concerning the 't Hooft couplings, remember that the phenomenological value and sign of the $\Sigma - \Lambda$ splitting (see ref. [5]) required the instanton-induced attraction between a non-strange–strange quark pair to be weaker than between a non-strange quark pair, *i.e.* $g_{ns} < g_{nn}$. In fact, this requirement is fairly well confirmed by the QCD-relations (A.2) due to the different Wick contractions of the original six-point 't Hooft vertex with one incoming and outgoing

quark of each flavor (u, d, s): g_{nn} involves the integration over the strange (s) quark loop, while in g_{ns} the lighter non-strange quark (u and d, respectively) is integrated over.

We should further mention that for a value $\rho = \rho_c = 0.44$ fm we find only a 6 % difference between the one-loop and two-loop approximation of the strong ρ-dependent running coupling constant $g(\rho)$ given in eq. (A.4), which still is small enough to be within the scope of the two-loop formula.

Unfortunately, the phenomenologically adjusted strange-quark mass is definitely too high to be compatible with the gap equation result at this critical instanton size $\rho_c \simeq 0.44$. But note that the derivation of the effective 't Hooft interaction assumes zero-mode dominance in the case of (almost) massless current quarks. Compared to the almost vanishing non-strange current quark mass $m_n^0 \simeq 9$ MeV, the strange quark mass $m_s^0 \simeq 150$ MeV, however, is quite big, so that in this case the zero-mode approximation might become less valid and consequently contributions to the strange quark mass that stem from non-zero modes could become important to explain a part of this missing mass. Moreover, the instanton-induced interaction is not necessarily the only source for contributions to the effective constituent quark masses. In principle there might be other contributions and hence it is hard to decide whether this discrepancy in the strange quark mass actually reflects a serious inconsistency.

In table 20 we additionally displayed the explicit absolute values for the masses and coupling constants obtained by the gap equations with a cutoff $\rho_c \simeq 0.44$ fm, in comparison to the corresponding fitted values of model $\mathcal{A}$.

Except for the much too low strange quark mass m_s the agreement with model $\mathcal{A}$ indeed is satisfying: In view of the sensitive dependence on the condensate values and the arbitrary regularization procedure, the deviations of ≤ 15 % of the calculated values for g_{nn}, g_{ns} and m_n from the phenomenological values are rather small. For the ratio g_{ns}/g_{nn} between the non-strange–strange and the non-strange coupling constants the QCD relation yields the explicit value $g_{ns}/g_{nn} = 0.78$ which also is in a satisfactory accordance with the value $g_{ns}/g_{nn} = 0.69$ obtained by the phenomenologically determined couplings.

In summary, we thus find a rather good consistency of our model $\mathcal{A}$ with the expectations from the theory of instantons and its relation to QCD, which strongly supports the spirit of our model that non-perturbative gluon configurations, *i.e.* the instantons, play the dominant role in the description of spin-spin forces for the light baryons. In comparison with the analogous couplings fitted in the meson calculations of ref. [40,41], our couplings are, however, too large. This admittedly indicates that our phenomenological approach needs further theoretical justifications.

References

1. E.E. Salpeter, H.A. Bethe, Phys. Rev. **84**, 1232 (1951).
2. J.G. Taylor, Phys. Rev. **150**, 1321 (1966).
3. E.E. Salpeter, Phys. Rev. **87**, 328 (1952).
4. U. Löring, K. Kretzschmar, B.Ch. Metsch, H.R. Petry, Eur. Phys. J. A **10**, 309 (2001).
5. U. Löring, B. Ch. Metsch, H.R. Petry, this issue, p. 395.
6. J. Carlson, J.B. Kogut, V.R. Pandhariapande, Phys. Rev. D **27**, 233 (1983).
7. J. Carlson, J.B. Kogut, V.R. Pandhariapande, Phys. Rev. D **28**, 2807 (1983).
8. G.S. Bali, hep-ph/0001312 (2000).
9. G. 't Hooft, Phys. Rev. D **14**, 3432 (1976); **18**, 2199(E) (1978).
10. M.A. Shifman, A.I. Vainshtein, V.I. Zakharov, Nucl. Phys. B **163**, 46 (1980).
11. V.V. Anisovich, Upton/BY, *AIP Conf. Proc.*, Vol. **432** (AIP, New York, 1997) p. 421.
12. V.V. Anisovich, Phys. Usp. **41**, 419 (1998).
13. V.V. Anisovich, Usp. Fiz. Nauk **168**, 481 (1998).
14. A.V. Anisovich, A.V. Sarantsev, hep-ph/9705401; see also Phys. Lett. B **413**, 137 (1997).
15. V.V. Anisovich, A.V. Sarantsev, Phys. Lett. B **382**, 429 (1996).
16. V.V. Anisovich, Yu.D. Prokoshkin, A.V. Sarantsev, Phys. Lett. B **389**, 388 (1996).
17. T. Schäfer, E.V. Shuryak, Rev. Mod. Phys. **70**, 323 (1998).
18. D.I. Dyakonov, V.Y. Petrov, Nucl. Phys. B **245**, 259 (1984).
19. D.I. Dyakonov, V.Y. Petrov, Sov. Phys. JETP **62**, 204, 431 (1985).
20. D.I. Dyakonov, V.Y. Petrov, Nucl. Phys. B **272**, 457 (1986).
21. D.I. Dyakonov, V.Y. Petrov, *Diquarks in the Instanton Picture*, in *Proceedings of the 99th WE-Heraeus Seminar on Quark Cluster Dynamics*, edited by K. Goeke, P. Kroll, H.R. Petry, *Lect. Notes Phys.*, Vol. **417** (Springer-Verlag, Heidelberg, 1992) p. 288.
22. M.A. Nowak, J.J.M. Verbaarschot, I. Zahed, Nucl. Phys. B **324**, 1 (1989).
23. M.A. Nowak, M. Rho, I. Zahed, *Chiral Nuclear Dynamics* (World Scientific, Singapore, 1996).
24. Particle Data Group, *Review of Particle Physics*, Eur. Phys. J. C **15**, 1-878 (2000).
25. Particle Data Group, *The Λ(1405)*, revised by R.H. Dalitz in *Review of Particle Physics*, Eur. Phys. J. C **15**, 748 (2000).
26. S. Capstick, W. Roberts, nucl-th/0008028 (2000).
27. M. Arima, S. Matsui, K. Shimizu, Phys. Rev. C **49**, 2831 (1994).
28. W.H. Blask, U. Bohn, M.G. Huber, B.C. Metsch, H.R. Petry, Z. Phys. A **337**, 327 (1990).
29. B.C. Metsch, *Hadron Spectroscopy with Instanton induced Forces*, in *Proceedings of the 99th WE-Heraeus Seminar on Quark Cluster Dynamics*, edited by K. Goeke, P. Kroll, H.R. Petry, *Lect. Notes Phys.*, Vol. **417** (Springer-Verlag, Heidelberg, 1992) p. 72.
30. N. Isgur, G. Karl, Phys. Rev. D **18**, 4187 (1978); Phys. Rev. D **19**, 2653 (1979).
31. S. Capstick, N. Isgur, Phys. Rev. D **34**, 2809 (1986).
32. R. Bijker, F. Iachello, A. Leviatant, Ann. Phys. **284**, 89 (2000).
33. K. Kretzschmar, *Electroweak Form Factors in a Covariant Quark Model of Baryons*, Ph.D. thesis, University of Bonn, TK-01-01 (2001).
34. S. Mandelstam, Proc. R. Soc. **233**, 248 (1955).

35. E.V. Shuryak, Nucl. Phys. B **203**, 93;116 (1982).
36. L.J. Reinders, H. Rubinstein, S. Yazaki, Phys. Rep. **127**, 1 (1985).
37. D. Smith, M. Teper, Phys. Rev. D **58**, 014505 (1998).
38. J.W, Negele, Nucl. Phys. Proc. Suppl. **73**, 92 (1999).
39. A. Ringwald, F.Schrempp, Phys. Lett. B **459**, 249 (1999).
40. M. Koll, R. Ricken, D. Merten, B.C. Metsch, H.R. Petry, Eur. Phys. J. A **9**, 73 (2000).
41. R. Ricken, M. Koll, D. Merten, B.C. Metsch, H.R. Petry, Eur. Phys. J. A **9**, 221 (2000).